SPI Report

ANALYSIS OF SPACE ENVIRONMENT DAMAGE TO SOLAR CELL ASSEMBLIES FROM LDEF EXPERIMENT A0171-GSFC TEST PLATE

by

David C. Hill & M. Frank Rose
Space Power Institute
231 Leach Center
Auburn University, AL 36849-5320

Work performed under NASA contract NAS8-39131
Sponsored by NASA George C. Marshall Space Flight Center, Huntsville, AL 35812

September 1994

89pp

AUBURN UNIVERSITY

FINAL REPORT

for

NASA CONTRACT

NAS8-39131

"Analysis of Space Environment Damage to Solar Cell Assemblies from LDEF Experiment A0171-GSFC Test Plate"

21 July 1993 - 19 August 1994

Auburn University

Space Power Insitute

231 Leach Center

Auburn University, AL 36849-5320

David C. Hill & M. Frank Rose

2 September 1994

TABLE OF CONTENTS

LIST OF TABLES

LIST OF FIGURES

EXECUTIVE SUMMARY

The contractor has completed the tasks as set out in the Scope of Work. The solar cell assemblies (SCAs) have been described in detail, resulting in a *Materials List - As Built; As Flown* (see pages 54-55) and two sets of SCA data sheets (pages 56-61 and pages 62-66). Crystal orientation cannot be determined without demounting and disassembling each SCA. Such work should be deferred until the test plate is disassembled, preferably by NASA personnel. Pre-flight electrical characteristics have been collated in detail for future reference. Post-flight electrical measurements conducted by NASA were extended and full current-voltage data for all LD-type cells were obtained. Current-voltage traces are appended to this document on pages 75-89. Task 2 activities were extended to encompass a full diagnosis and data analysis of the electrically-conductive surface coatings and electrical bond materials. Task 3 activities are included in the relevant sections indicating the effects of the space particulate and atomic oxygen environments with a summary provided at the end of the report.

Meteoroid and debris (M&D) impact locations were scanned using Space Power Institute facilities to determine whether the M&D environment has a significant effect on SCA structural integrity and electrical performance. Impact site location and dimensions data shall be inserted into the LDEF M&D SIG Database maintained by Lockheed ESCO, NASA Johnson Space Center.

An anomalous cluster of impact sites was located on cells S-2 and S-3. A major impact event on cell S-10 resulted in extensive cracking of the coversheet, which caused several sectors of the coversheet to become electrically isolated. Electrical continuity could be restored by applying mechanical force to such areas implying that thermal cycling could result in partial intermittent electrical continuity across the coversheet surface.

A coversheet penetration flux distribution was derived from the M&D impact data, allowing for the estimation of solar cell damage. Of 397 identified M&D sites only two penetrated the coversheet material. The area erosion effect due to impact site spallation is of negligible importance in scattering radiation and reducing solar cell output. Solar cell maximum power reduction is inversely proportional to coversheet thickness, indicating that for the coversheet thicknesses deployed here (6 mil, 12 mil, 40 mil) radiation darkening of the coversheet is significant and that the coversheets provided adequate radiation protection to the cells.

Indium oxide electrically-conductive coatings are subject to atomic oxygen degradation, resulting in an increase in surface resistivity. Adhesive-based electrically conductive bonds

(EBPs) appear to be subject to vacuum outgassing resulting in reduced resistivity, whereas solder-based EBPs showed increased resistance most likely due to the greater thermal expansion coefficient mismatch between the EBP and the coversheet.

Further analysis is recommended in the areas of (i) M&D impact site clusters, (ii) coversheet penetration effects on solar cell performance, (iii) differential charging/discharging effects for isolated areas on nominally electrically-conductive solar cell coversheets.

SCOPE OF WORK

The Scope of Work is presented here for completeness as taken from the NASA Delivery Order Proposal and Acceptance package for this project (delivery order no. 18, contract NAS8-39131).

The Long Duration Exposure facility (LDEF) experiment A0171 was composed of many separate experiments, some of which contained solar cells. These solar cells require post-flight analysis.

Task 1: The contractor shall analyze these solar cells from LDEF experiment A0171 and provide the following data, as available.

solar cell description
substrate composition and thickness, crystal orientation, anti-reflective coating composition and thickness

pre-flight characteristics
V (open circuit), I (short circuit), V (at maximum power), I (at maximum power), maximum power and efficiency

post-flight characteristics
V (open circuit), I (short circuit), V (at maximum power), I (at maximum power), maximum power and efficiency

The solar cell description and pre-flight characteristics will be provided by NASA, as available.

Task 2: perform solar cell measurements as necessary to complete task 1.

Task 3: provide an analysis summary and conclusion of findings related to Space Environmental Effects (SEE) on solar cells in Low Earth Orbit (LEO).

INTRODUCTION

The space environment in earth orbit has been extensively studied and documented. The most serious factors influencing electrical systems (including solar arrays) are the local radiation environment, thermal cycling effects, local plama density, neutral particle density, spacecraft surfaces outgassing/effluent products, and the meteoroid and debris flux. The radiation environment (proton, electron, and photon), fueled primarily by the sun but also by other stellar sources, encountered by spacecraft in earth orbit is complex and depends upon such factors as orbital altitude, inclination, and current solar activity levels, and can result in exposures which vary over several orders of magnitude per orbit. The effects of these particles and electromagnetic radiation can cause major changes in the properties of insulators and semiconductors by ionization, atomic displacements or local changes due to chemical reactions. The severity of a radiation-induced change under multi-factor stressing depends on the total dose, intensity, particle species, impingement angle, presence of shielding, mechanical stress, local induced environment, temperature, and the presence of system-generated electromegnetic fields.

Repeated thermal cycling with moderate to large temperature excursions are responsible for the degration of materials mechanical and electrical characteristics. For example, thermal control paints can be embrittled as the binder degrades. Thermally- or mechanically-induced flexing of the substrate may lead to paint flakes being ejected form the surface, contaminating the spacecraft local environment and contibuting to the space debris environment. Immersion of a spacecraft in the ionospheric environment, typical of low earth orbit (LEO) altitudes (250 km to 1000 km), leads to a local induced environment produced by the complex interaction of the spacecraft structure and systems with the ambient environment. The induced environment may depend heavily on the out-gassing and de-gassing characteristics of the spacecraft surfaces, especially for surfaces with long vent paths. Atomic oxygen exposure is known (ref. 1) to be especially damaging for materials which suffer oxidation easily. Solar cell silver interconnects have been found to be particularly susceptible as have numerous polymeric materials such as Kapton®.

Where spacecraft surfaces are exposed to the space particulate (meteoroid and debris -M&D) environment the threat of hypervelocity micro-particle cratering, perforation, and impact-induced electrical breakdown (both volume breakdown and surface flashover) exists. The term *"hypervelocity micro-particle impact"* implies impact by micron-scale to sub-millimeter-scale space particles, including space debris particles (SDPs) and interplanetary dust (meteoroids) particles (IDPs) at velocities in excess of 4-6 km/s. Such particles typically impact spacecraft and space structures in LEO at average velocities in the range 7-25 km/s and, because of their excessive kinetic energy, generate shock waves in target material, liberate copious amounts of ejecta and initiate the production of hot plasma. Physical phenomena of these types are known to be extremely damaging to low voltage spacecraft power systems operating exposed to the space environment (refs 2-5). For solar arrays, cells, and other associated materials such as coversheets, the problem is significant. Impacts cause large areas of spallation around impact craters in brittle materials such as glass. Thin laminated structures such as solar cell or multilayer dielectric stacks can suffer extensive delamination. Cratering in optical substrates causes scattering and loss of transmission and the build-up of such sites reduces effective aperture. Recently, Russian research has indicated that the shock processing of the solar cell that occurs under impact can increase the cell shunt resistance significantly, producing a dramatic reduction in efficiency and thus total power output (ref. 6).

The sum total of these effects on spacecraft materials, components, and systems, can only be evaluated by long term exposure. Therefore, NASA designed, flew, and retrieved the LDEF spacecraft, which remained in orbit for 69 months from April 1984 to January 1990. Included in the experiment inventory were several experiments designed to measure the effects of long duration exposure to the space environment on solar array materials, solar cells, and associated array manufacturing technologies. The purpose of the work reported here was to conduct an analysis of the solar cell stacks flown on LDEF as part of experiment A0171 (Solar Array Materials Passive LDEF Experiment -SAMPLE), in particular, the Goddard Space Flight Center (GSFC) provided test plate.

LDEF ORIENTATION & EXPERIMENT EXPOSURE GEOMETRY

The LDEF was deployed into Earth orbit on 7 April 1984 at a time of near-minimum solar activity and was retrieved 69 months later on 12 January 1990 at a time of near-maximum solar activity (ref. 7) after completing 32,422 orbits. The spacecraft flew in a circular orbit, inclined at 28.5°, with an initial altitude of 257 nm (476 km). On retrieval, the orbit had decayed to an altitude of approximately 179 nm (332 km).

A passive, gravity-gradient 3-axis stabilization scheme was utilized for attitude control. Figure 1 shows the spacecraft structural configuration and identification of experiment locations relative to the spacecraft body coordinate system. The 12 faces (experiment rows) of the structure are numbered 1 through 12 in a clockwise direction when looking at the Earth-facing end. The 6 longitudinal locations on each row are identified as Bay A through Bay F starting at the Earth end of the spacecraft. Nominally, the LDEF was to fly orientated with the Row 9 surface normal (+Z axis) parallel to the spacecraft velocity vector and the spacecraft +X axis

(Space-facing end normal vector) parallel to the orbit radius vector. In reality, the spacecraft was yawed 8° to starboard and pitched 2° forward. Figure 2 shows the spacecraft attitude relative to the Earth and the effect of the 8° yaw on the relative orientations of the various experiment tray rows.

The GSFC test plate which is the subject of this report was part of LDEF experiment A0171 which was located in Bay A08, close to the spacecraft leading edge. The experiment comprised specimens of various solar array materials mounted in a standard 3" deep LDEF peripheral tray. Figure 3 shows the post-deintegration view of the front of the entire A08 experiment tray (ref. 8) with the GSFC test plate being located in the lower left corner. Figure 4 is a schematic of the A0171 experiment layout indicating the position of the GSFC test plate relative to other LDEF bays and the spacecraft attitude. Due to the location of the GSFC test plate, *i.e.* close to the wall of the tray, it was necessary to determine the relative exposure geometry with respect to the spacecraft flight vector. This is critical for atomic oxygen (ATOX) exposure effects since part of the GSFC test plate was partially shielded from the ATOX RAM direction.

Similarly, there is a "RAM-effect" for M&D particles due to the fact that the average arrival velocity of such particles is comparable to the spacecraft velocity. Measurement of M&D impact crater rates for all LDEF surfaces has yielded a RAM-to-WAKE impact ratio of between 5 and 10 to 1, the exact value being a function of particle type (*i.e.* either meteoroid or debris), particle velocity and size (refs 9-11). For a partially-shielded RAM-facing surface the M&D impact rate should show the effect of such shielding. Figure 5 shows the relative exposure geometry for the GSFC test plate. It can be seen that the whole of one row of solar cell assemblies (SCAs), the row containing SCA S-1, is shielded from the direct ATOX RAM flux. Also, this row should suffer fewer impacts due to M&D particles.

GSFC TEST PLATE EXPERIMENTAL CONFIGURATION

The GSFC test plate was designed to test the space environmental effects (radiation, atomic oxygen, thermal cycling, meteroid & debris) on conductively coated solar cell coversheets, various electrical bond materials, solar cell performance, and other materials properties where feasible. The test plate contained twenty-eight 2 cm X 2 cm silicon solar cells (S-type), 305 μm (12 mil) thick, with silicon monoxide (SiO) anti-reflection (AR) coatings, covered by 305 μm thick fused silica (SiO_2) coversheets with indium oxide (In_2O_3) conductive coatings, and fifteen 2 cm X 6 cm, 305 μm thick, silicon solar cells (LD-type) with tantalum pentoxide (Ta_2O_5) AR coatings, boron-doped back surface field (BSF), aluminum back surface mirror (BSM), covered by various thickness (6 mil, 12 mil, and 40 mil) fused silica coversheets with MgF_2 AR coatings and UV blocking filters. Figure 6 shows the layout of the test plate, indicating the electrical connection points. A complete materials list (as-built, as-flown), a data sheets for S-type SCAs, and data sheets for LD-type SCAs are presented on pages 54-66.

2 cm X 2 cm Silicon Solar Cells

The S-type cells (note that the type designation, S- and LD-, are project specific) were bonded to the experiment faceplate (epoxy board) using Dow-Corning adhesive 93-500. Electrical connections were made to the coversheet front face using a variety of solders or conductively-loaded adhesives, the objective of which was to determine the best method of providing electrical continuity to the front face of the solar cell coversheet. Therefore, the cell contacts, nominally titanium-palladium-silver (Ti:Pd:Ag), were irrelevant to this part of the experiment. No measurements of cell current-voltage characteristics were possible. Figure 7 shows the S-type SCA cross-sectional geometry.

Four vapor-deposited metallic (material undefined) pads are located on the front surface of each S-type cell coversheet, one in each corner. Pad-to-pad measurements of electrical resistance allows the surface coating resistivity to be characterized both pre- and post-flight. Each cell also has four electrical bond pads (EBPs) connected to terminal posts via 24-AWG copper (Cu) wire of either unplated or tin (Sb) plated type. Again, the S-type SCA data sheets give the specific combinations for each cell stack. Space environmental exposure of the various EBP materials was expected to modify or degrade the resistivity of the material. Terminal-to-pad measurements of resistance can indicate the relative degree of degradation, although due to the irregular nature of each EBP no estimate of resistivity could be obtained from such data. Figure 8 shows the metallic-pad and EBP layout for the S-type cells.

2 cm X 6 cm Silicon Solar Cells with Various Thickness Coversheets

The LD-type cells were bonded to the experiment faceplate again using Dow-Corning adhesive 93-500. Cell electrical connections to terminal posts were made via Ti:Pd:Ag contacts to silver (Ag) mesh busbars which were mostly encapsulated in the 93-500 RTV silicone adhesive, except for those areas close to the terminal posts where the mesh was cut and twisted to make a connecting "wire" for soldering to the terminal itself. Coversheets of various thicknesses were bonded to the cells using 93-500 adhesive, although in the case of two SCAs (LD-1 and LD-4) the coversheet was deleted to obtain the maximum level of environmental degradation possible (*i.e.* no ATOX protection of the contacts and no radiation protection from the coversheet). Two of the 40 mil (1.02 mm) thick coversheets on SCAs LD-11 and LD-14 did not have the UV blocking filter that was applied to the other LD-type cell coversheets. The UV filter geometry (*e.g.* multi-layer) and material is undefined and so too is the 50% transmission cut-on wavelength.

Figure 9 shows the cross-sectional geometry of the LD-type SCAs. These stacks were configured to allow electrical characterization of each cell. Pre-flight measurements of open circuit voltage (V_{OC}), short circuit current (I_{SC}), and maximum power (P_{MAX}) were made for AM0 conditions at an unspecified (although estimated at 25-28°C) temperature. Post-flight measurements of the same parameters were made by NASA GSFC personnel, again at an undefined temperature. Further post-flight complete electrical characterizations of the cells (including efficiency and fill factor) were made by Auburn University and NASA LeRC personnel (see pages 75-89).

METEOROID AND DEBRIS RESULTS

An optical scan of the surfaces of the solar cell coversheets was made to determine the number of meteoroid and debris (M&D) impact sites. The minimum diameter impact site recorded was 8μm although there is no guarantee that all sites of that size scale were located due to the high levels of particulate contamination. We are confident that virtually all sites greater than 20μm in diameter were located. Figure 10 is a scatter plot of the M&D impact sites located. A total of 397 sites larger than 8μm were located on a total surface area of 260 cm^2, excluding SCAs S-2, S-3, LD-1, and LD-4 SCAs S-2 and S-3 were excluded from this number on the grounds that they exhibited a significant number of impact craters clustered together, 222 and 66, respectively, representing either a fragmented particle impact or a secondary ejecta crater field produced by a primary impact on the tray wall close by. SCAs LD-1 and LD-4 were uncovered cells and thus the M&D impacts occur in silicon.

Typical hypervelocity impact damage in glass coversheets comprised a circular inner crater with a peripheral spall zone extending out typically 2-3 crater diameters and as much as 6 crater diameters (see figures 11a&b). Where possible the inner (crater) diameter, D_C, and the outer (spall zone) diameter, D_S, were measured (see figure 12 for definitions). Frequently, the inner crater was undefined, being ejected during the impact process. This phenomena is indicative of higher velocities, over 4-6 km/s (refs 12-15). Figure 13 shows the cumulative fluence distribution as a function of impact site (spall zone) diameter for all sites on glass coversheet substrates. Due to the partial-shielding geometry it was instructuve to determine whether the 3" recessed location of the experiment contributed to a non-uniformity in the M&D flux across the surface of the test plate. The data were broken out as a function of row number and normalized to the exposure area of ROW-3 (60 cm^2) to account for the differences in exposure area in each row (*i.e.* there are different numbers of SCAs in each row). Figures 14 and 15 show the cumulative fluence distributions of crater diameter and spall zone diameter for all rows. Also, impact site data were binned according to ROW number for the coversheet impacts and normalized for exposure area (see figure 16). The partially-shielded row, ROW-5, contained 60 impact sites whereas the other four rows contained, on average, 96 sites (SD = 4.4), confirming the hypothesis that relatively more of the M&D particles appear to come from the RAM direction for an orbiting spacecraft. The 3" tray wall provided such shielding as to reduce the number of M&D impacts on average by ~40%.

Where the inner crater diameter was reasonably well-defined a measurement was recorded. The ratio of spallation diameter to crater diameter was computed for each site, numbering 189, and was then binned. This ratio is a function of impact velocity with faster impacts generating higher ratios of spall diameter to crater diameter. A number distribution for such ratios was plotted (see figure 17), indicating a median ratio of 2 to 2.25 and a maximum ratio of almost 10. Future work could relate the spall-crater ratio to impact velocity producing an estimate of the impact velocity distribution for the specific spacecraft surface. All that can be said, at present, is that the spall-crater ratio distribution exhibits a reassuring qualitative similarity with the NASA SP-8013 meteoroid velocity distribution.

Since cells LD-1 and LD-4 were uncovered, and the impact response of silicon is substantially different with respect to coversheet glass, the data from these cells were analyzed separately. The cumulative fluence distribution for cells LD-1 and LD-4 is shown in figure 18. In particular, the impact sites in silicon do not exhibit the inner crater/outer spall zone geometry, rather they show merely spalled out pits (see figure 19). Therefore, site-to-site diameter correlations should not be made between impact sites on silicon and glass since for a given particle diameter and impact velocity the resultant crater diameter will be larger for silicon with respect to glass.

Since M&D flux increases with decreasing particle diameter the LD-1 and LD-4 cells should exhibit more detectable impact sites, which is the case. The partially shielded LD-1 has 25 sites and LD-4 has 27 sites, whereas LD-7, LD-10, and LD-13 have 19, 15, and 20 sites, respectively. All of the 52 detected impact sites in the silicon solar cells are sufficiently deep to penetrate the depletion layer (junction) which in such cells is typically no more than 3-5 μm from the upper surface of the cell, including the anti-reflection coating. It is possible that the presence of such penetrations has shunted the cell significantly, contributing to the radiation and ATOX erosion-induced degradation of the cell performance.

For completeness, we executed a further photographic survey of the SCAs. Figures 20-22 show typical M&D impact induced damage phenomena. Figure 20 shows the major impact site (1.74mm dia.) on SCA S-10 showing the maximum extent of damage that can be expected from the M&D environment short of total perforation of the spacecraft structure. The brittle nature of the coversheet and the solar cell along with the multi-layer nature of the SCA induces significant peripheral fracture, extending out to distance of at least 1cm. Note that the impact has "punched through" to the epoxy board faceplate and as such could have resulted in a cell short circuit on a real solar array. Figure 21 shows a cluster of impact sites on SCA S-3, possibly attributable to the ejection of particles from a primary impact site on the experiment tray wall close by. Figure 22 shows ejecta spray material on the surface of SCA S-4 generated by an impact that occurred on the edge of terminal post #3 of SCA S-5. The incoming particle was fragmented, melted, and possibly partially vaporized and the fragmentation products impinged across the surface of SCA S-4. Note the way in which the EBP has shielded part of the coversheet surface from ejecta contamination.

A survey of all impact sites was made to determine how many coversheet penetration events occurred during the mission. Only two (2) such sites, both on the S-type cells, were categorically determined for the various thickness coversheets in this experiment. As a result, the effect of coversheet penetration on cell electrical performance could not be determined. There were no such events on the LD-type cells which did have the required electrical connections for the solar cells.

It appears that the M&D impact damage present in this experiment was not sufficient to cause significant damage to the solar cells themselves due to the presence to the coversheets. However, the majority of coversheet thicknesses used in this experiment are thicker than those typically used in most LEO solar arrays, *e.g.* EURECA and HST both used 150 μm thick coversheets

CONDUCTIVE MATERIALS RESULTS

Coversheet Conductive Coating Electrical Resistivity

The S-type cell assemblies were constructed to allow measurements of the solar cell coversheet coating electrical resistance. Pre-flight measurements of all combinations of pad-to-pad resistance (1-2, 1-3, 1-4, 2-3, 3-4) for each cell were made by NASA GSFC personnel. Post-flight measurements were made by NASA GSFC personnel (23-30 June 1992) and by Auburn University personnel (28 July 1993). Derived statistical data over all 28 S-type cells is presented in Table 1, below.

	pre-FLT-GSFC [kΩ]	post-FLT-GSFC [kΩ]	post-FLT-AU [kΩ]
MIN	3.2	4.1	4.1
MAX	9.6	35.2	32.3
Mean	5.1	11.4	11.0
SD	1.8	6.6	6.0
Std Error	0.3	1.3	1.2

Table 1. *Statistical resistance data for 28 S-type silicon solar cell assemblies with indium oxide (In_2O_3) conductive coatings on the front of the fused silica (SiO_2) coversheet.*

This first-cut analysis shows that the mean value of the conductive coating resistance increased by over 100% across the whole sample. Further analysis revealed that the increases in resistance are not similar for all cells. Two aspects of the data require explanation. Firstly, the row containing cells S-1 to S-6, *i.e.* the row nearest the experiment tray wall which was partially-shielded from the ATOX RAM flux exhibited significantly less degradation than those cells fully-exposed to the RAM flux (see figure 23). Clearly, the different ATOX fluences over the exposure period for the different locations imply that the indium oxide coating is subject to degradation by the ATOX environment. Further analysis of the data, confirming that coating degradation rather than pad degradation is the root cause of the resistance changes, is presented below.

Cell S-10 was a particularly interesting cell since it was impacted by a large meteoroid or space debris particle which penetrated the cell assembly completely exposing the epoxy substrate (figure 20). This impact site, approximately 1.2mm in diamater was surrounded by peripheral cracking of the coversheet out to a distance of ~1.5 cm. This cracking, induced by impact-induced shock waves interacting with the coversheet free surface, caused the destruction of PAD #4 and isolated electrically PAD #3. Figure 24 shows a schematic of this cell front surface, indicating the cracking effects on electrical resistance across the surface of the coversheet. During the measurement of these point-to-point resistances another phenomena became apparent. For point-to-point measurements indicating very high resistance (>100 kΩ) or open circuit behavior, application of pressure on the ohmmeter probes could result in intermittent closed circuit behavior with resistances measured in the 5-20 kΩ regime. Clearly, the conductive paths can be mechanically restored which leads to the possibility of variations in impact damaged coversheet point-to-point resistances under thermal cycling, where the expansion and/or contraction of the cracked coversheet elements can make or break electrical continuity across the surface.

Cell S-18 showed anomalously large increases (5.5 to 8 times) in surface coating resistance (see figure 23). There is no general difference in appearance for S-18 with respect to the other cells. The level of particulate contamination is similar and there is no significant surface cracking. Conversely, the surrounding cells, S-12, S-13, S-19, and S-24, do not exhibit the same large increases in resistance, and so the S-18 cell increases can only be explained as a statistical maximum. The resistance data were reviewed to determine whether the magnitudes of the pre-flight pad-to-pad resistance measurements for S-18 were significantly different from those of S-12, S-13, S-19, and S-24. No discrepancy was found, indicating that the pad deposition process was not compromised for cell S-18.

Further statistical analyses were made to determine whether the degree of resistance increase correlated with the magnitudes of the pre-flight pad-to-pad resistance paths. The data were separated into a ROW-5 data set, i.e. the partially-shielded row, and an all other rows (1-4) data set. Mean and standard deviation parameters were computed for each set as shown in Table 2 below.

	$\langle R_{PP} \rangle$[kΩ]	σ_{PP} [kΩ]	$\langle R_{post}/R_{pre} \rangle$	$\sigma_{R_{post}/R_{pre}}$
ROW-5	6.39	1.41	1.09	0.23
ROWS 1-4	4.59	2.41	2.75	1.12

Table 2. *Computed statistical parameters for surface resistance data.* $\langle R_{PP} \rangle$ *= mean pad-to-pad resistance;* σ_{PP} *= pad-to-pad resistance standard deviation;* $\langle R_{post}/R_{pre} \rangle$ *= mean of post-flight-to-pre-flight resistance ratios;* $\sigma_{R_{post}/R_{pre}}$ *= standard deviation of post-flight-to-pre-flight resistance ratios.*

Since there were outlier points in the rows 1-4 data set, all points which exhibited a 3σ variation with respect to the mean were discarded. This was not the case for the ROW-5 data set. A correlation of $\langle R_{PP} \rangle$ versus $\langle R_{post}/R_{pre} \rangle$ was attempted for both data sets. For ROW-5 there was effectively no correlation between the two variables, the correlation coefficient being C_R = -0.064. For rows 1-4, *i.e.* the fully-exposed rows with respect to the ATOX RAM flux, the correlation coefficient was C_R = 0.748, indicating that the degree of resistance increase correlates with the magnitude of the initial resistance. If the pad-to-pad resistance is dominated by the pad-to-surface interface resistance then there would be little change in the resistance since the interface would be protected from ATOX erosion effects. Alternatively, if the pad-to-pad resistance is dominated by the surface coating resistance, which is assumed to be thicker for lower initial resistance values since resistance is inversely proportional to the cross-sectional area of the resistance path, and that the coating is degraded to a constant depth for all ATOX exposed surfaces, then the thicker coatings (lower resistance) would be expected to suffer relatively less degradation than the thinner coatings (higher resistance). This appears to be the case here.

EBP Conductive Bond Materials

Each S-type cell has four EBPs attached to the coversheet front surface. Measurements of terminal-to-pad resistance for each of the EBPs was made to each of the two nearest pads. Figure 25 shows the pre-flight resistance for all terminal-to-pad combinations for all cells. Estimated EBP resistance is computed by correcting for the surface coating resistance between the two pads adjacent to the EBP. Figure 8 indicates the pad and EBP identification scheme. A simple resistive network, as shown in figure 26, can be envisaged to exist for the terminal to pad resistance paths. The EBP resistance, $R_{EBP-\#}$, is computed using the following equations:

$$R_{EBP-1} = \frac{R_{TP-11} + R_{TP-12} - R_{PP-12}}{2}$$

$$R_{EBP-2} = \frac{R_{TP-22} + R_{TP-23} - R_{PP-23}}{2}$$

$$R_{EBP-3} = \frac{R_{TP-33} + R_{TP-34} - R_{PP-34}}{2}$$

$$R_{EBP-4} = \frac{R_{TP-44} + R_{TP-41} - R_{PP-41}}{2}$$

where $R_{TP\text{-}\#\#}$ = terminal-to-pad resistance
$R_{PP\text{-}\#\#}$ = pad-to-pad resistance

The statistical data for the various bond types, pre-flight, are shown in table 3, below. It is apparent from the pre-flight data that SOLDER #3 has the lowest resistivity assuming approximately similar EBP dimensions, followed by SOLDER #1, EPON815, Eccobond 56C w/10% alcohol, Eccobond 56CH w/10% toluene, and Eccobond 56C w/10% toluene. Also, the solder-based bonds were the most reproducible, having the lowest value of $SD_n/\langle R \rangle$. Post-flight measurements of terminal-to-pad resistances were made by NASA GSFC personnel. Corrections for changes in surface coating resistance were made and the post-flight EBP resistances were computed, resulting in the statistical data shown in table 4. The NASA GSFC post-flight data indicates that the adhesive-based bonds suffered a decrease in resistivity on

bond-composition-plating	<R> [kΩ]	SD_n	SD_n/<R>
Ecc56C-10%TOL-unPL	64±5	24.6	0.38
Ecc56C-10%ALC-unPL	46±4	18.5	0.40
Ecc56CH-10%TOL-unPL	51±4	24.0	0.47
EPON815-SnPL	20±4	15.4	0.75
SOLDR#1-50%In50%Sn-SnPL	0.28±0.01	0.05	0.18
SOLDR#3-90%In10%Sn-SnPL	0.21±0.01	0.05	0.24

Table 3. *Pre-flight EBP resistance data. <R> is the bond resistance averaged across all cells. SD_n is the standard deviation in the data. The variable SDn/<R> is a relative measure of the spread in the data about the mean value of resistance, indicating that the SOLDER #1 and #3 bonds were the most reproducible and the EPON815 were the least reproducible. Note too that the resistance is dependent on undefined parameters such as bond length-area ratio and surface cleanliness.*

average, whereas the solder-based bonds exhibited an increase in resistivity. One can speculate that a combination of bond outgassing and thermal cycling may account for this phenomenon. It is possible that outgassing decreases the resistivity in the bulk of the adhesive bonds, but obviously does not affect the resistivity in the bulk of the solder bonds, whereas thermal cycling causes greater stresses at the coversheet-EBP interface for the solder bonds than for the adhesive-based EBPs due to the relative mis-match between thermal expansion coefficients for the solder-glass combinations and the adhesive-glass combinations. The ratio of average post-flight EBP resistance to average pre-flight EBP resistance was plotted for each

bond-composition-plating	<R> [kΩ]	$<R_{post}>/<R_{pre}>$	SD_n	SD_n/<R>
Ecc56C-10%TOL-unPL	3.2±0.6	0.05±0.01	2.7	0.84
Ecc56C-10%ALC-unPL	5±1	0.11±0.03	4.6	0.92
Ecc56CH-10%TOL-unPL	3.2±0.6	0.06±0.02	2.4	0.75
EPON815-SnPL	2.6±0.5	0.13±0.05	1.8	0.69
SOLDR#1-50%In50%Sn-SnPL	0.56±0.04	2.00±0.21	0.21	0.38
SOLDR#3-90%In10%Sn-SnPL	0.36±0.04	1.71±0.27	0.16	0.44

Table 4. *Post-flight EBP resistance data. as measured by NASA GSFC personnel (June 1992). <R> is the bond resistance averaged across all cells. SD_n is the standard deviation in the data. The variable SD_n/<R> is a relative measure of the spread in the data about the mean value of resistance. This data excludes all open circuit terminal-to-pad combinations.*

cell (see figure 27). As a result there appears to be no difference in the ratio as a function of cell location, *i.e.* the EBP resistance ratios for cells S-1 through S-6, those partially-shielded from the ATOX RAM flux, are similar to those for cells in the other 4 rows. This finding is in accordance with the surface coating resistance variations, which did vary as a function of ATOX RAM flux exposure, since EBP resistance changes are due to bulk material changes (*i.e.* not dependent on exposed surface interactions) and also most probably EBP-coversheet interface changes due mainly to thermal cycling.

Further measurements of terminal-to-pad resistance were made by Auburn University personnel. The ratio of post-flight to pre-flight resistance are plotted in figure 28 for each S-type SCA. The most significant feature of this data is the fact that all of the non-solder EBPs show significant increases in terminal-to-pad resistance. In most cases the post-flight to pre-flight ratio increases from the range 0.1-1 up to the range 5,000-200,000. All of the solder based EBPs showed no signs of degradation other than for cell S-12. During the period between the NASA GSFC measurements and the Auburn University measurements, a period of one year, the test plate was not maintained in a controlled environment. It can only be assumed that the non-solder EBPs suffered significant degradation as a result of terrestrial environment stressors such as humidity fluctuations and/or handling. These findings have implications for post-retrieval operations for spacecraft designed for re-flight.

SOLAR CELL ELECTRICAL CHARACTERISTICS

Current-Voltage Characteristics

Pre-flight measurements of LD-type cell performance parameters, including open circuit voltage (V_{OC}), short circuit current (I_{SC}), and maximum power (P_{MAX}), but excluding cell temperature were made by NASA GSFC personnel. Similar post-flight measurements were also made. Further post-flight measurements were made by Auburn University and NASA LeRC personnel, determining the complete current-voltage (I-V) curve for each cell at AM0 and 25°C. Table 5 shows the NASA GSFC pre- and post-flight data. Data obtained during the course of this project at NASA LeRC (see pages 75-89) confirm the NASA GSFC post-flight data to within ±7mA for I_{SC}, with one cell (LD-14) showing a -10mA difference, within ±5mV for V_{OC}, with no outliers, and within ±5mW for P_{MAX}. The post-flight measurements by GSFC personnel were made in 1990, whereas the more recent Auburn University/NASA LeRC measurements were made in July 1994. There are no discernible changes in electrical characteristics between these two post-flight data sets for any cell, suggesting that radiation damage annealing effects are insignificant over this time period and that cell damage due to space exposure is irreversible.

cell ID	cover		I_{SC}	frac	V_{OC}	frac	P_{MAX}	frac	FF	ΔFF
LD-1	NO	PRE	495		580		215		74.9	
		POST	469	0.95	454	0.78	112	0.52	52.6	-22.3
LD-2	12 mil w/f	PRE	507		595		218		72.3	
		POST	509	1.00	580	0.97	211	0.97	71.5	-0.8
LD-3	6 mil w/f	PRE	503		591		220		74.0	
		POST	506	1.01	578	0.98	214	0.97	73.2	-0.8
LD-4	NO	PRE	497		592		221		75.1	
		POST	465	0.94	452	0.76	139	0.63	66.1	-9.0
LD-5	40 mil w/f	PRE	511		594		220		72.5	
		POST	507	0.99	578	0.97	211	0.96	72.0	-0.5
LD-6	6 mil w/f	PRE	507		587		225		75.6	
		POST	507	1.00	578	0.98	220	0.98	75.1	-0.5
LD-7	6 mil w/f	PRE	508		577		189		64.5	
		POST	511	1.01	571	0.99	188	0.99	64.4	-0.1
LD-8	40 mil w/f	PRE	516		586		225		74.4	
		POST	510	0.99	574	0.98	218	0.97	74.5	+0.1
LD-9	12 mil w/f	PRE	508		577		200		68.2	
		POST	502	0.99	569	0.99	197	0.99	69.0	+1.1
LD-10	6 mil w/f	PRE	505		584		223		75.6	
		POST	505	1.00	573	0.98	218	0.98	75.3	-0.3
LD-11	40 mil wo/f	PRE	519		593		233		75.7	
		POST	514	1.01	582	0.98	227	0.97	75.9	+0.2
LD-12	40 mil w/f	PRE	521		591		231		75.0	
		POST	514	0.99	579	0.98	223	0.97	74.9	-0.1
LD-13	12 mil w/f	PRE	510		585		227		76.1	
		POST	505	0.99	572	0.98	219	0.96	75.8	-0.3
LD-14	40 mil wo/f	PRE	521		591		231		75.0	
		POST	509	0.98	579	0.98	221	0.96	75.0	0.0
LD-15	40 mil w/f	PRE	521		584		229		75.3	
		POST	512	0.98	577	0.99	223	0.97	75.5	+0.3

Table 5. *Pre- and post-flight electrical characteristics (NASA GSFC data). Note w/f = with UV filter, wo/f = without UV filter, I_{SC} = short circuit current [milliamperes], V_{OC} = open circuit voltage [millivolts], P_{MAX} = maximum power [milliwatts].*

For completeness, we computed approximate I-V curves for the pre-flight data, using a three parameter equation and the three data points available for each cell, namely I_{SC}, V_{OC}, and P_{MAX}. A typical 5-parameter model for solar cell operation is;

$$I = I_{ph} - I_0\left\{\exp\left(\frac{e(V + IR_S)}{nkT}\right) - 1\right\} - \frac{V + IR_S}{R_{SH}}$$

where

I_{ph}	=	*photogenerated current*
I_0	=	*reverse bias saturation current*
n	=	*diode ideality factor*
R_S	=	*cell series resistance*
R_{SH}	=	*cell shunt resistance*
e	=	*electron charge*
k	=	*Boltzmann's constant*
T	=	*temperature*

Since there are only have three data for each cell and one, P_{MAX}, is the product $I_{MAX}V_{MAX}$ it was necessary to use a 3-parameter approximation. We found that the following equation provided a reasonable approximation across the whole range of cell voltages (0-V_{OC});

$$I = m_1 - m_2 \, \mathbf{exp}(m_3 V)$$

A system of four simultaneous equations in four unknowns is, therefore, constructed:

$$0 = m_1 - m_2 \, \mathbf{exp}(m_3 V_{OC})$$

$$I_{SC} = m_1 - m_2$$

$$P_{MAX} = I_{MAX} V_{MAX} = m_1 V_{MAX} - m_2 \, \mathbf{exp}(m_3 V_{MAX})$$

$$\left.\frac{dP}{dV}\right|_{V=V_{MAX}} = m_1 - m_2 \, \mathbf{exp}(m_3 V_{MAX}) - m_2 m_3 V_{MAX} \, \mathbf{exp}(m_3 V_{MAX}) = 0$$

This system of equations was solved for all fifteen cells using the iterative Levenberg-Marquardt method to solve for several constraints simultaneously (Mathcad® v3.1, Mathsoft, Inc.). The derived estimated I-V curves for pre-flight conditions are shown on pages 67-74. Two cells, LD-7 and LD-9 exhibit lower maximum power ratings with correspondingly lower fill factors, 64.5 and 68.2 respectively, than the other cells. Short circuit current and open circuit voltage are similar for all cells, the average values being 510±2 mA and 587±2 mV, respectively.

The post-flight data are characterized by discernible reductions in I_{SC} and P_{MAX} as a function of coversheet thickness with greater thickness causing greater reductions. These reductions may be attributed to radiation darkening of the coversheet bulk and the coversheet-cell adhesive layer. Figure 29 shows a plot of the power reduction curves, including maximum and minimum power reduction as a function of coversheet thickness. The adhesive layer thickness is undefined. The following function was fitted to the data to provide for engineering computations, giving the average reduction in maximum power $\langle \Pi_R \rangle$;

$$\langle \Pi_R \rangle = \frac{0.036}{1 + (t/7)^{-1.75}}$$

where Π_R = *fractional reduction in maximum power*
t = *thickness of coverslide [mil]*

The fractional reduction in maximum power is defined as;

$$\Pi_R = 1 - \frac{P_{EOL}}{P_{BOL}}$$

where P_{EOL} = *maximum power at end-of-life*
P_{BOL} = *maximum power at beginning-of-life*

For the maximum degree of degradation the function is:

$$\langle \Pi_{MAX} \rangle = \frac{0.044}{1+(t/4)^{-1.35}}$$

For the minimum degree of degradation the function is:

$$\langle \Pi_{MIN} \rangle = \frac{0.028}{1+(t/11.5)^{-2.30}}$$

Plots of post-flight to pre-flight ratios for I_{SC}, V_{OC} and P_{MAX}, excluding the uncovered cells LD-1 and LD-4 are shown in figures 30-32. Post-flight degradation values of I_{SC} correlate with coversheet thickness, with thicker coversheets showing greater reduction in I_{SC}. Note that some post-flight values of I_{SC} for 6 mil and 12 mil coversheets are greater than the measured pre-flight values. We attribute that to calibration errors in the data acquisition process since the exact pre-flight test parameters could not be recreated during the post-flight tests. Note, too, that the errors appear to be systematic since all 6 mil thick coversheets appear to produce an increase in I_{SC}, whereas one 12 mil coversheet produced an increase and no 40 mil coversheets did so (see figure 33). The presence of the UV blocking filter on the underside of two of the coversheets (LD-11 and LD-14) produced no discernible advantage with respect to post-flight I_{SC} reduction for the 40 mil coversheets. The uncovered cells, LD-1 and LD-4, showed minimal degradation in I_{SC}, the values being 95% and 94% of their pre-flight values, respectively. Due to the systematic test calibration errors, these values could be as low as 93% and 92%, respectively.

Post-flight values of V_{OC}, although degraded in all cases, show no firm correlation to coversheet thickness (see figure 34) and so no conclusion about the degradation mechanism can be advanced other than that degradation in V_{OC} does occur to approximately the same degree for coversheets in the thickness range 6 - 40 mil. The uncovered cells showed a strong degration in V_{OC}, the values being 78% and 76% of their pre-flight values, respectively. Again, the presence of the UV blocking filter produced no apparent advantage in mitigating cell degradation for V_{OC}.

Finally, a comparison of the characteristics of those cell assemblies which were partially shielded from the ATOX RAM flux, cells LD-1, LD-2, and LD-3, and those which were unshielded was made. Within the statistical limits of this experiment, *i.e.* only fifteen cells, there is no significant difference in the post-flight characteristics of partially shielded cell assemblies and unshielded cell assemblies. Therefore, no effects due to the differences in ATOX exposure are present in the data. All covered cells appeared to be protected to the same degree from the effects of ATOX erosion of materials. The uncovered cells suffered significant erosion of their front surface contacts (see figure 35) which most likely caused an increase in the cell assembly series resistance, degrading the cell I-V profiles in conjunction with radiation damage (see pages 75-78 and compare with pages 67 and 68).

CONCLUSIONS & RECOMMENDATIONS

As a result of the analysis of M&D damage and electrical characteristics, certain limited conclusions regarding space environmental effects on solar cell assemblies can be made.

1 For a 69 month exposure of a 260 cm^2 area with a 38° normal to the spacecraft RAM direction, there were only two (2) meteoroid or debris coversheet penetration events, one of which "punched" through to the epoxy matrix faceplate. This results in a flux rate of $13\pm9\ m^{-2}.yr^{-1}$ for an average coversheet thickness of 474 µm. Punch-through events have been implicated in solar cell short circuit failures (ref. 4), although data is scarce. A series of tests to determine the actual failure modes induced by M&D impacts as a function of cell protection (*i.e.* coversheet thickness), impact velocity and impactor diameter need to be executed to provide a quantifiable baseline.

2 Assuming crater depth, p, to be $(0.50\pm0.05)D_C$, where D_C is the crater diameter, a cumulative flux, F, distribution for coversheet penetration events per square meter per year as a function of coversheet thickness, f, measured in micrometers, has been developed, *i.e.*:

$$\log_{10}(F) = (4.82 \pm 0.06) - (1.38 \pm 0.01)\log_{10}(f)$$

The significance of coversheet penetration events for damage in the solar cell junction region, usually located no more than 5 µm from the upper surface of the cell, cannot be ascertained from this experiment since no coversheet penetration events occurred on the 13 LD-type cell with coversheets. However, research exists (ref. 6) suggesting that a cell shunt failure mode may exist that needs to be quantified.

3 The 397 M&D impact sites studied produced a total spall area of $0.14\pm0.06\ cm^2$ over the exposure area of 260 cm^2, resulting in no more than 0.05% erosion of the coversheet surfaces. The area erosion effect is negligible in terms of solar cell performance degradation. This was confirmed by the post-flight electrical performance data which showed that cell short circuit current was reduced by ~5-7%, attributable to coversheet radiation-induced darkening and solar cell radiation damage. Coversheet thickness did

affect the degree of maximum power reduction with the thinner 6 mil (152 μm) coversheets causing the least reduction and the thicker 40 mil ones causing the greatest reduction. Clearly, with no data for thinner coversheets we cannot determine where the radiation damage effect begins to cut-in. The degree of performance degradation across the 13 covered cells was minimal with P_{MAX} being reduced by no more than 4%. The UV blocking filters appeared to have no quantifiable effect within the limits of this data set.

4 The uncovered cells LD-1 and LD-4 showed significant reduction in maximum power, post-flight values being 52% and 63% of their pre-flight values, respectively, indicating significant radiation damage. The effect, if any, of M&D impact penetrations cannot be separated from the radiation damage effects. Also, front contact erosion by atomic oxygen may have contributed to I-V profile degradation by increasing series resistance.

5 Indium oxide conductive coatings on solar cell coversheets are subject to degradation by the ATOX environment. Partially-shielded cells in ROW-5 exhibited little increase in coating resistance (~9% on average), whereas the fully-exposed cells in ROWs 1-4 exhibited an increase of ~175%. A further degradation mode was found whereby large M&D impacts (*e.g.* impact on cell S-10) cause surface cracking, leading to electrical isolation of parts of the coversheet surface. Such isolation can be restored mechanically by applying pressure to isolated areas bringing them back into contact with their surrounds implying that thermal cycling may cause intermittent restoration of electrical continuity also. There are implications for differential charging/ discharging occurrences where isolated areas become charged, being discharged when electrical continuity is restored. Further work in this area should be conducted to quantify this effect.

6 The electrical bond pads showed various levels of resistance changes. Typically, the resistance of the adhesive-based bond pads decreased, most probably due to outgassing, whereas the resistance of the solder-based bond pads typically increased, indicating thermally-induced stresses occured at the coversheet-EBP interface due to a greater thermal expansion mismatch. Use of such techniques and materials to alleviate coversheet front surface charging is not recommended at their level of development indicated here due to their instability in the space environment.

7 The cluster events on SCAs S-2 and S-3 warrant some further investigation to determine their origin and size distribution characteristics. Removal of coversheets for electron microscopy studies would be useful to improve impact site measurements and to characterize any retained residue.

REFERENCES

1. Stein, B.A. (1993). "LDEF materials overview," *LDEF - 69 Months in Space: 2nd Post-Retrieval Symp.*, NASA CP-3194, III, pp741-789.

2. McDonnell, J.A.M. & Carey, W.C. (1984). "ECS solar cell tolerance to meteoroid hazard," Space Sciences Lab., Univ. of Kent Report (Canterbury, Kent, UK).

3. Bogus, K. *et al.* (1985) (with Claassens, C. & Lechte, H.). "Investigations and conclusions on the ECS solar array in-orbit power anomalies," *Proc. 18th IEEE Photovoltaic Specialists Conf.*, (Las Vegas, NV, USA), pp368-375.

4. Schneider, E. (1986). "Micrometeorite Impact on solar panels", *Proc. 5th Eur. Symp. Photovoltaic Generators in Space*, ESA SP-267, pp171-174.

5. Weishaupt, U. *et al.* (1986) (with Kuczera, H. & Rott, M.). "Micrometeorite exposure of solar arrays," *Proc. 5th Eur. Symp. Photovoltaic Generators in Space*, ESA SP-267, pp175-180.

6. Burgasov, M.P. & Nadiradzer, A.B. (1993). "Assessments of the solar cell degradation caused by space debris impact," *Proc. 3rd Eur. Space Power Conf.*, ESA WPP-054, 2, pp767-772.

7. Kinard WH & Martin GD (1991). "Long Duration Exposure Facility (LDEF) space environments overview," *LDEF - 69 Months in Space: 1st Post-Retrieval Symp.*, NASA CP-3194, I, pp49-60.

8. See, T.H. *et al.* (1990) (with Allbrooks, M.K., Atkinson, D.R., Simon, C.G. & Zolensky, M.E.). "Meteoroid and debris impact features documented on the Long Duration Exposure Facility: a preliminary report," NASA JSC 24608.

9. Mandeville, J-C. (1993). "Micrometeoroids and debris on LDEF," *LDEF - 69 Months in Space: 2nd Post-Retrieval Symp.*, NASA CP-3194, II, pp303-312.

10. See, T.H. *et al.* (1993). (with Mack, K.S., Warren, J.L., Zolensky, M.E. & Zook, H.A.) "Continued investigations of LDEF's frame and thermal blankets by the Meteoroid and Debris Spaecial Investigation Group," *LDEF - 69 Months in Space: 2nd Post-Retrieval Symp.*, NASA CP-3194, II, pp313-324.

11. Drolshagen, G. (1993). "Predicted and observed directional dependence of meteoroid/ debris impacts on LDEF thermal blankets," *LDEF - 69 Months in Space: 2nd Post-Retrieval Symp.*, NASA CP-3194, II, pp25-338.

12. Flaherty, R.E. (1969). "Impact characteristics in fused silica," *Proc. AIAA Hypervelocity Impact Conf.*, AIAA Paper No. 69-367.

13. Mandeville, J-C. (1972). "Profile and depth of microcraters formed in glass," *Earth Planet. Sci. Lett.*, **15**, pp110-112.

14. Mandeville, J-C. (1979). "Microcraters produced in brittle materials in the 1 to 20 km/s velocity range," *Proc. Comet Halley Micrometeoroid Hazard Workshop*, ESA SP-153, pp99-100.

15. Vedder, J.F. (1971). "Microcraters in glass and minerals," *Earth Planet. Sci. Lett.*, 11, pp291-296.

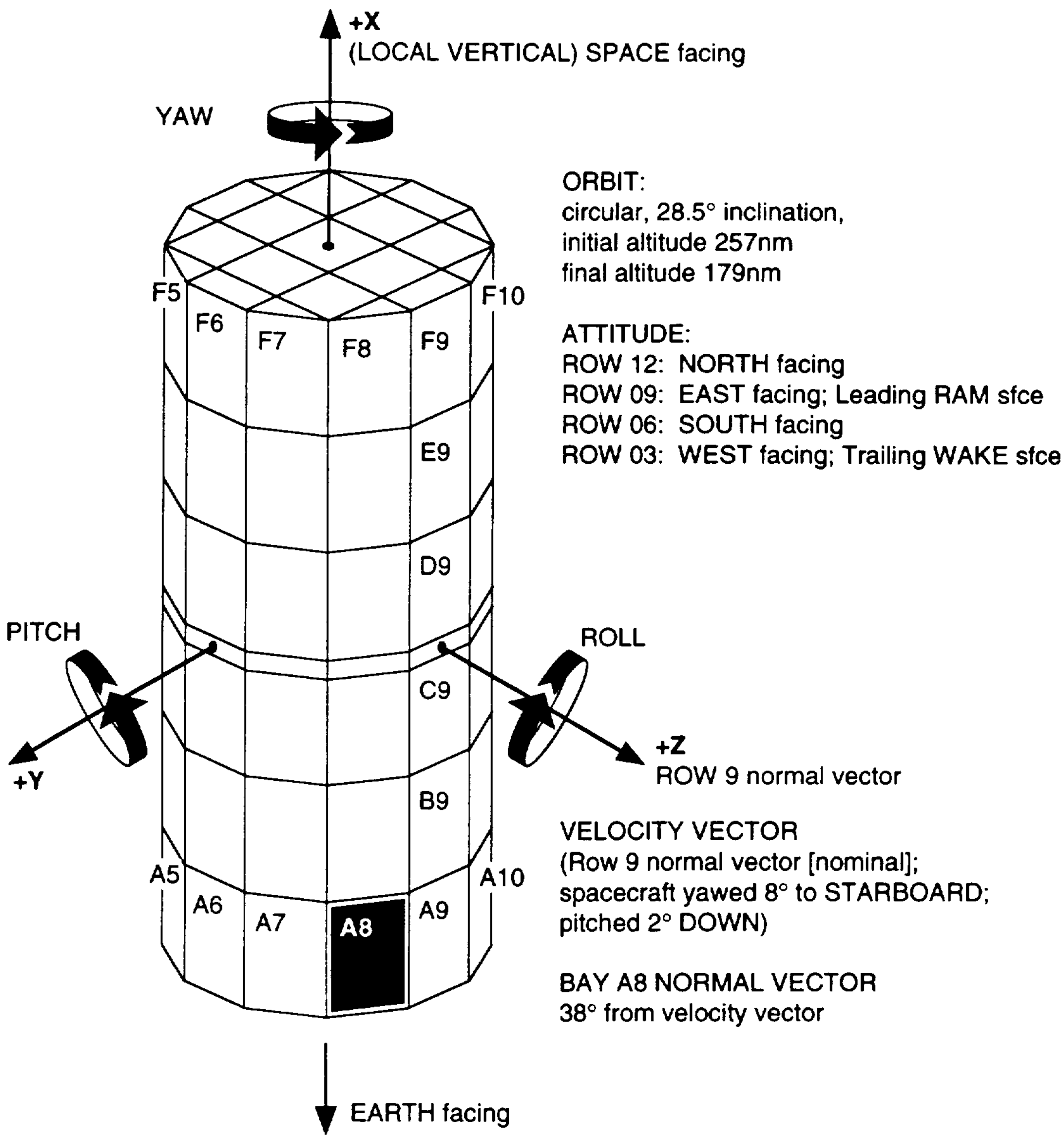

Figure 1. *LDEF orientation and location of experiment A0171 in Bay A8.*

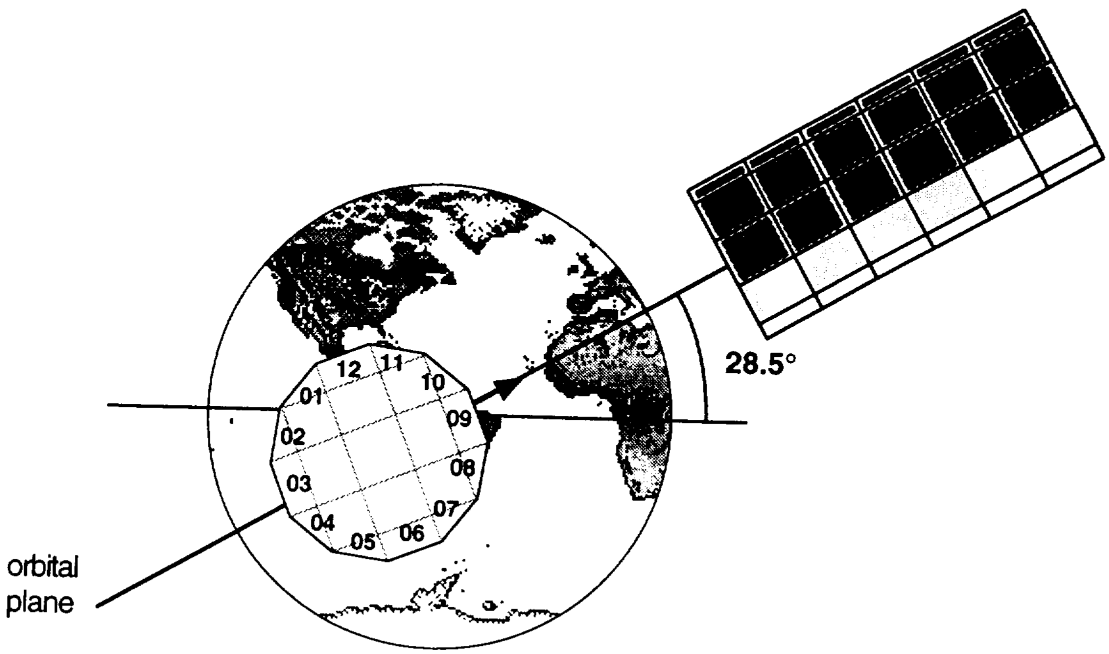

Figure 2. *LDEF flight orientation showing 28.5° orbital inclination, the relative location of the rows 01-12, and the 8° YAW to starboard. ROW 09 is "East-facing," ROW 03 is "West-facing," ROW 12 is "North-facing," and ROW 06 is "South-facing."*

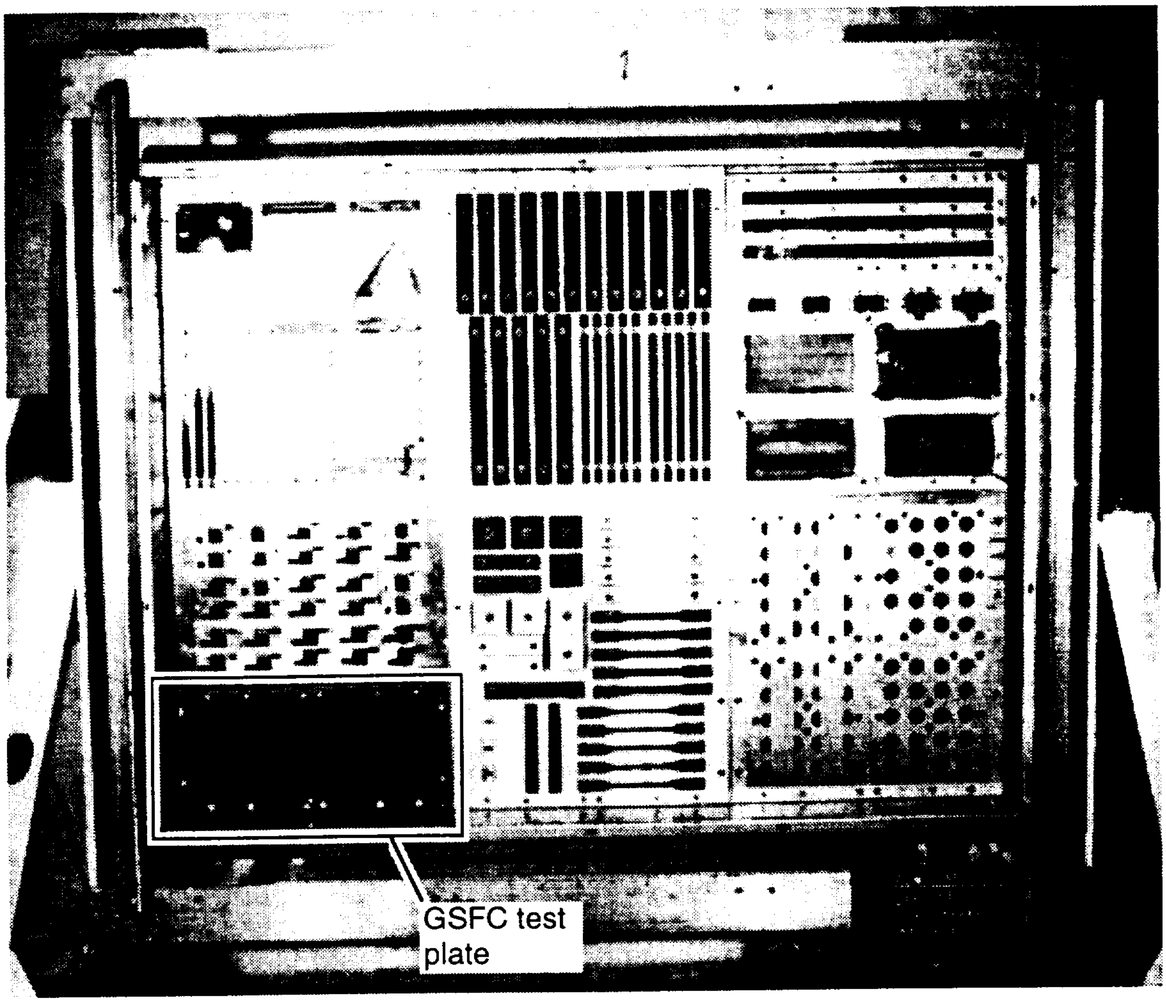

Figure 3. *Post de-integration view of the LDEF experiment A0171 tray, showing the location of the GSFC test plate (ref. 8).*

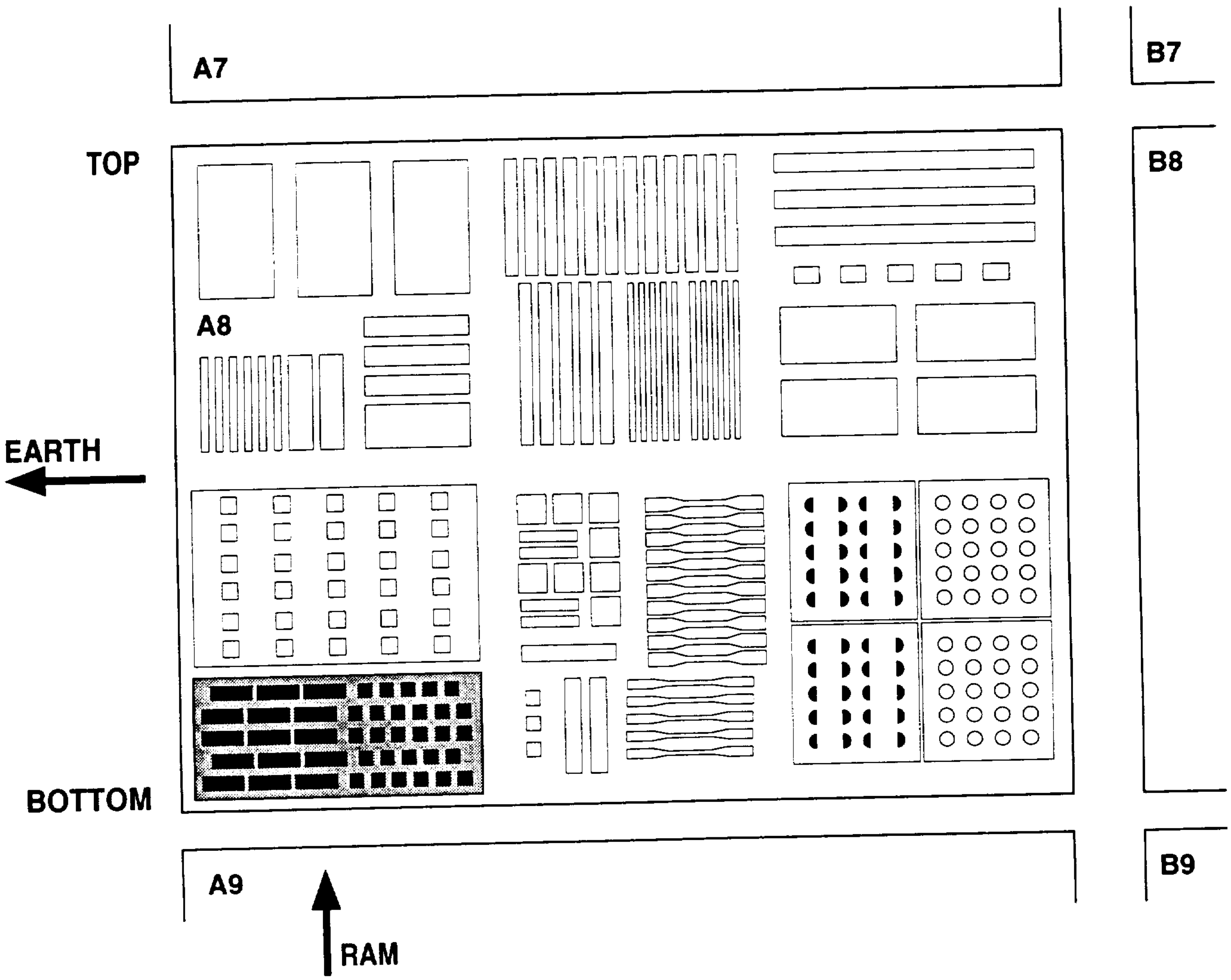

Figure 4. *Schematic of the A0171 tray (using the same protocol as the de-integration team), showing the relative locations of the GSFC test plate, other experiment trays, and the vehicle orientation parameters. Note that since the experiment was mounted in a 3" deep tray the GSFC test plate was partially shielded from the ATOX RAM flux vector.*

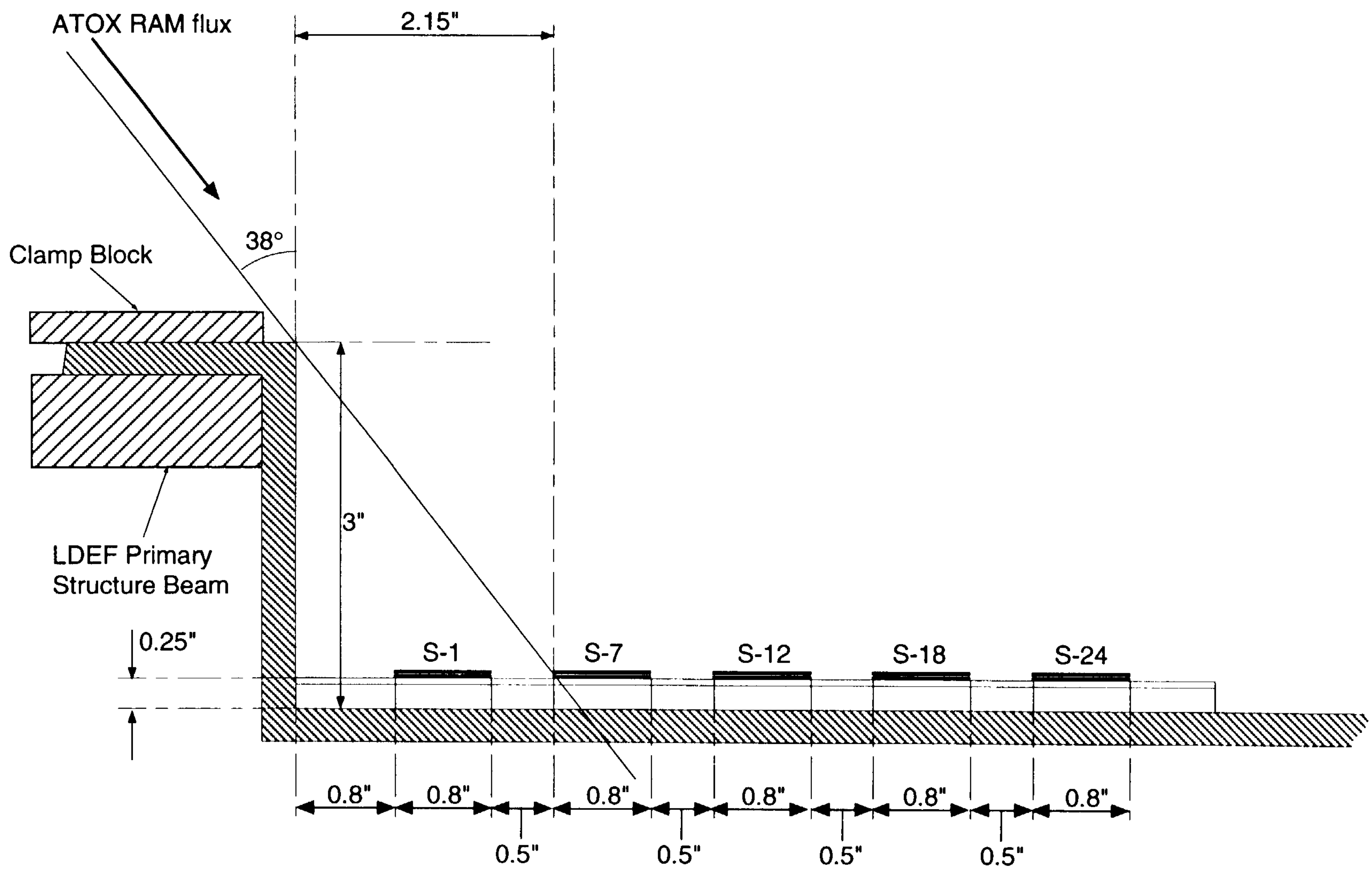

Figure 5. *Orientation and location of the GSFC test plate with respect to the ATOX RAM vector showing the degree of shielding. Effectively, cells in the row containing cell S-1 are shielded from the worst effects of the ATOX flux. M&D shielding effects should result from this type of geometry also.*

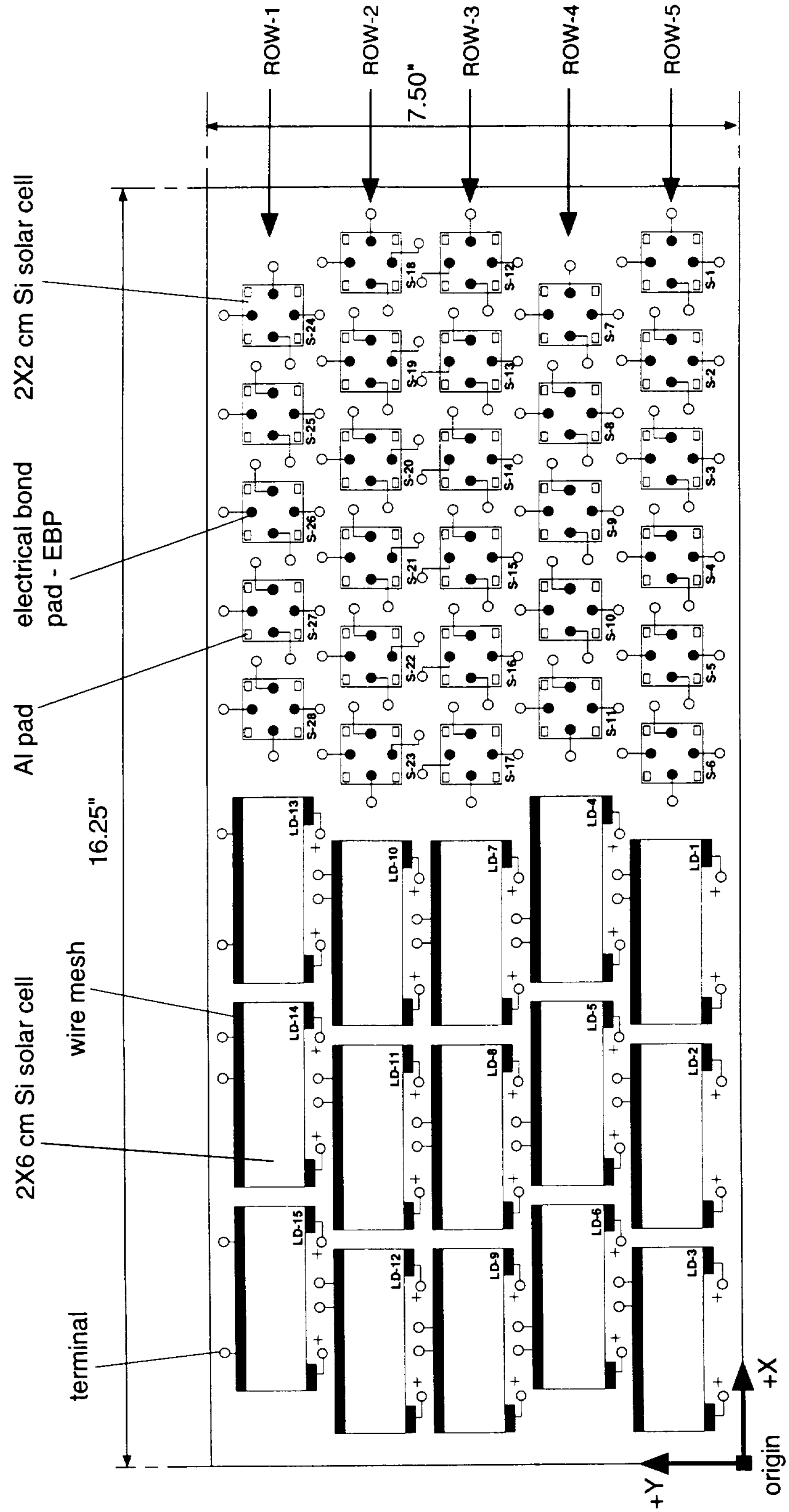

***Figure 6.** GSFC test plate layout, showing electrical connections and cell identification.*

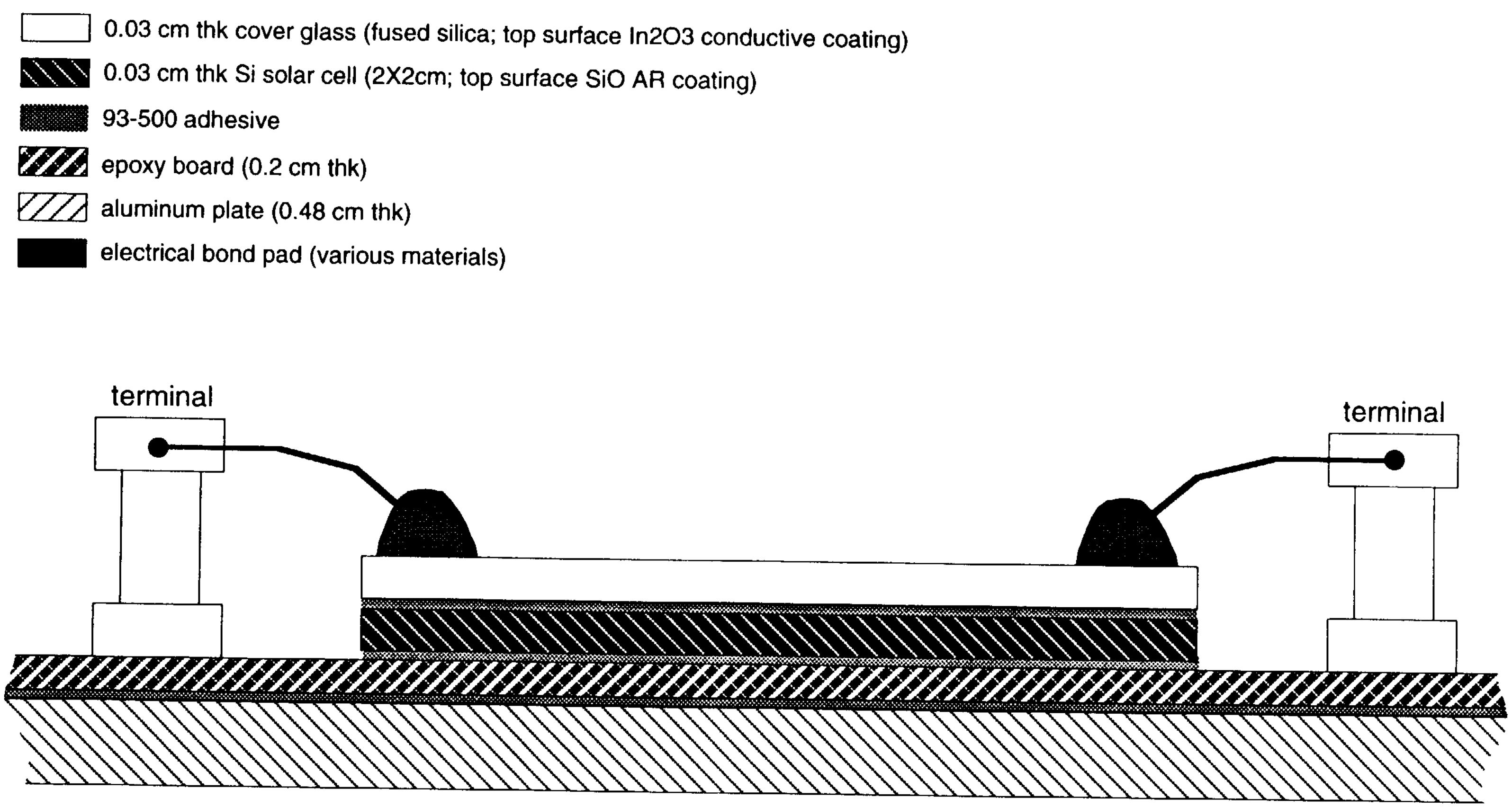

Figure 7. *S-type solar cell assembly (SCA) cross-section, showing electrical connections to terminals for characterization of electrical bond pad resistance.*

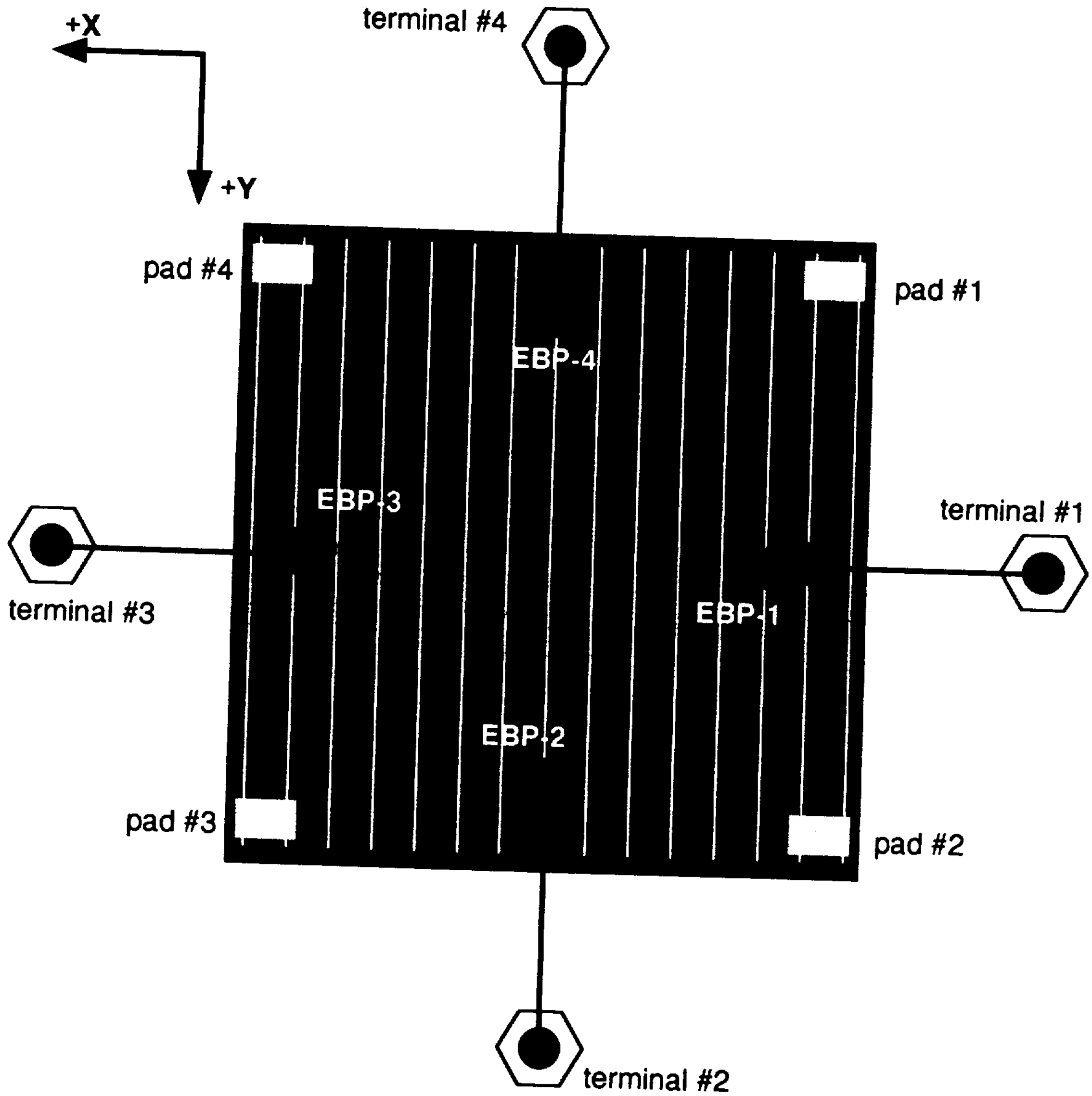

Figure 8. Electrical bond pad (EBP) and corner pad layout for S-type 2X2cm cells.

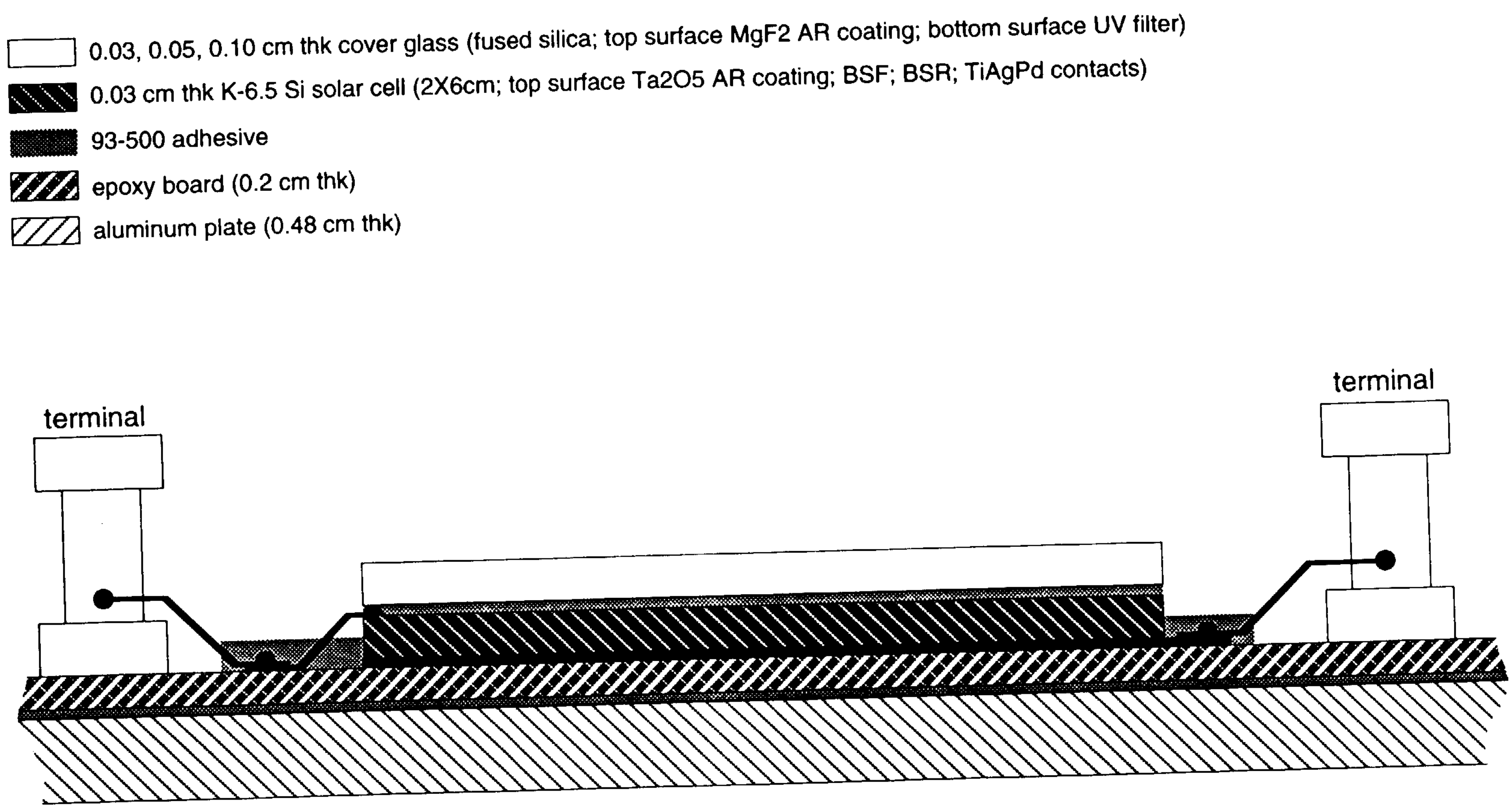

Figure 9. *LD-type solar cell assembly (SCA) cross-section, showing electrical connections to terminals for characterization of pre- and post-flight current-voltage performance.*

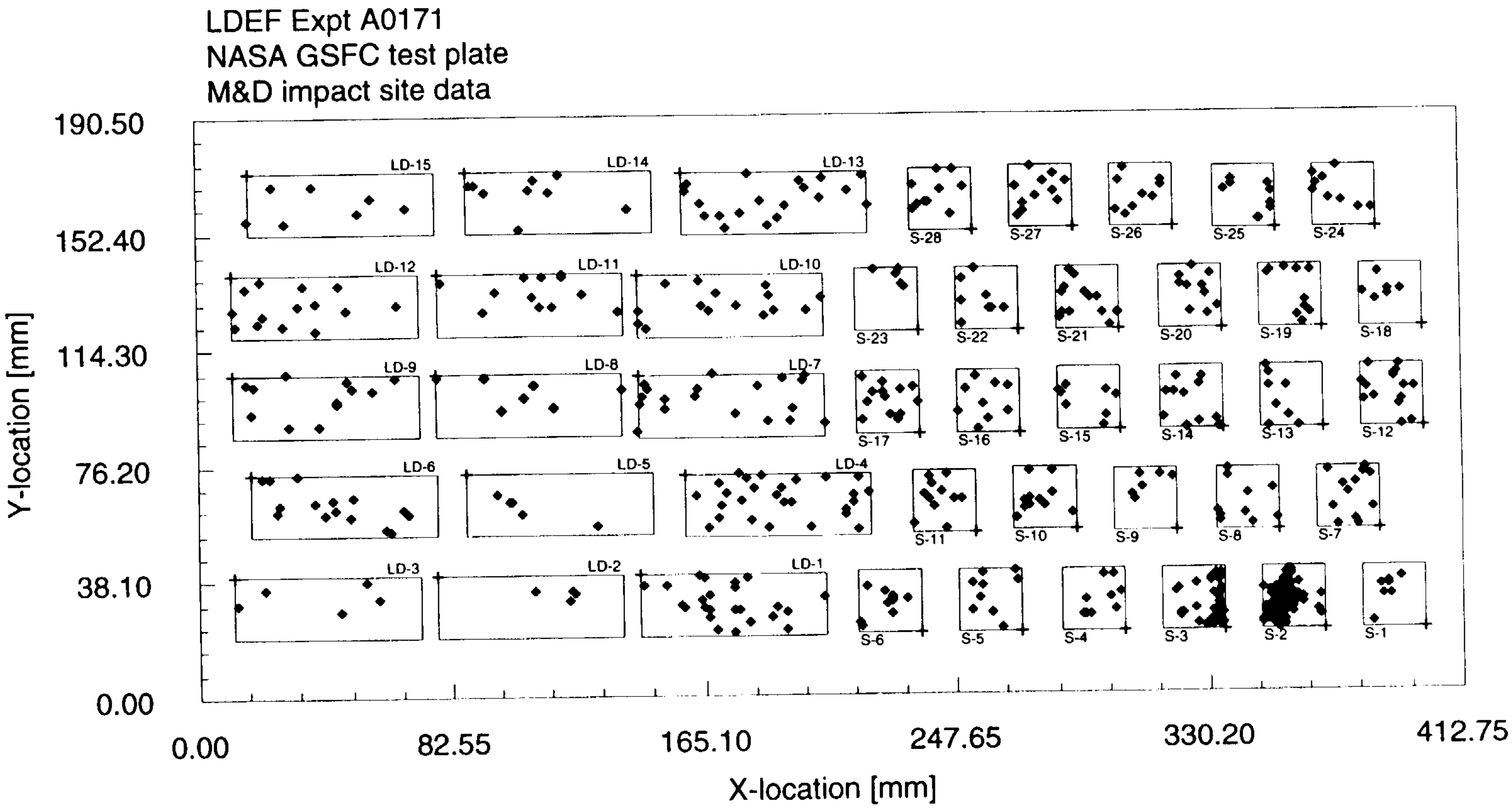

Figure 10. *Scatter plot of M&D impact sites greater than ~8 µm diameter on solar cell assemblies. Note the clusters of impacts on cells S-2 and S-3, indicating secondary sites generated by ejecta from an impact site on the tray wall close by. Cells LD-1 and LD-4 were uncovered, exposing silicon to the M&D environment. Impact sites on these cells will be larger than sites on the coversheet glass for a similar particle diameter and impact velocity.*

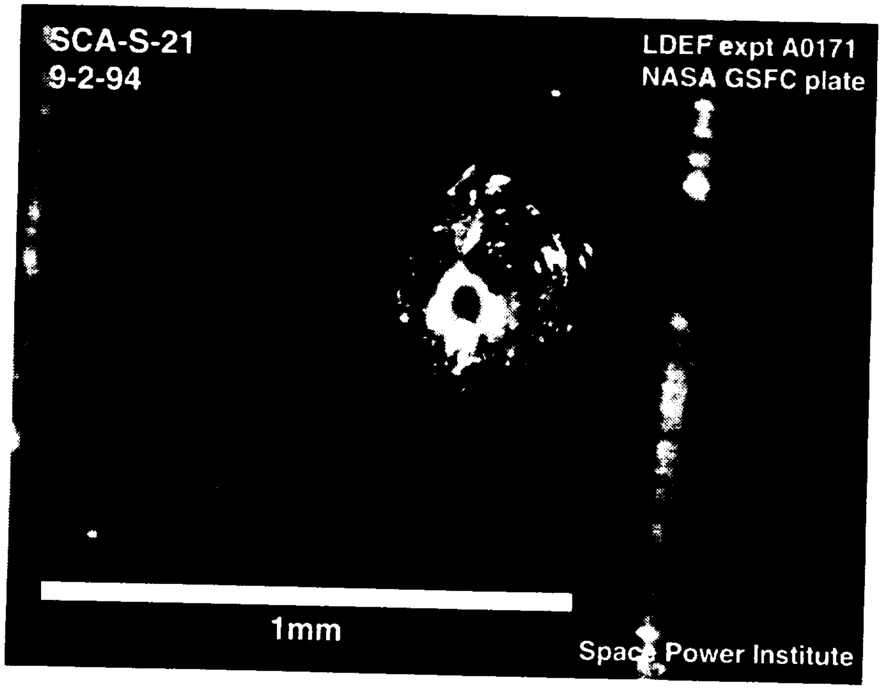

Figure 11a. *Photograph of a typical M&D impact site in the SCA coversheet material. Note the pronounced inner crater and extensive outer spallation zone with radial cracking.*

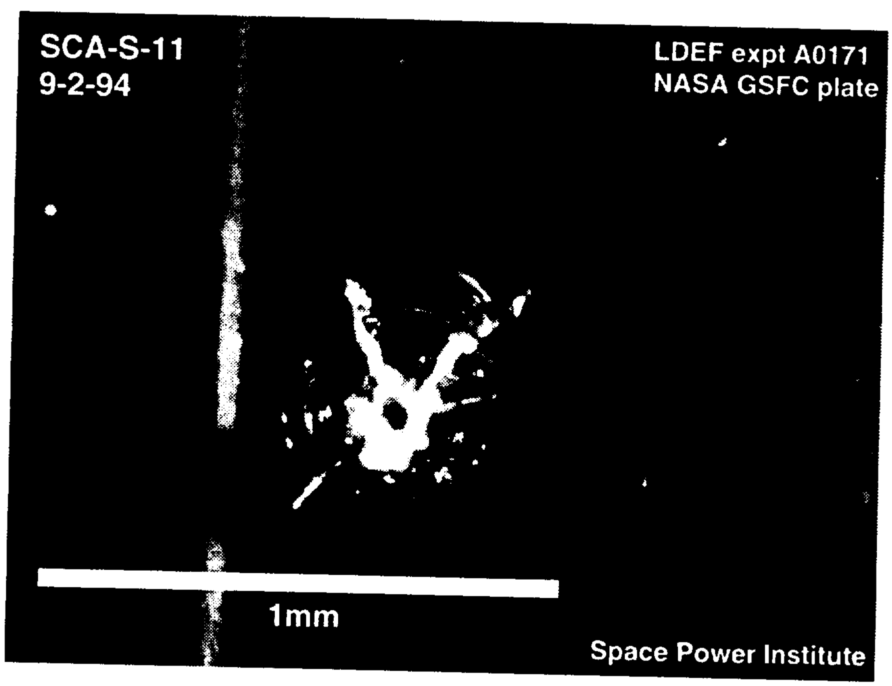

Figure 11b. *Photograph of a typical M&D impact site in the SCA coversheet material. Again, there is a pronounced inner crater and extensive outer spallation zone with radial cracking, but the degree of cracking is different from the previous figure, indicating a different impact velocity and/or impactor material.*

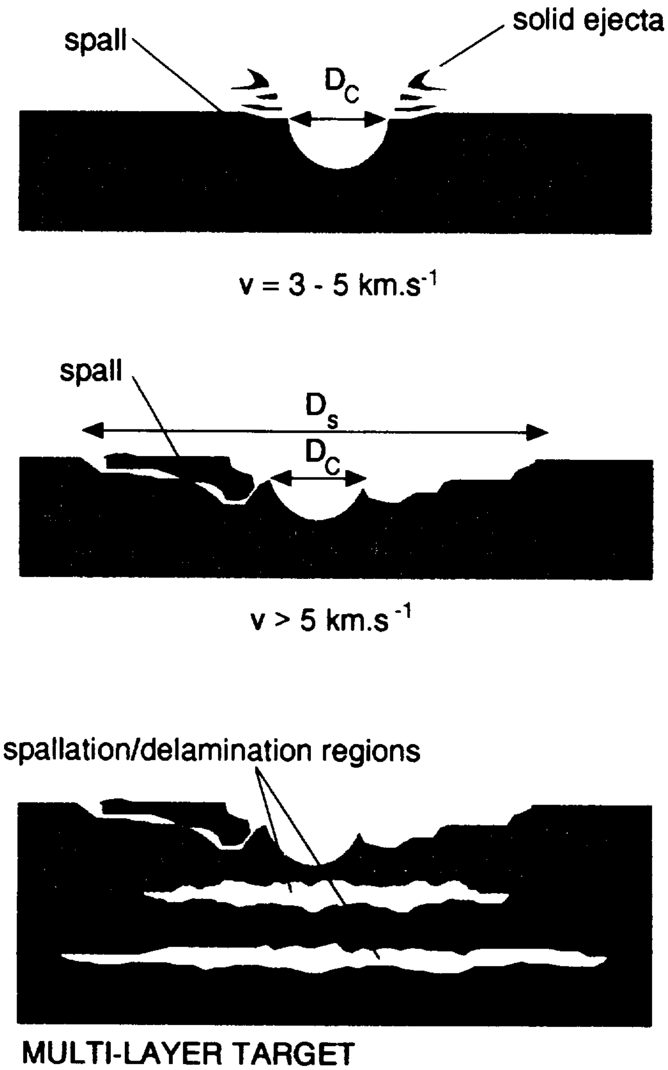

Figure 12. *Schematics of impact damage site cross-sections in brittle materials. D_s is the outer spall zone diameter; D_c is the inner crater diameter.*

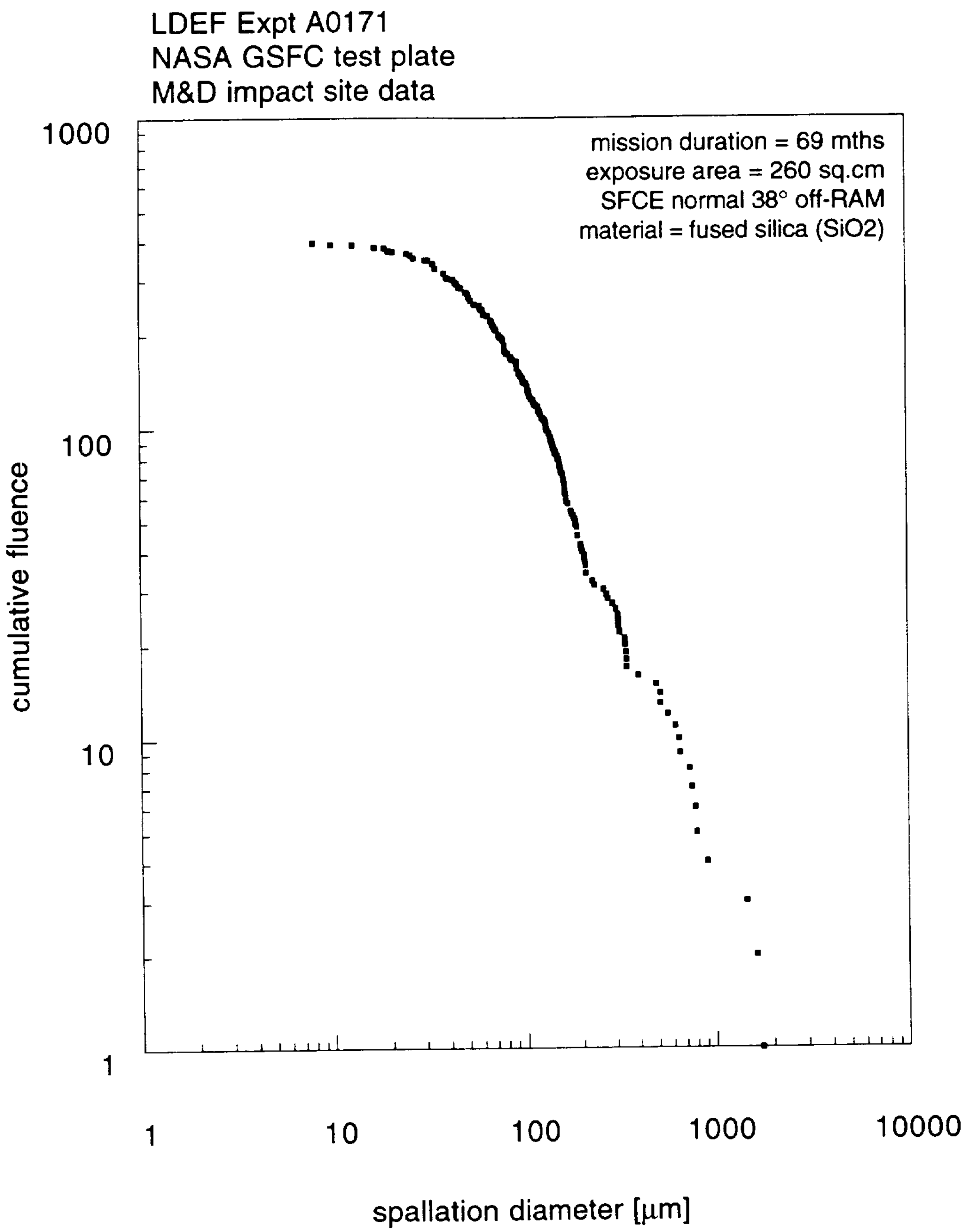

Figure 13. *Cumulative fluence distribution for all identified impact site spallation diameters on SCA fused silica coversheets.*

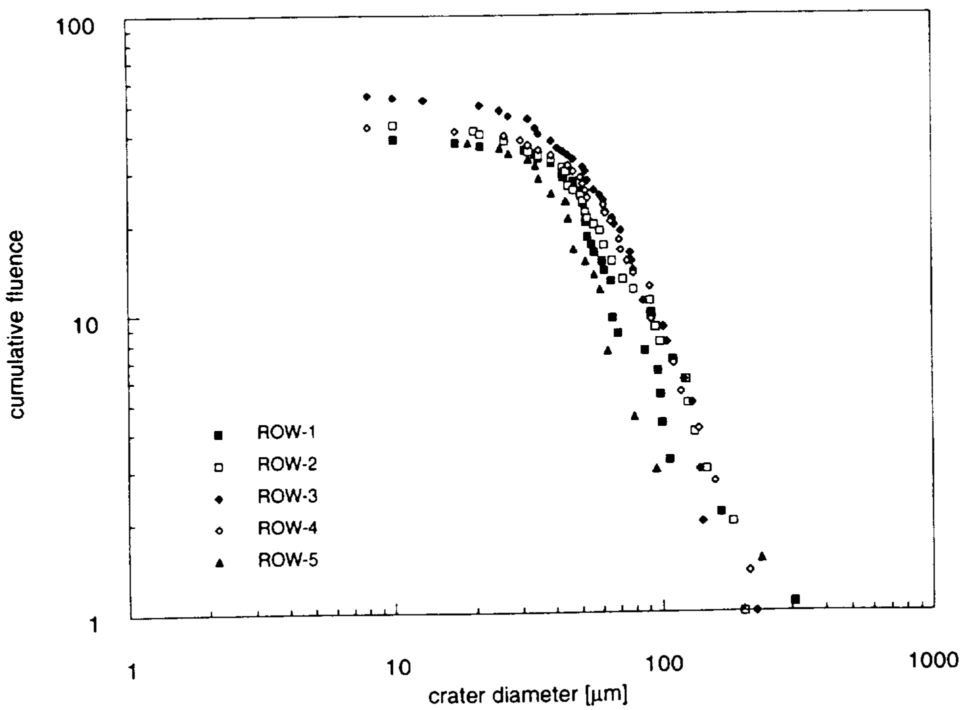

Figure 14. *Cumulative fluence plot for impact site crater diameters on SCA coversheets. Note the significant reduction in fluence for the partially-shielded row, ROW-5. All data are normalized to an exposure area per row of 60 sq.cm.*

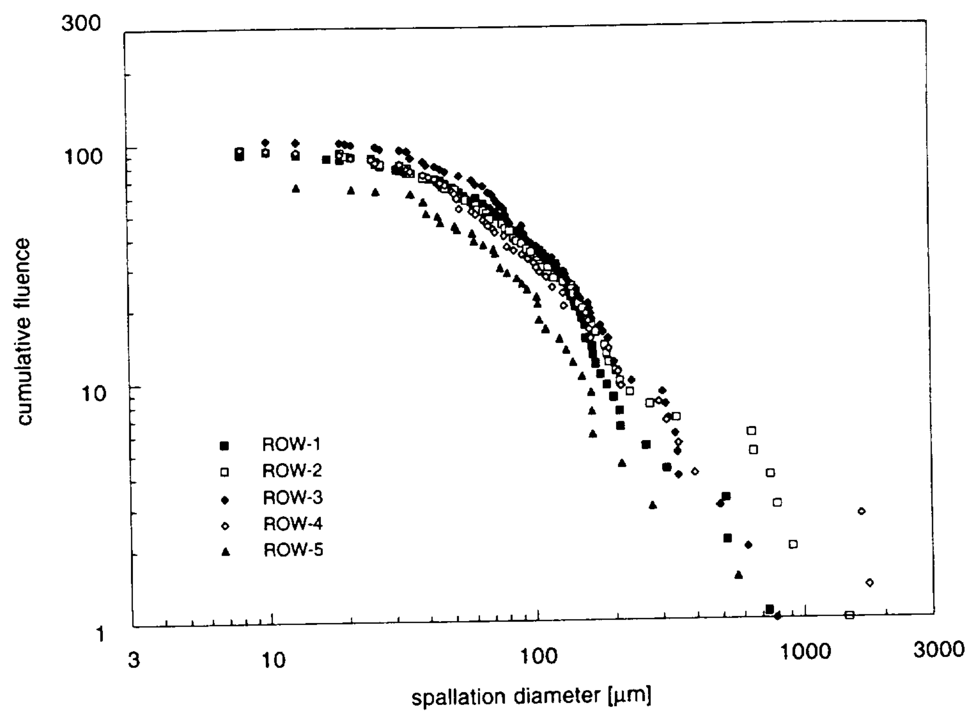

Figure 15. *Cumulative fluence plot for impact site spallation diameters on SCA coversheets. All data are normalized to an exposure area per row of 60 sq.cm. Data set is larger than the crater diameter data set since some crater diameters could not be resolved.*

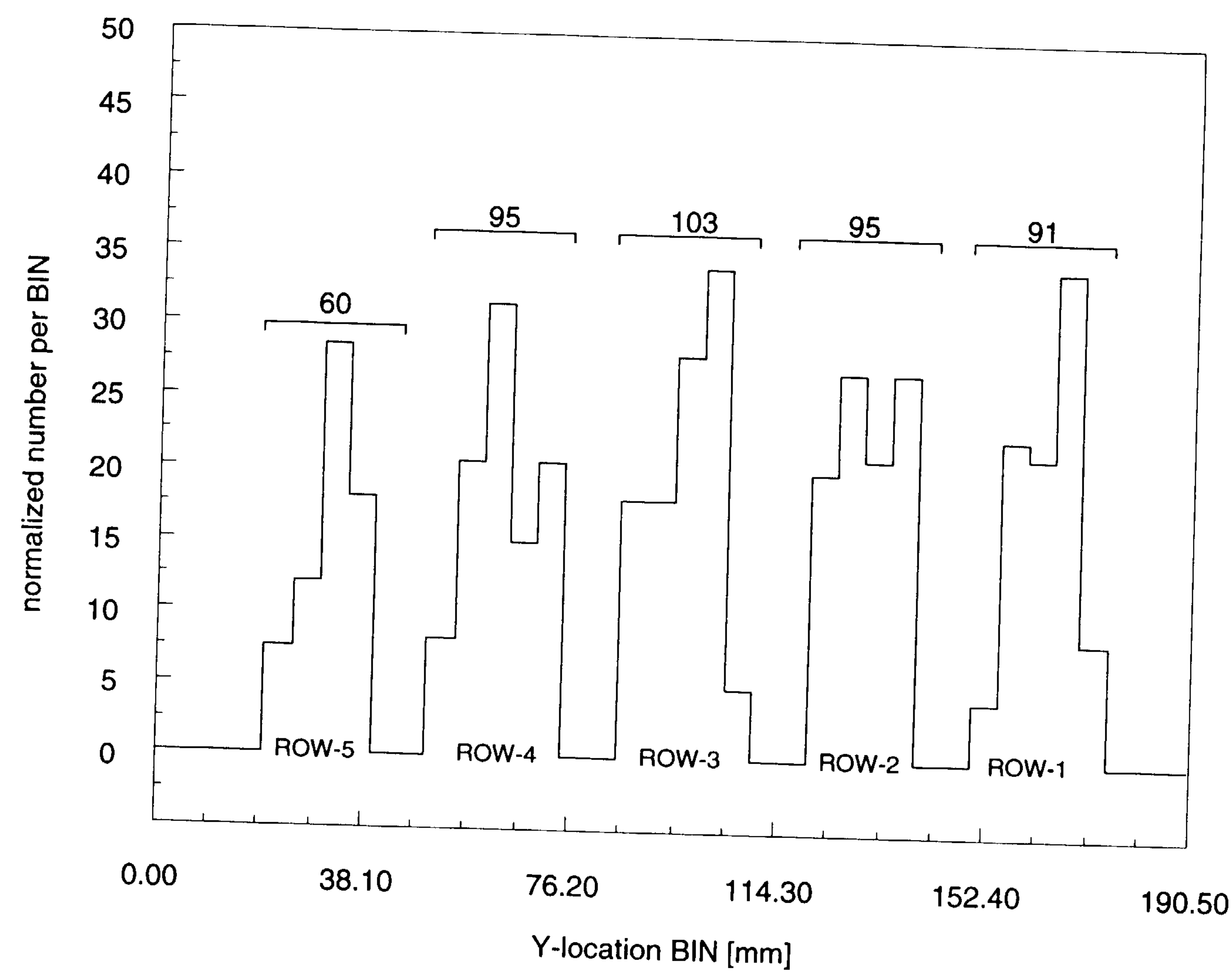

Figure 16. *Step plot of number of impact sites as a function of Y-location. ROW-5 is the row closest to the tray side wall and is partially shielded from the RAM direction. Note the low number (60) of impacts for cells in ROW-5 with respect to the mean number of impacts per row for ROW-4, ROW-3, ROW-2 and ROW-1, i.e. 96. This indicates that even a 3" recess depth for a surface oriented at 38° wrt the spacecraft velocity vector can produce significant shielding effects, ~40%, for the M&D environment. Cells LD-1, LD-4 were excluded since they were uncovered. Cells S-2 and S-3 were excluded since these cells exhibited substantial secondary sites. The number per BIN was normalized to the area exposed by the ROW-3 cells, i.e. 60 sq.cm.*

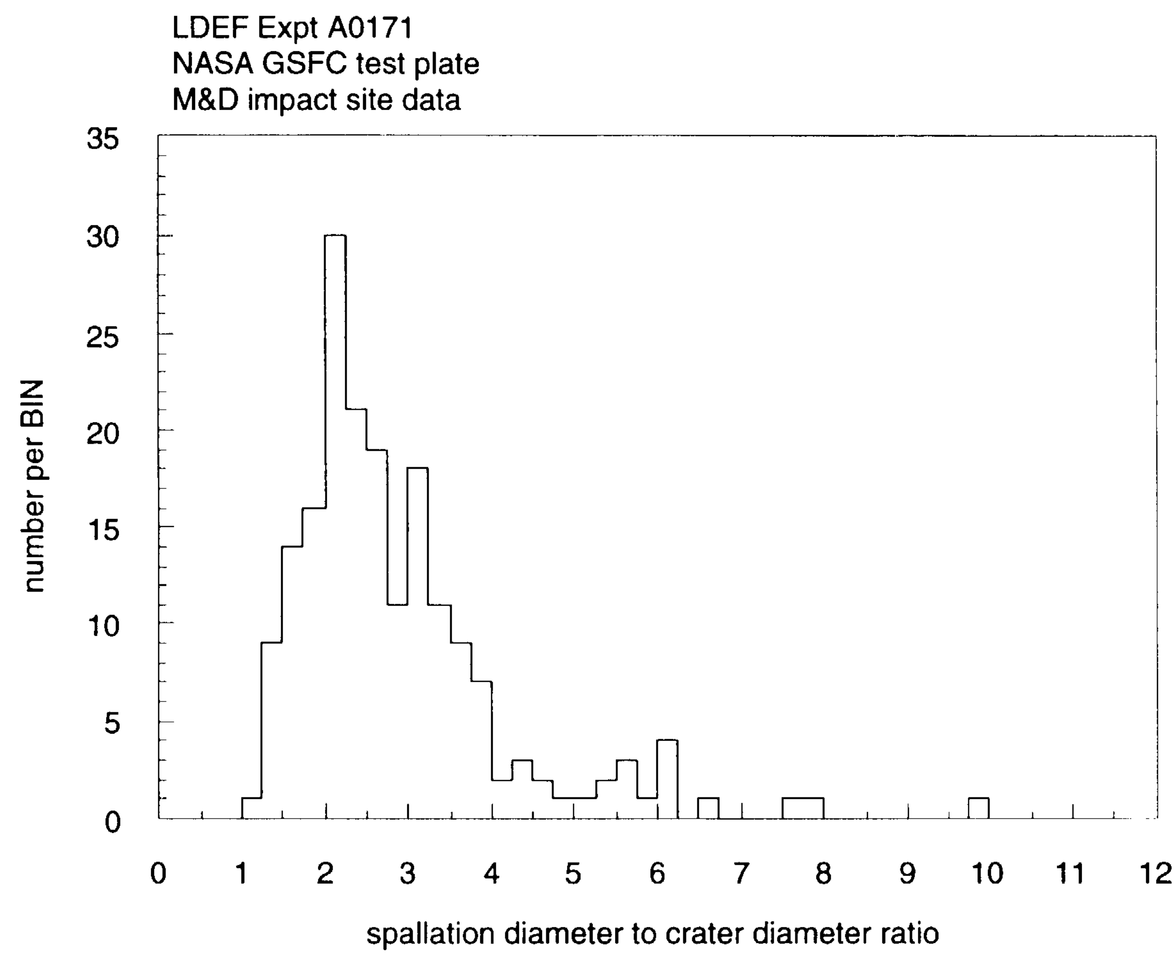

Figure 17. *Number distribution of spallation diameter to crater diameter ratio. This ratio is a function of impact velocity with the faster impacts generating higher ratios of spall diameter to crater diameter. At present, a quantitative relationship between spall-crater diameter ratio and impact velocity is unavailable.*

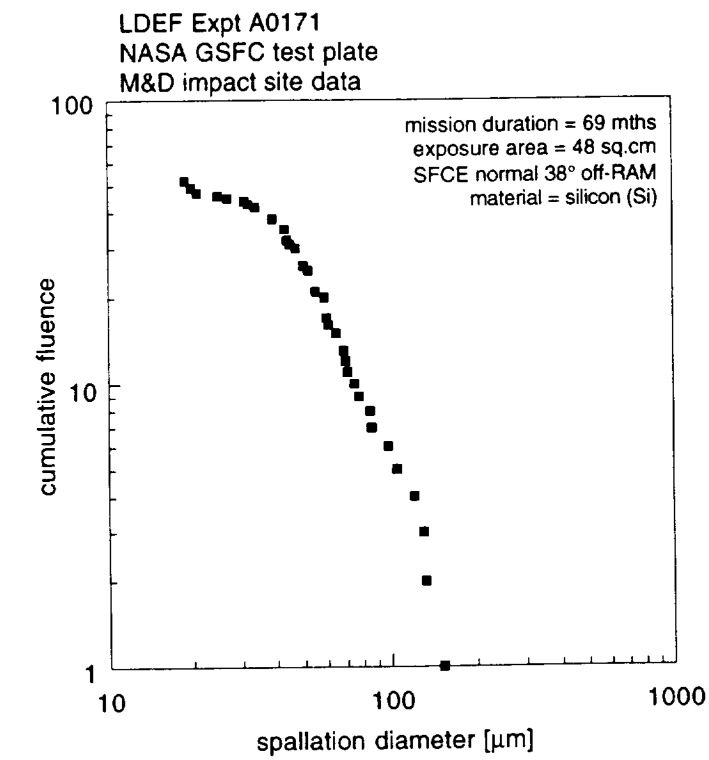

Figure 18. Cumulative fluence plot for impact site crater diameters on exposed solar cells LD-1 and LD-4. Exposure area is 24 sq.cm.

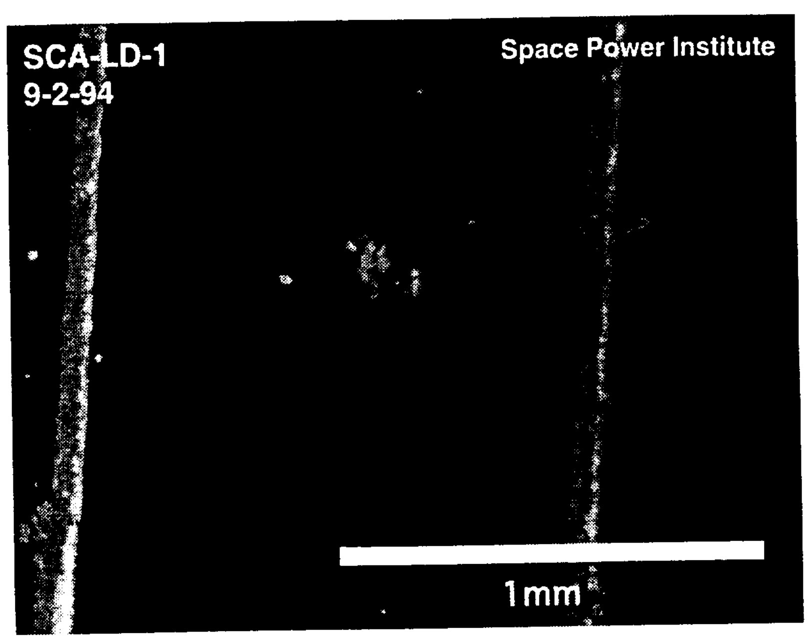

Figure 19. Photograph of a typical M&D impact site in exposed silicon solar cell. Note the absence of a central pit, the whole area being merely spalled out.

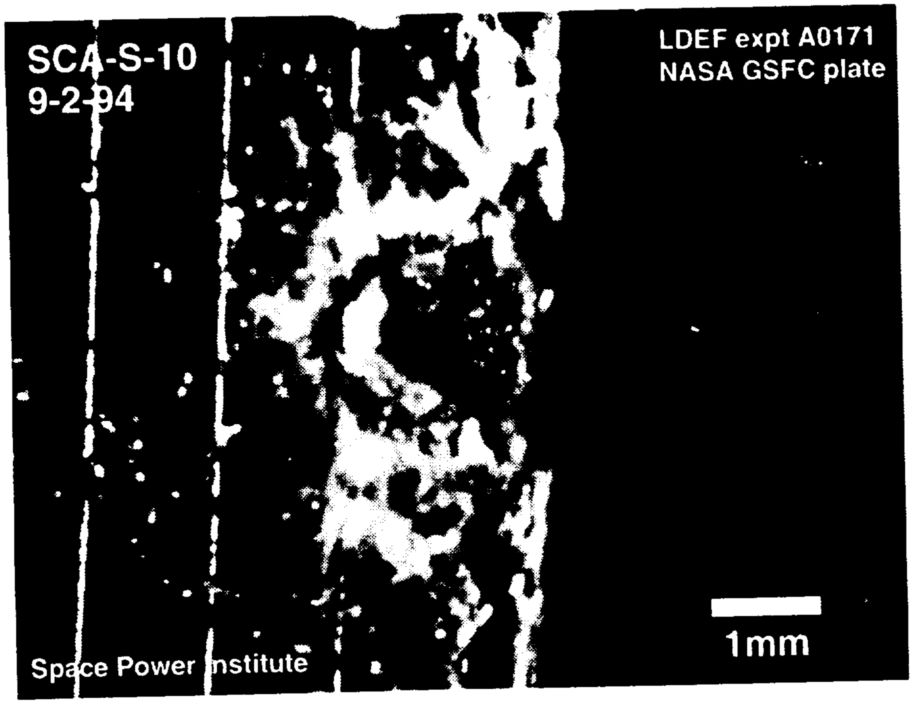

Figure 20. *Photograph of major impact site on the S-10 SCA showing the degree of damage that can occur to thin laminated structures. Note the extensive peripheral fracture zones. This impact has "punched through" to the epoxy board faceplate and as such could have resulted in a cell short circuit on a real solar array.*

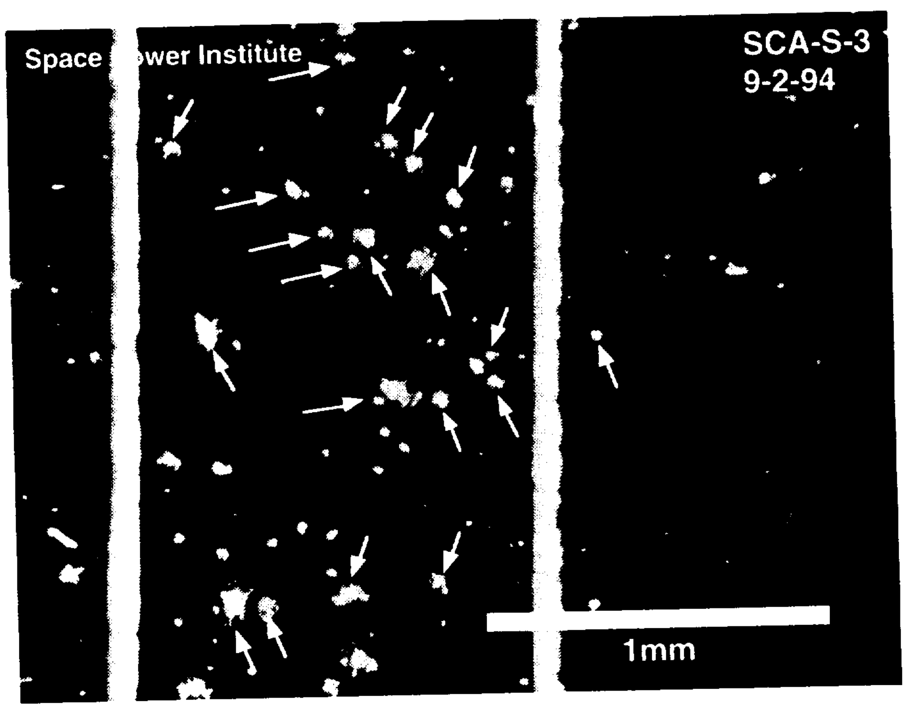

Figure 21. *Photograph of a cluster of M&D impact sites on the coversheet of SCA S-3. Both cells S-2 and S-3 exhibited such large numbers of small impact sites possibly attributable to the ejection of particles from a primary impact site on the experiment tray wall close by.*

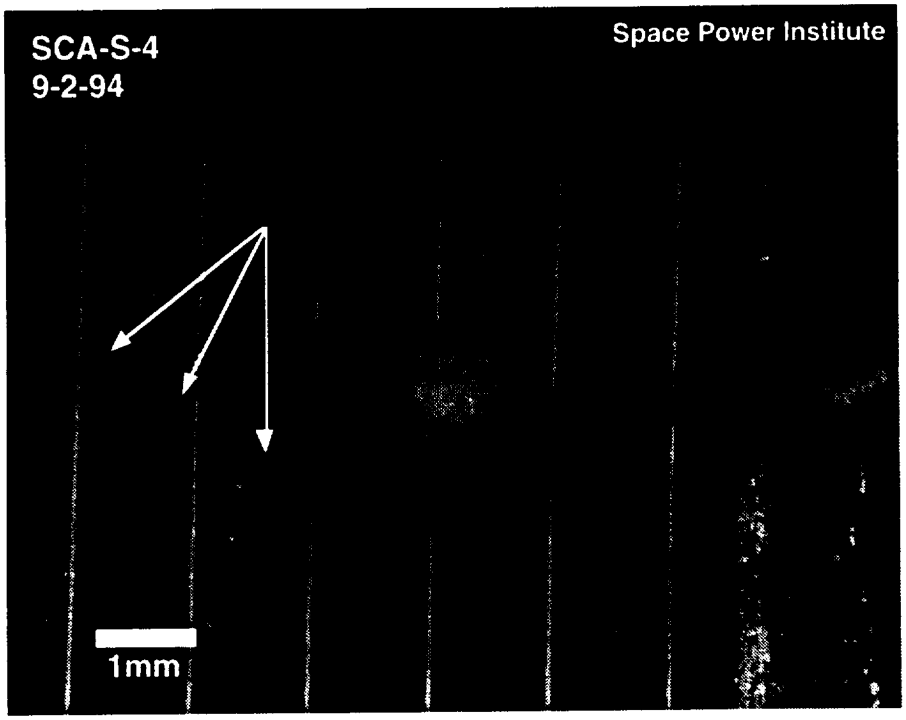

Figure 22. *Photograph of ejecta spray material (very pronounced at lower right) on the coversheet surface of SCA S-4. This ejecta was generated by an impact that occurred on the edge of terminal post #3 of SCA S-5 which is located beyond the right-hand edge of the image. The incoming particle was clearly fragmented on impact and the ejecta impacted the surface of SCA S-4. The large central object is EBP-1 with its connecting wire extending to the right. The arrows define the edge of the spray contamination region where the EBP has shielded the coversheet surface from secondary impacts.*

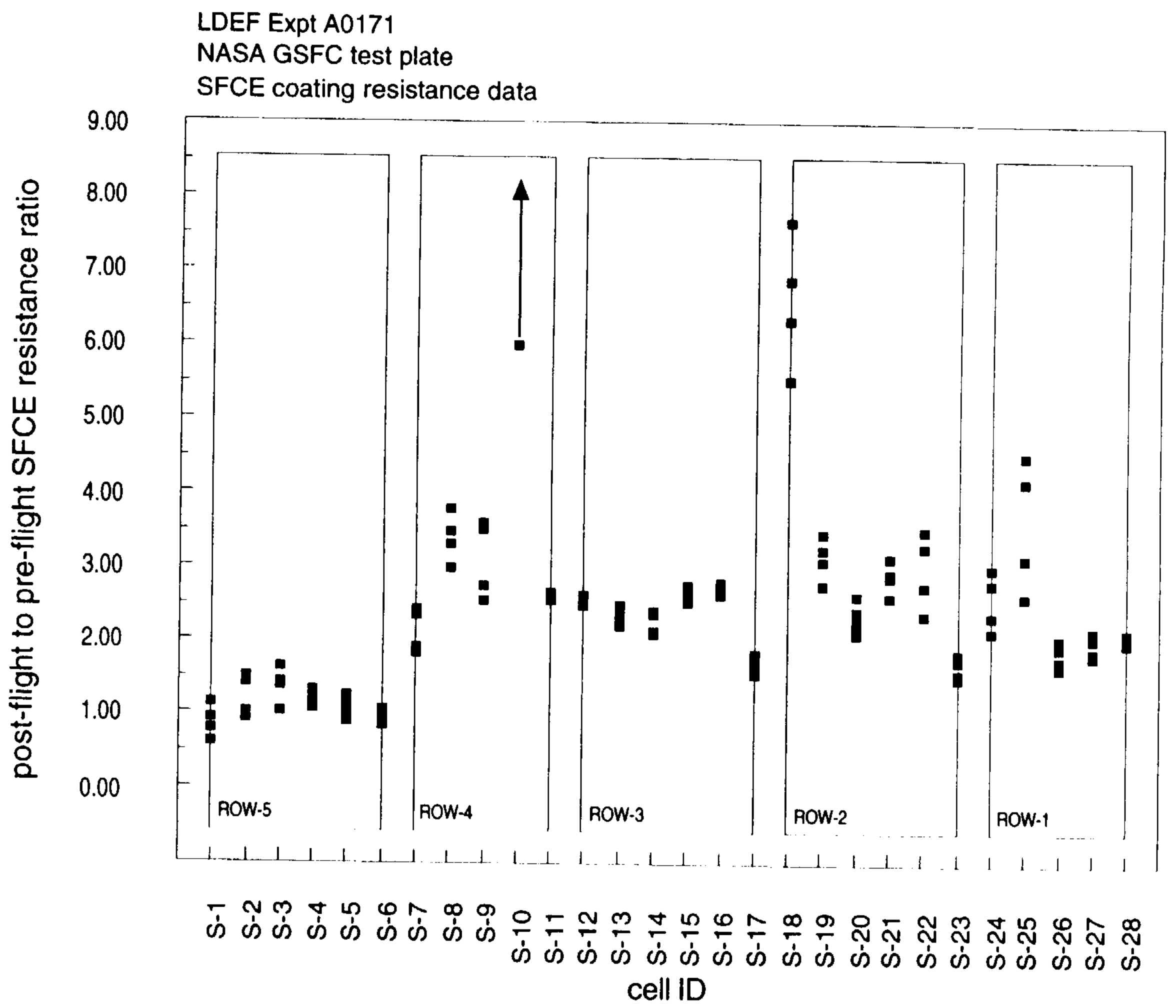

Figure 23. *Plot of post-flight to pre-flight surface coating resistance ratio versus cell number for the 28 S-type SCAs. Note the minimal degradation of the ROW-5 surface coating resistance due to its partial shielding from the ATOX RAM flux by the experiment tray wall. S-10 ratios are dominated by open circuit behavior in pad-to-pad resistance measurements due to the presence of a very large M&D impact site which caused extensive cracking of the SCA coversheet. No explanation of the anomalously large values of resistance ratio for cell S-18 could be found, i.e. there were no significant damage features present on the surface of the coversheet.*

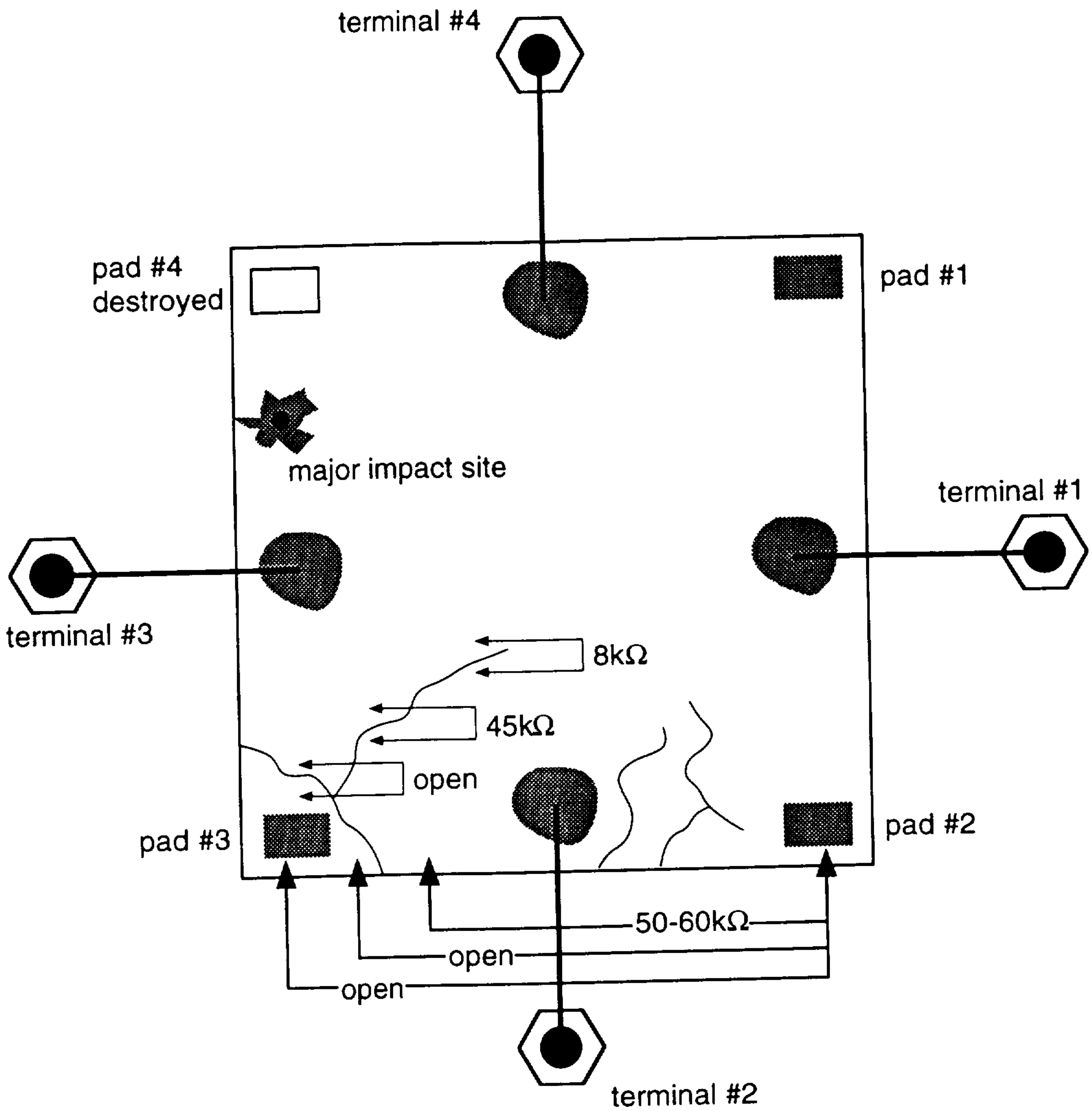

Figure 24. *Schematic of cell S-10, showing the surface resistance effects due to the coversheet cracking caused by the major impact at the left-hand edge. This illustrates a potential failure mode initiator where electrical continuity is lost across the coversheet surface allowing for possible charge build-up in isolated areas.*

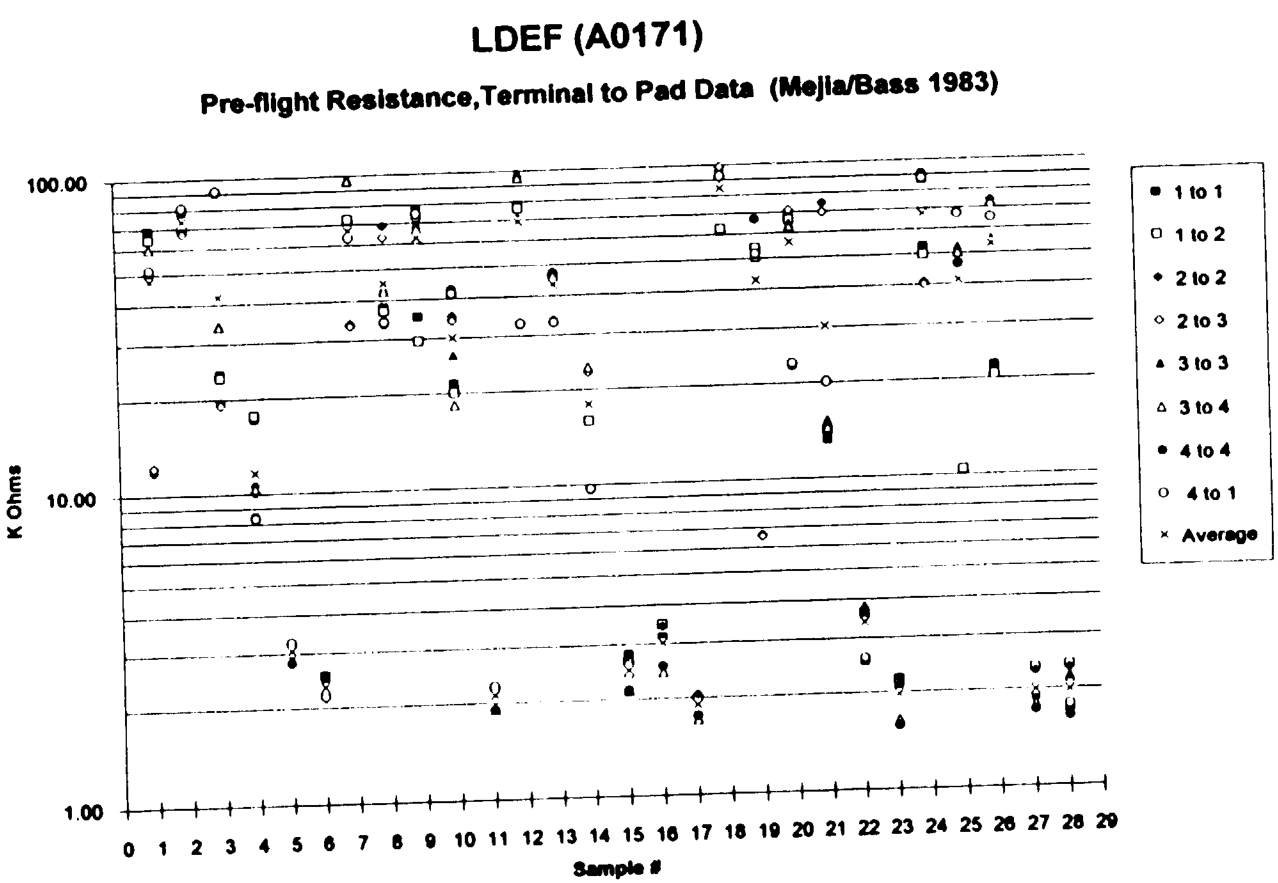

Figure 25. Plot of pre-flight terminal-to-pad resistance for all such combinations on all 28 S-type SCAs. Note that the solder-based EBPs have the lowest values of resistance, whereas the conductively-loaded adhesive based EBPs have higher resistances and also exhibit a greater variation in magnitude for each SCA indicating a significant variation in reproducibility for this type of electrical bond process.

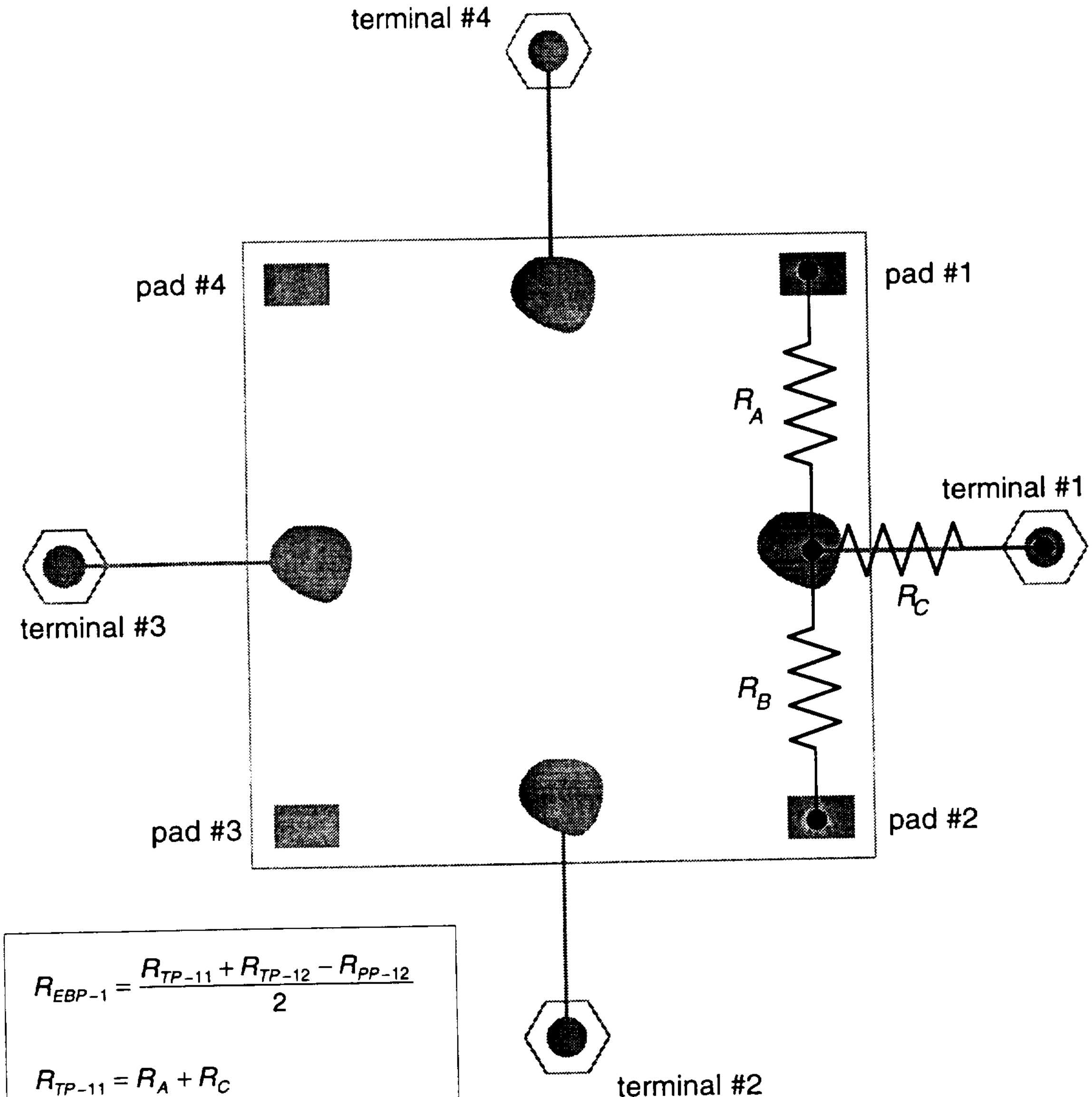

$$R_{EBP-1} = \frac{R_{TP-11} + R_{TP-12} - R_{PP-12}}{2}$$

$$R_{TP-11} = R_A + R_C$$
$$R_{TP-12} = R_B + R_C$$
$$R_{PP-12} = R_A + R_B$$

Figure 26. *Simple resistive network for the terminal, pads, and surface resistances to allow computation of the EBP resistance without surface resistance effects. Similar networks are set up for the other three EBPs, although they are not shown here for the sake of clarity.*

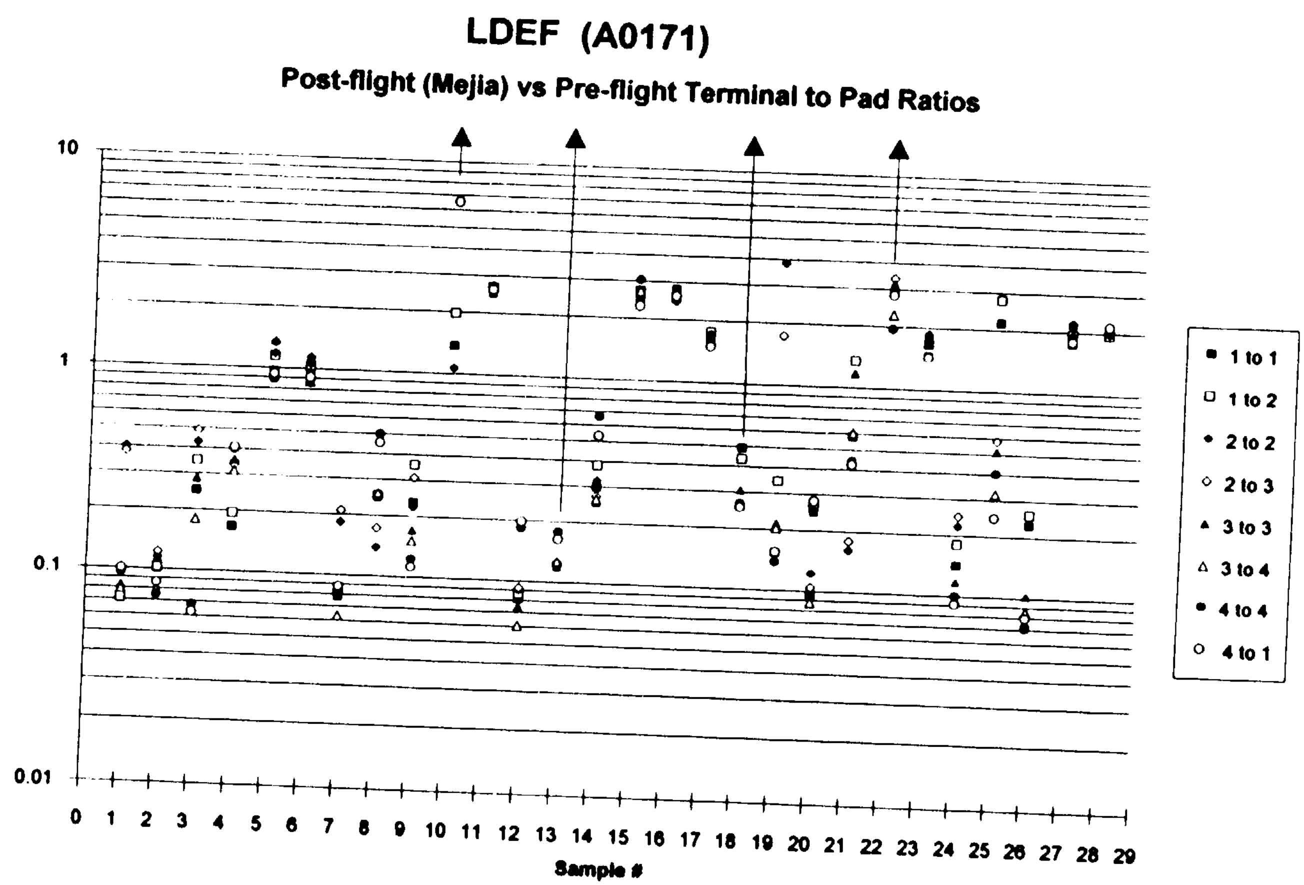

Figure 27. *Plot of post-flight to pre-flight terminal-to-pad resistance ratios (NASA GSFC data) for all such combinations on all 28 S-type SCAs. Note that the solder-based EBPs exhibit minimal changes in resistance, whereas the conductively-loaded adhesive based EBPs typically show reductions in resistance, although some cells exhibit increases due mainly to surface damage such as for cell S-10.*

LDEF (A0171)

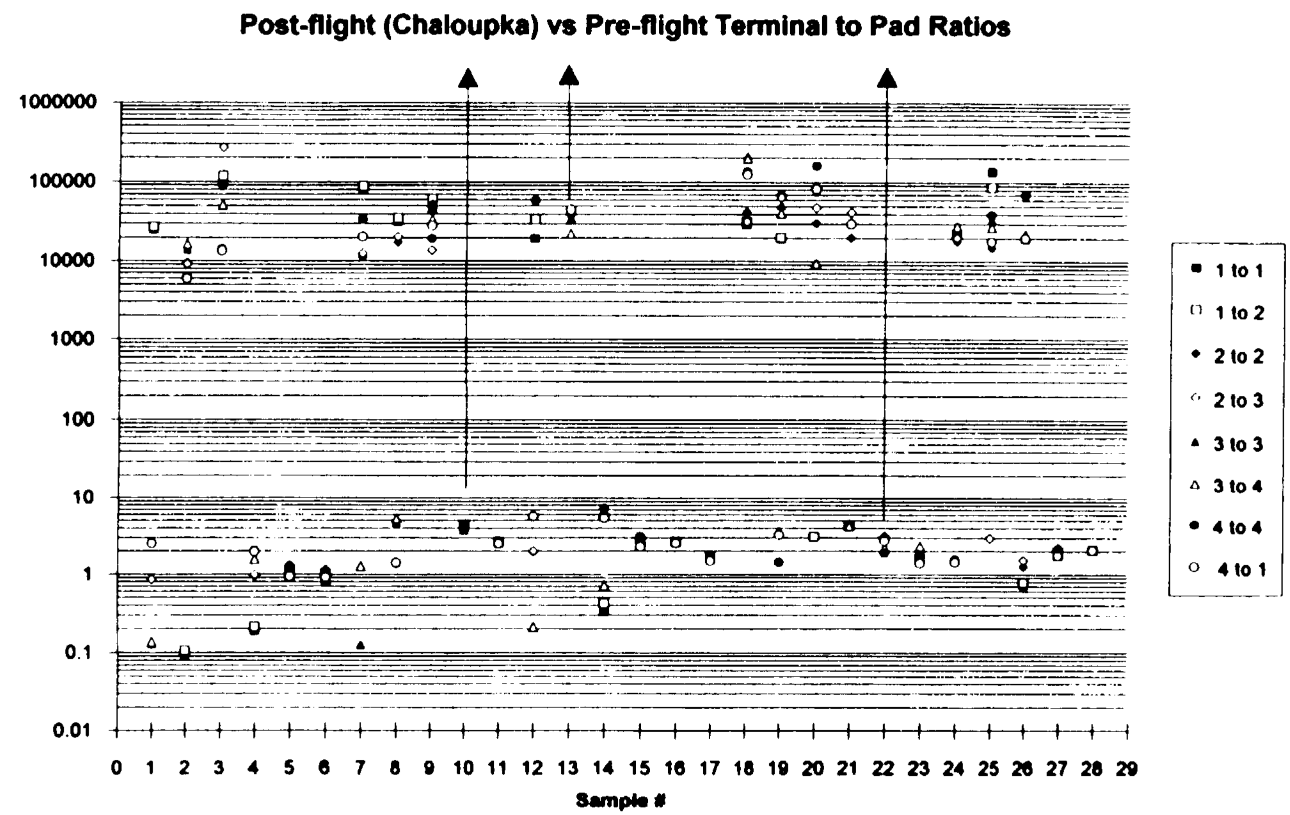

Figure 28. *Plot of post-flight to pre-flight terminal-to-pad resistance ratios (Auburn University data) for all such combinations on all 28 S-type SCAs. Note that the solder-based EBPs exhibit no changes in resistance with respect to the NASA GSFC data, whereas the conductively-loaded adhesive based EBPs typically show massive increases in resistance. This appears to be due to a failure to maintain the test plate in a controlled environment which has lead to further degradation in resistance characteristics.*

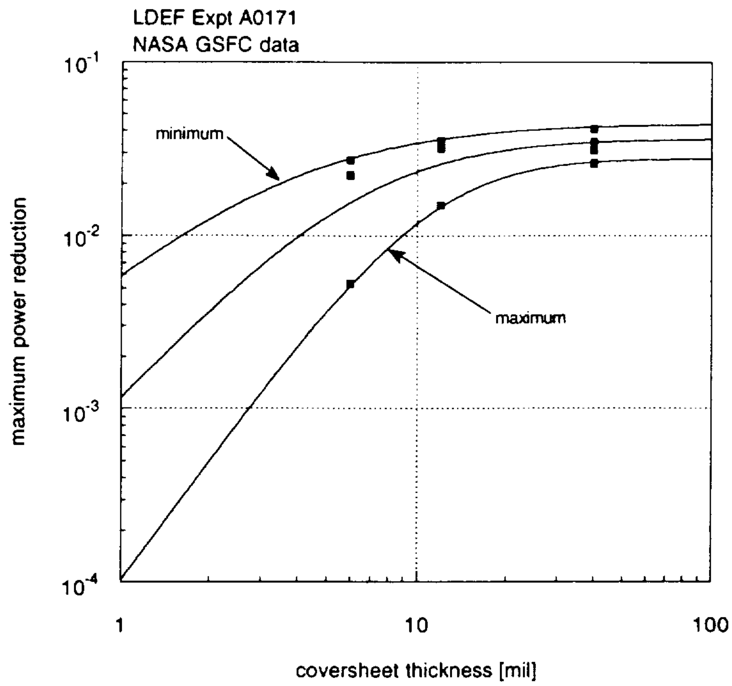

Figure 29. *Plot of* P_{MAX} *reduction,* Π_{MAX}*, as a function of coversheet thickness*

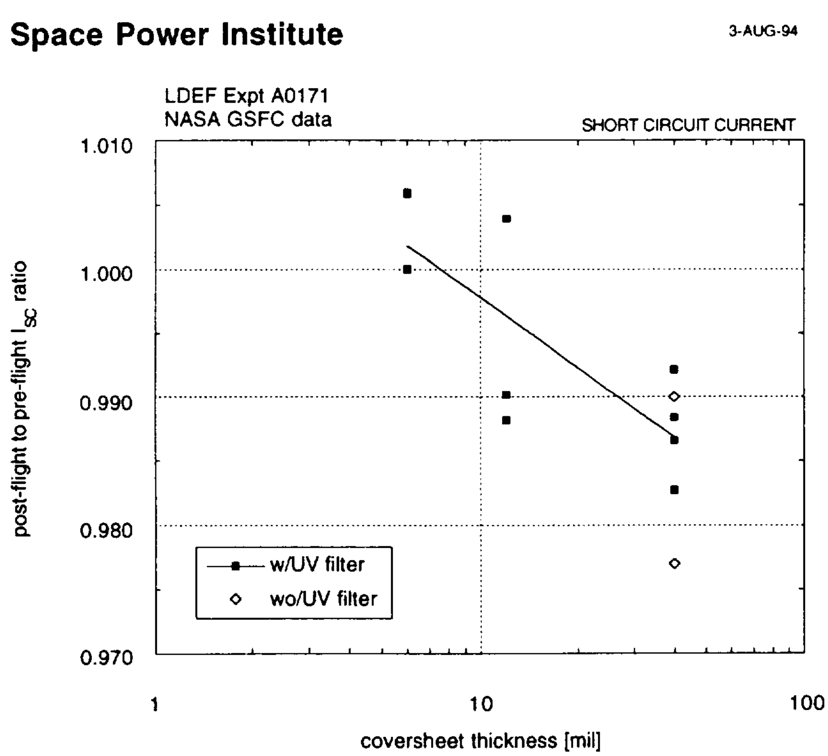

Figure 30. *Plot of post-flight to pre-flight* I_{SC} *ratio versus coversheet thickness.*

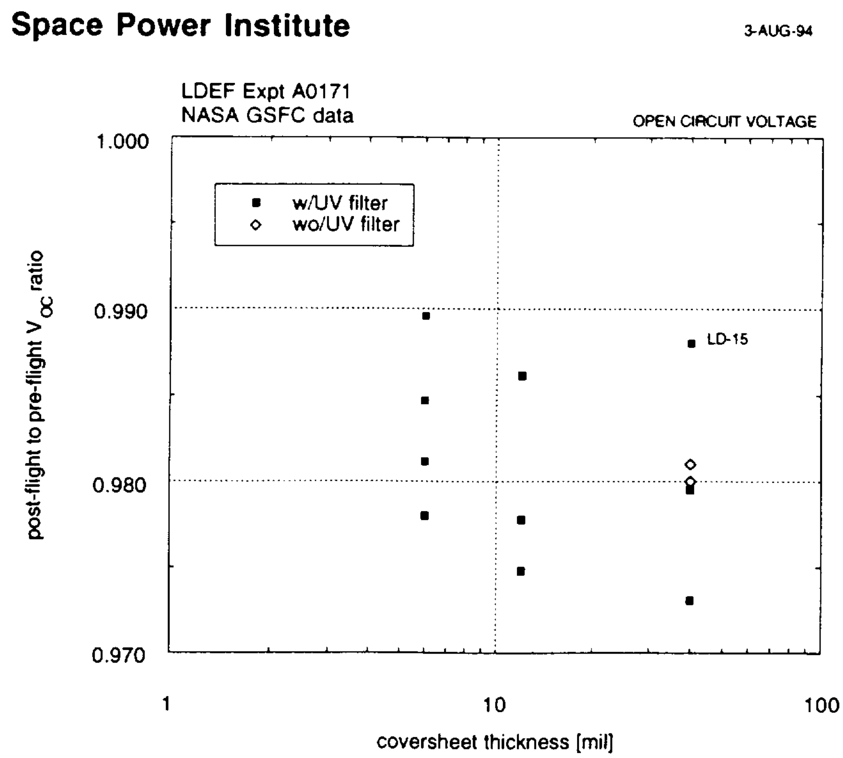

Figure 31. *Plot of post-flight to pre-flight* V_{OC} *ratio versus coversheet thickness.*

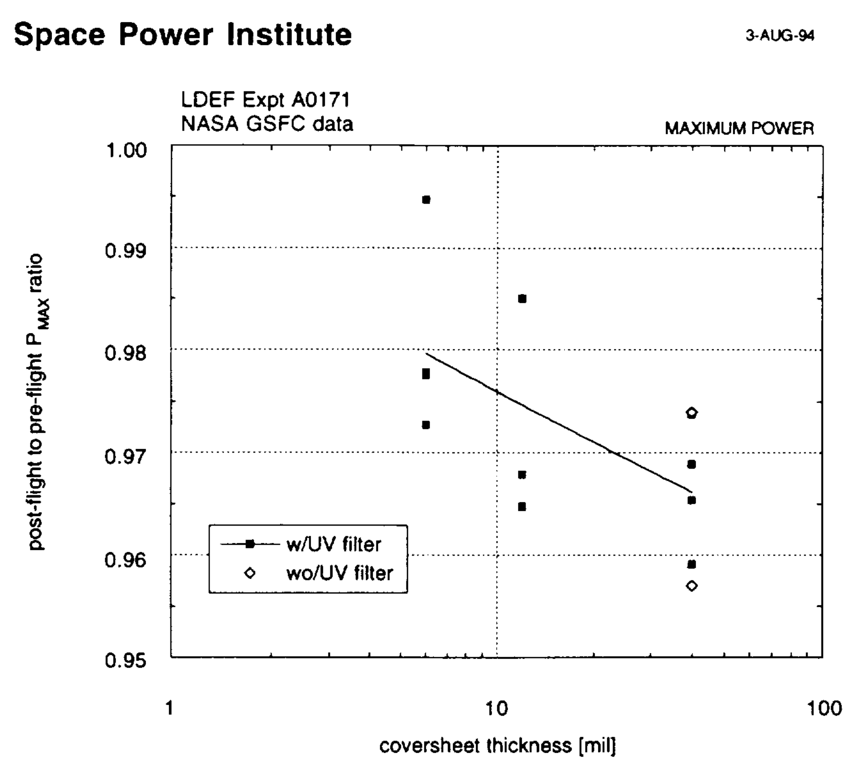

Figure 32. *Plot of post-flight to pre-flight* P_{MAX} *ratio versus coversheet thickness.*

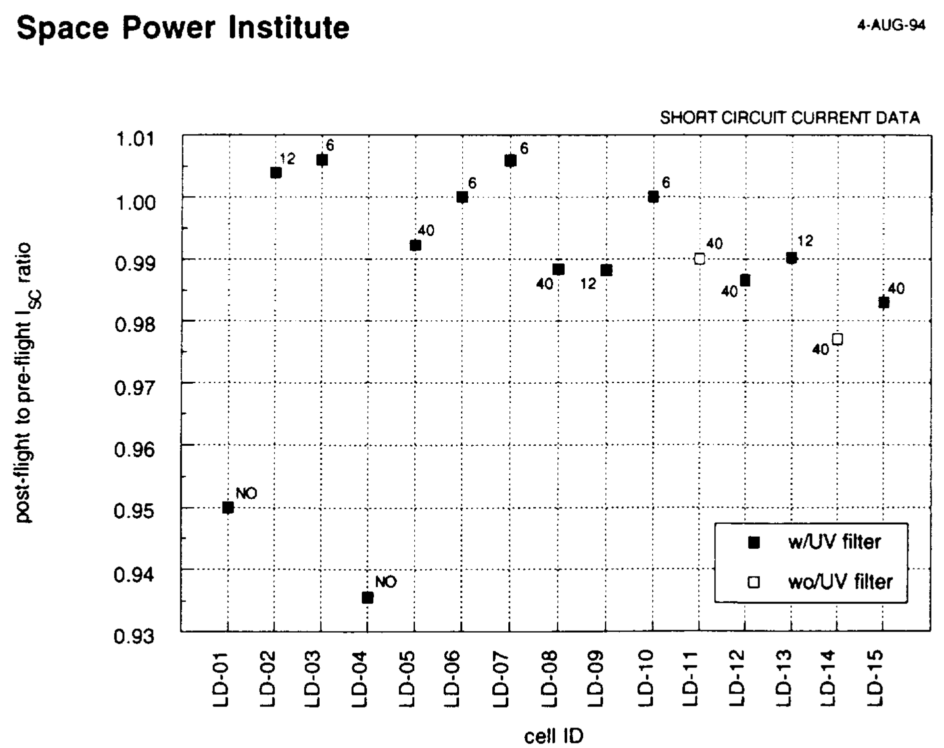

Figure 33. *Plot of post-flight to pre-flight* I_{SC} *ratio for each LD-type cell.*

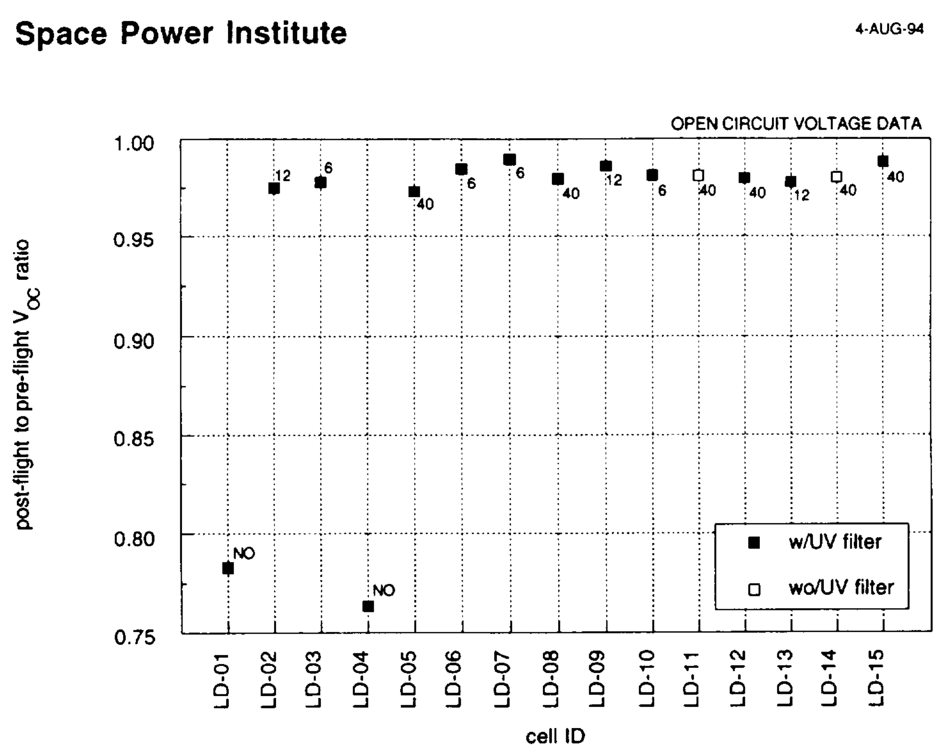

Figure 34. *Plot of post-flight to pre-flight* V_{OC} *ratio for each LD-type cell.*

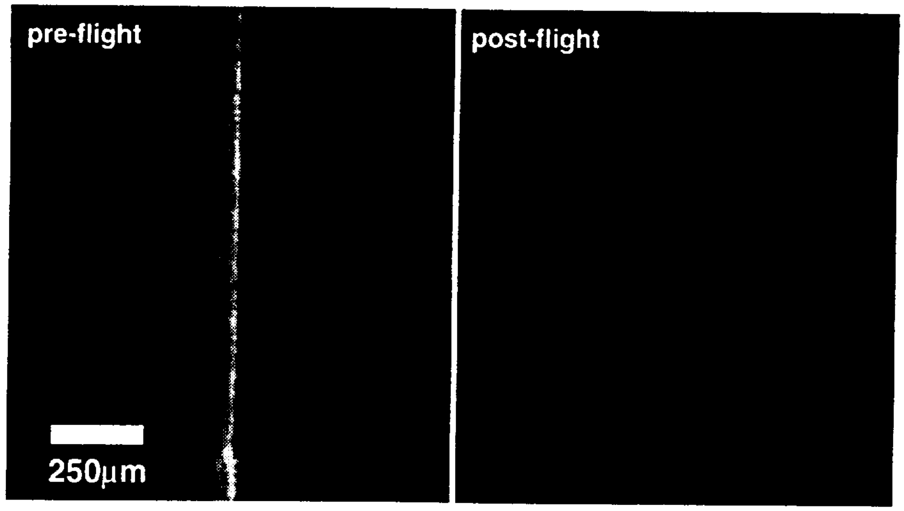

Figure 35. *Photographs, pre- and post-flight of solar cell front surface contacts. Note how the ATOX environment erodes the contact, spreading material out across the surface of the solar cell close to the original edge of the contact (right-hand image).*

SAMPLE Solar Array Materials Passive LDEF Experiment	date: August 30, 1994
LDEF EXPT #: A0171 **ROW:** 8 **BAY:** A **EXPT SUB-ELEMENT:** NASA GSFC module	**document title:** MATERIALS LIST - AS BUILT; AS FLOWN

ITEM	NUMBER	TOTAL WEIGHT	DESCRIPTION
S-type solar cell 2 cm X 2 cm X 0.03 cm	28	7.7 g (0.276 g/cell)	silicon (Si; $\rho = 2.33$ g.cm^{-3}) with silicon monoxide (SiO) anti-reflection coating and titanium palladium silver (Ti:Pd:Ag) contacts.
conductively coated coverslide 2 cm X 2 cm X 0.03 cm	28	7.4 g	fused silica (SiO_2; $\rho = 2.20$ g.cm^{-3}) with vapor-deposited indium oxide (In_2O_3) conductive coating.
LD-type K-6.5 solar cell 2 cm X 6 cm X 0.03 cm	15	12.4 g (0.828 g/cell)	silicon (Si; $\rho = 2.33$ g.cm^{-3}) with tantalum pentoxide (Ta_2O_5) anti-reflection coating and titanium palladium silver (Ti:Pd:Ag) contacts.
6 mil coverslide 2 cm X 6 cm X 0.015 cm	4	1.58 g	fused silica (SiO_2; $\rho = 2.20$ g.cm^{-3}) with magnesium fluoride (MgF_2) anti-reflection coating and UV interference filter.
12 mil coverslide 2 cm X 6 cm X 0.03 cm	3	2.38 g	fused silica (SiO_2; $\rho = 2.20$ g.cm^{-3}) with magnesium fluoride (MgF_2) anti-reflection coating and UV interference filter.
40 mil coverslide 2 cm X 6 cm X 0.10 cm	4	10.6 g	fused silica (SiO_2; $\rho = 2.20$ g.cm^{-3}) with magnesium fluoride (MgF_2) anti-reflection coating and UV interference filter.
40 mil coverslide 2 cm X 6 cm X 0.10 cm	2	5.28 g	fused silica (SiO_2; $\rho = 2.20$ g.cm^{-3}) with magnesium fluoride (MgF_2) anti-reflection coating.
coverslide adhesive 2 cm X 2 cm	28	3.36 g	Dow Corning 93-500, ~0.03 cm thk, $\rho = 1.08$ g.cm^{-3} @ 0.03 g.cm^{-2}
coverslide adhesive 2 cm X 6 cm	15	5.40 g	Dow Corning 93-500, ~0.03 cm thk, $\rho = 1.08$ g.cm^{-3} @ 0.03 g.cm^{-2}
solar cell adhesive 2 cm X 2 cm	28	3.36 g	Dow Corning 93-500, ~0.03 cm thk, $\rho = 1.08$ g.cm^{-3} @ 0.03 g.cm^{-2}
solar cell adhesive 2 cm X 6 cm	15	5.40 g	Dow Corning 93-500, ~0.03 cm thk, $\rho = 1.08$ g.cm^{-3} @ 0.03 g.cm^{-2}
epoxy board adhesive 41.4 cm X 19.1 cm X 0.20 cm	2	78.6 g	Dow Corning 93-500, ~0.05 cm thk, $\rho = 1.08$ g.cm^{-3} @ 0.05 g.cm^{-2}

SAMPLE Solar Array Materials Passive LDEF Experiment	page 2 of 2 date: August 30, 1994
LDEF EXPT #: A0171 **ROW:** 8 **BAY:** A **EXPT SUB-ELEMENT:** NASA GSFC module	**document title:** MATERIALS LIST - AS BUILT; AS FLOWN

ITEM	NUMBER	TOTAL WEIGHT	DESCRIPTION
coverslide wiring (4 per cell)	56	0.78 g	unplated 24-AWG copper (Cu) wire, 0.011" dia. X 1" long; ρ = 8.96 g.cm^{-3}, 0.0055 g.cm^{-1}
coverslide wiring (4 per cell)	56	0.78 g	tin (Sn) plated 24-AWG copper (Cu) wire, 0.011" dia. X 1" long; ρ = 8.96 g.cm^{-3}, 0.0055 g.cm^{-1}
epoxy board 41.4 cm X 19.1 cm X 0.20 cm	1	225.4 g	0.2 cm thk epoxy board (ρ = 1.43 g.cm^{-3})
LD-type solar cell contact mesh 183 cm^2	15	2.2 g	silver (Ag) mesh; 0.012 g.cm^{-2}
Eccobond 56C 2 cm X 6 cm X 0.03 cm	56 pads	0.56 g	silver (Ag) filled epoxy adhesive; 0.01 g/pad
Indium-tin solder #1	20 pads	0.40 g	50% indium (In), 50% tin (Sn); 0.02 g/pad
Indium-silver solder #3	20 pads	0.40 g	90% indium (In), 10% silver (Ag); 0.02 g/pad
EPON 815	16 pads	0.16 g	0.01 g/pad
terminal 0.30" X 0.125" X 0.10"	172	90.1 g	brass with 0.0003" solder plating; 0.524 g ea.
solar cell hook-up wire	60	n/a	silver (Ag) mesh; 0.012 g.cm^{-2}; two strands, twisted ~0.75" long
terminal mounting screw	172	41.3 g	flat head stainless steel machine, #2-56, 3/8" long, 0.24 g ea.
tray interface plate 41.4 cm X 19.1 cm X 0.20 cm	1	1024.8 g	aluminum (alloy not specified), ρ ~ 2.7 g.cm^{-3}
washer	4	2.3 g	stainless steel, 0.58 g ea.
nut	4	6.0 g	stainless steel, 1.50 g ea.
wire and terminal adhesive	172	8.6 g	Dow Corning 93-500, ρ = 1.08 g.cm^{-3}, @ 0.05 g.cm^{-2}, ~1 cm^2 ea. bond area

SAMPLE Solar Array Materials Passive LDEF Experiment	page 1 of 6 date: September 13, 1994
LDEF EXPT #: A0171 **ROW:** 8 **BAY:** A **EXPT SUB-ELEMENT:** NASA GSFC module	**document title:** S-TYPE SCAs DATA [as-built, as-flown]

cell ID	CONFIGURATION & MATERIALS
S-1	• 305 μm (12 mil) thk 2 cm X 2 cm silicon solar cell with silicon monoxide (SiO) anti-reflection coating and Ti:Pd:Ag contacts • 305 μm (12 mil) thk fused silica (SiO_2) coverslide with indium oxide (In_2O_3) conductive coating • 4 Eccobond 56C (w/10% toluene solvent) pads • 4 unplated 24-AWG copper (Cu) contact wires • Dow Corning 93-500 cell and coverslide adhesive
S-2	• 305 μm (12 mil) thk 2 cm X 2 cm silicon solar cell with silicon monoxide (SiO) anti-reflection coating and Ti:Pd:Ag contacts • 305 μm (12 mil) thk fused silica (SiO_2) coverslide with indium oxide (In_2O_3) conductive coating • 4 Eccobond 56C (w/10% alcohol solvent) pads • 4 unplated 24-AWG copper (Cu) contact wires • Dow Corning 93-500 cell and coverslide adhesive
S-3	• 305 μm (12 mil) thk 2 cm X 2 cm silicon solar cell with silicon monoxide (SiO) anti-reflection coating and Ti:Pd:Ag contacts • 305 μm (12 mil) thk fused silica (SiO_2) coverslide with indium oxide (In_2O_3) conductive coating • 4 Eccobond 56C-H (w/10% toluene solvent) pads • 4 unplated 24-AWG copper (Cu) contact wires • Dow Corning 93-500 cell and coverslide adhesive
S-4	• 305 μm (12 mil) thk 2 cm X 2 cm silicon solar cell with silicon monoxide (SiO) anti-reflection coating and Ti:Pd:Ag contacts • 305 μm (12 mil) thk fused silica (SiO_2) coverslide with indium oxide (In_2O_3) conductive coating • 4 EPON 815 pads • 4 tin (Sn) plated 24-AWG copper (Cu) contact wires • Dow Corning 93-500 cell and coverslide adhesive
S-5	• 305 μm (12 mil) thk 2 cm X 2 cm silicon solar cell with silicon monoxide (SiO) anti-reflection coating and Ti:Pd:Ag contacts • 305 μm (12 mil) thk fused silica (SiO_2) coverslide with indium oxide (In_2O_3) conductive coating • 4 indium-tin (50:50) solder #1 pads • 4 tin (Sn) plated 24-AWG copper (Cu) contact wires • Dow Corning 93-500 cell and coverslide adhesive

cell ID	CONFIGURATION & MATERIALS
S-6	• 305 µm (12 mil) thk 2 cm X 2 cm silicon solar cell with silicon monoxide (SiO) anti-reflection coating and Ti:Pd:Ag contacts • 305 µm (12 mil) thk fused silica (SiO_2) coverslide with indium oxide (In_2O_3) conductive coating • 4 indium-silver (90:10) solder #3 pads • 4 tin (Sn) plated 24-AWG copper (Cu) contact wires • Dow Corning 93-500 cell and coverslide adhesive
S-7	• 305 µm (12 mil) thk 2 cm X 2 cm silicon solar cell with silicon monoxide (SiO) anti-reflection coating and Ti:Pd:Ag contacts • 305 µm (12 mil) thk fused silica (SiO_2) coverslide with indium oxide (In_2O_3) conductive coating • 4 Eccobond 56C (w/10% toluene solvent) pads • 4 unplated 24-AWG copper (Cu) contact wires • Dow Corning 93-500 cell and coverslide adhesive
S-8	• 305 µm (12 mil) thk 2 cm X 2 cm silicon solar cell with silicon monoxide (SiO) anti-reflection coating and Ti:Pd:Ag contacts • 305 µm (12 mil) thk fused silica (SiO_2) coverslide with indium oxide (In_2O_3) conductive coating • 4 Eccobond 56C (w/10% alcohol solvent) pads • 4 unplated 24-AWG copper (Cu) contact wires • Dow Corning 93-500 cell and coverslide adhesive
S-9	• 305 µm (12 mil) thk 2 cm X 2 cm silicon solar cell with silicon monoxide (SiO) anti-reflection coating and Ti:Pd:Ag contacts • 305 µm (12 mil) thk fused silica (SiO_2) coverslide with indium oxide (In_2O_3) conductive coating • 4 Eccobond 56C-H (w/10% toluene solvent) pads • 4 unplated 24-AWG copper (Cu) contact wires • Dow Corning 93-500 cell and coverslide adhesive
S-10	• 305 µm (12 mil) thk 2 cm X 2 cm silicon solar cell with silicon monoxide (SiO) anti-reflection coating and Ti:Pd:Ag contacts • 305 µm (12 mil) thk fused silica (SiO_2) coverslide with indium oxide (InO) conductive coating • 4 EPON 815 pads • 4 tin (Sn) plated 24-AWG copper (Cu) contact wires • Dow Corning 93-500 cell and coverslide adhesive

cell ID	CONFIGURATION & MATERIALS
S-11	• 305 μm (12 mil) thk 2 cm X 2 cm silicon solar cell with silicon monoxide (SiO) anti-reflection coating and Ti:Pd:Ag contacts • 305 μm (12 mil) thk fused silica (SiO_2) coverslide with indium oxide (In_2O_3) conductive coating • 4 indium-tin (50:50) solder #1 pads • 4 tin (Sn) plated 24-AWG copper (Cu) contact wires • Dow Corning 93-500 cell and coverslide adhesive
S-12	• 305 μm (12 mil) thk 2 cm X 2 cm silicon solar cell with silicon monoxide (SiO) anti-reflection coating and Ti:Pd:Ag contacts • 305 μm (12 mil) thk fused silica (SiO_2) coverslide with indium oxide (In_2O_3) conductive coating • 4 Eccobond 56C (w/10% toluene solvent) pads • 4 unplated 24-AWG copper (Cu) contact wires • Dow Corning 93-500 cell and coverslide adhesive
S-13	• 305 μm (12 mil) thk 2 cm X 2 cm silicon solar cell with silicon monoxide (SiO) anti-reflection coating and Ti:Pd:Ag contacts • 305 μm (12 mil) thk fused silica (SiO_2) coverslide with indium oxide (In_2O_3) conductive coating • 4 Eccobond 56C (w/10% alcohol solvent) pads • 4 unplated 24-AWG copper (Cu) contact wires • Dow Corning 93-500 cell and coverslide adhesive
S-14	• 305 μm (12 mil) thk 2 cm X 2 cm silicon solar cell with silicon monoxide (SiO) anti-reflection coating and Ti:Pd:Ag contacts • 305 μm (12 mil) thk fused silica (SiO_2) coverslide with indium oxide (In_2O_3) conductive coating • 4 EPON 815 pads • 4 tin (Sn) plated 24-AWG copper (Cu) contact wires • Dow Corning 93-500 cell and coverslide adhesive
S-15	• 305 μm (12 mil) thk 2 cm X 2 cm silicon solar cell with silicon monoxide (SiO) anti-reflection coating and Ti:Pd:Ag contacts • 305 μm (12 mil) thk fused silica (SiO_2) coverslide with indium oxide (In_2O_3) conductive coating • 4 indium-tin (50:50) solder #1 pads • 4 tin (Sn) plated 24-AWG copper (Cu) contact wires • Dow Corning 93-500 cell and coverslide adhesive

cell ID	CONFIGURATION & MATERIALS
S-16	• 305 µm (12 mil) thk 2 cm X 2 cm silicon solar cell with silicon monoxide (SiO) anti-reflection coating and Ti:Pd:Ag contacts • 305 µm (12 mil) thk fused silica (SiO_2) coverslide with indium oxide (In_2O_3) conductive coating • 4 indium-silver (90:10) solder #3 pads • 4 tin (Sn) plated 24-AWG copper (Cu) contact wires • Dow Corning 93-500 cell and coverslide adhesive
S-17	• 305 µm (12 mil) thk 2 cm X 2 cm silicon solar cell with silicon monoxide (SiO) anti-reflection coating and Ti:Pd:Ag contacts • 305 µm (12 mil) thk fused silica (SiO_2) coverslide with indium oxide (In_2O_3) conductive coating • 4 indium-silver (90:10) solder #3 pads • 4 tin (Sn) plated 24-AWG copper (Cu) contact wires • Dow Corning 93-500 cell and coverslide adhesive
S-18	• 305 µm (12 mil) thk 2 cm X 2 cm silicon solar cell with silicon monoxide (SiO) anti-reflection coating and Ti:Pd:Ag contacts • 305 µm (12 mil) thk fused silica (SiO_2) coverslide with indium oxide (In_2O_3) conductive coating • 4 Eccobond 56C (w/10% toluene solvent) pads • 4 unplated 24-AWG copper (Cu) contact wires
S-19	• 305 µm (12 mil) thk 2 cm X 2 cm silicon solar cell with silicon monoxide (SiO) anti-reflection coating and Ti:Pd:Ag contacts • 305 µm (12 mil) thk fused silica (SiO_2) coverslide with indium oxide (In_2O_3) conductive coating • 4 Eccobond 56C (w/10% alcohol solvent) pads • 4 unplated 24-AWG copper (Cu) contact wires • Dow Corning 93-500 cell and coverslide adhesive
S-20	• 305 µm (12 mil) thk 2 cm X 2 cm silicon solar cell with silicon monoxide (SiO) anti-reflection coating and Ti:Pd:Ag contacts • 305 µm (12 mil) thk fused silica (SiO_2) coverslide with indium oxide (In_2O_3) conductive coating • 4 Eccobond 56C-H (w/10% toluene solvent) pads • 4 unplated 24-AWG copper (Cu) contact wires • Dow Corning 93-500 cell and coverslide adhesive

SAMPLE Solar Array Materials Passive LDEF Experiment	page 5 of 6 date: September 13, 1994
LDEF EXPT #: A0171 ROW: 8 BAY: A EXPT SUB-ELEMENT: NASA GSFC module	document title: S-TYPE SCAs DATA [as-built, as-flown]

cell ID	CONFIGURATION & MATERIALS
S-21	• 305 μm (12 mil) thk 2 cm X 2 cm silicon solar cell with silicon monoxide (SiO) anti-reflection coating and Ti:Pd:Ag contacts • 305 μm (12 mil) thk fused silica (SiO_2) coverslide with indium oxide (In_2O_3) conductive coating • 4 EPON 815 pads • 4 tin (Sn) plated 24-AWG copper (Cu) contact wires • Dow Corning 93-500 cell and coverslide adhesive
S-22	• 305 μm (12 mil) thk 2 cm X 2 cm silicon solar cell with silicon monoxide (SiO) anti-reflection coating and Ti:Pd:Ag contacts • 305 μm (12 mil) thk fused silica (SiO_2) coverslide with indium oxide (In_2O_3) conductive coating • 4 indium-tin (50:50) solder #1 pads • 4 tin (Sn) plated 24-AWG copper (Cu) contact wires • Dow Corning 93-500 cell and coverslide adhesive
S-23	• 305 μm (12 mil) thk 2 cm X 2 cm silicon solar cell with silicon monoxide (SiO) anti-reflection coating and Ti:Pd:Ag contacts • 305 μm (12 mil) thk fused silica (SiO_2) coverslide with indium oxide (In_2O_3) conductive coating • 4 indium-silver (90:10) solder #3 pads • 4 tin (Sn) plated 24-AWG copper (Cu) contact wires • Dow Corning 93-500 cell and coverslide adhesive
S-24	• 305 μm (12 mil) thk 2 cm X 2 cm silicon solar cell with silicon monoxide (SiO) anti-reflection coating and Ti:Pd:Ag contacts • 305 μm (12 mil) thk fused silica (SiO_2) coverslide with indium oxide (In_2O_3) conductive coating • 4 Eccobond 56C (w/10% toluene solvent) pads • 4 unplated 24-AWG copper (Cu) contact wires • Dow Corning 93-500 cell and coverslide adhesive
S-25	• 305 μm (12 mil) thk 2 cm X 2 cm silicon solar cell with silicon monoxide (SiO) anti-reflection coating and Ti:Pd:Ag contacts • 305 μm (12 mil) thk fused silica (SiO_2) coverslide with indium oxide (In_2O_3) conductive coating • 4 Eccobond 56C (w/10% alcohol solvent) pads • 4 unplated 24-AWG copper (Cu) contact wires • Dow Corning 93-500 cell and coverslide adhesive

SAMPLE Solar Array Materials Passive LDEF Experiment	**page** 6 **of** 6 **date:** September 13, 1994
LDEF EXPT #: A0171 **ROW:** 8 **BAY:** A **EXPT SUB-ELEMENT:** NASA GSFC module	**document title:** S-TYPE SCAs DATA [as-built, as-flown]

cell ID	CONFIGURATION & MATERIALS
S-26	• 305 µm (12 mil) thk 2 cm X 2 cm silicon solar cell with silicon monoxide (SiO) anti-reflection coating and Ti:Pd:Ag contacts • 305 µm (12 mil) thk fused silica (SiO_2) coverslide with indium oxide (In_2O_3) conductive coating • 4 Eccobond 56C-H (w/10% toluene solvent) pads • 4 unplated 24-AWG copper (Cu) contact wires • Dow Corning 93-500 cell and coverslide adhesive
S-27	• 305 µm (12 mil) thk 2 cm X 2 cm silicon solar cell with silicon monoxide (SiO) anti-reflection coating and Ti:Pd:Ag contacts • 305 µm (12 mil) thk fused silica (SiO_2) coverslide with indium oxide (In_2O_3) conductive coating • 4 indium-tin (50:50) solder #1 pads • 4 tin (Sn) plated 24-AWG copper (Cu) contact wires • Dow Corning 93-500 cell and coverslide adhesive
S-28	• 305 µm (12 mil) thk 2 cm X 2 cm silicon solar cell with silicon monoxide (SiO) anti-reflection coating and Ti:Pd:Ag contacts • 305 µm (12 mil) thk fused silica (SiO_2) coverslide with indium oxide (In_2O_3) conductive coating • 4 indium-silver (90:10) solder #3 pads • 4 tin (Sn) plated 24-AWG copper (Cu) contact wires • Dow Corning 93-500 cell and coverslide adhesive

SAMPLE Solar Array Materials Passive LDEF Experiment	page 1 of 5 date: September 13, 1994
LDEF EXPT #: A0171 **ROW:** 8 **BAY:** A **EXPT SUB-ELEMENT:** NASA GSFC module	**document:** LD-TYPE SCAs DATA [as-built, as-flown]

Cell ID	CONFIGURATION & MATERIALS		
LD-1	• CELL	type	2 cm X 6 cm K-6.5 silicon
		thk	305 μm (12 mil)
		AR coating	Ta_2O_5
		contacts	Ti:Pd:Ag
		busbars	silver (Ag) mesh
	• COVERSLIDE	material	NO
		thk	n/a
		AR coating	n/a
		UV filter	n/a
	• ADHESIVES	coverslide-to-cell	NO
		cell-to-faceplate	Dow Corning 93-500
LD-2	• CELL	type	2 cm X 6 cm K-6.5 silicon
		thk	305 μm (12 mil)
		AR coating	Ta_2O_5
		contacts	Ti:Pd:Ag
		busbars	silver (Ag) mesh
	• COVERSLIDE	material	fused silica (SiO_2)
		thk	305 μm (12 mil)
		AR coating	MgF_2
		UV filter	YES
	• ADHESIVES	coverslide-to-cell	Dow Corning 93-500
		cell-to-faceplate	Dow Corning 93-500
LD-3	• CELL	type	2 cm X 6 cm K-6.5 silicon
		thk	305 μm (12 mil)
		AR coating	Ta_2O_5
		contacts	Ti:Pd:Ag
		busbars	silver (Ag) mesh
	• COVERSLIDE	material	fused silica (SiO_2)
		thk	152 μm (6 mil)
		AR coating	MgF_2
		UV filter	YES
	• ADHESIVES	coverslide-to-cell	Dow Corning 93-500
		cell-to-faceplate	Dow Corning 93-500

SAMPLE Solar Array Materials Passive LDEF Experiment	page 2 of 5 date: September 13, 1994
LDEF EXPT #: A0171 **ROW:** 8 **BAY:** A **EXPT SUB-ELEMENT:** NASA GSFC module	**document:** LD-TYPE SCAs DATA [as-built, as-flown]

Cell ID	CONFIGURATION & MATERIALS		
LD-4	• CELL	type	2 cm X 6 cm K-6.5 silicon
		thk	305 µm (12 mil)
		AR coating	Ta_2O_5
		contacts	Ti:Pd:Ag
		busbars	silver (Ag) mesh
	• COVERSLIDE	material	NO
		thk	n/a
		AR coating	n/a
		UV filter	n/a
	• ADHESIVES	coverslide-to-cell	NO
		cell-to-faceplate	Dow Corning 93-500
LD-5	• CELL	type	2 cm X 6 cm K-6.5 silicon
		thk	305 µm (12 mil)
		AR coating	Ta_2O_5
		contacts	Ti:Pd:Ag
		busbars	silver (Ag) mesh
	• COVERSLIDE	material	fused silica (SiO_2)
		thk	1.02 mm (40 mil)
		AR coating	MgF_2
		UV filter	YES
	• ADHESIVES	coverslide-to-cell	Dow Corning 93-500
		cell-to-faceplate	Dow Corning 93-500
LD-6	• CELL	type	2 cm X 6 cm K-6.5 silicon
		thk	305 µm (12 mil)
		AR coating	Ta_2O_5
		contacts	Ti:Pd:Ag
		busbars	silver (Ag) mesh
	• COVERSLIDE	material	fused silica (SiO_2)
		thk	152 µm (6 mil)
		AR coating	MgF_2
		UV filter	YES
	• ADHESIVES	coverslide-to-cell	Dow Corning 93-500
		cell-to-faceplate	Dow Corning 93-500

Cell ID	CONFIGURATION & MATERIALS		
LD-7	• CELL	type	2 cm X 6 cm K-6.5 silicon
		thk	305 μm (12 mil)
		AR coating	Ta_2O_5
		contacts	Ti:Pd:Ag
		busbars	silver (Ag) mesh
	• COVERSLIDE	material	fused silica (SiO_2)
		thk	152 μm (6 mil)
		AR coating	MgF_2
		UV filter	YES
	• ADHESIVES	coverslide-to-cell	Dow Corning 93-500
		cell-to-faceplate	Dow Corning 93-500
LD-8	• CELL	type	2 cm X 6 cm K-6.5 silicon
		thk	305 μm (12 mil)
		AR coating	Ta_2O_5
		contacts	Ti:Pd:Ag
		busbars	silver (Ag) mesh
	• COVERSLIDE	material	fused silica (SiO_2)
		thk	1.02 mm (40 mil)
		AR coating	MgF_2
		UV filter	YES
	• ADHESIVES	coverslide-to-cell	Dow Corning 93-500
		cell-to-faceplate	Dow Corning 93-500
LD-9	• CELL	type	2 cm X 6 cm K-6.5 silicon
		thk	305 μm (12 mil)
		AR coating	Ta_2O_5
		contacts	Ti:Pd:Ag
		busbars	silver (Ag) mesh
	• COVERSLIDE	material	fused silica (SiO_2)
		thk	305 μm (12 mil)
		AR coating	MgF_2
		UV filter	YES
	• ADHESIVES	coverslide-to-cell	Dow Corning 93-500
		cell-to-faceplate	Dow Corning 93-500

Cell ID	CONFIGURATION & MATERIALS		
LD-10	• CELL	type	2 cm X 6 cm K-6.5 silicon
		thk	305 μm (12 mil)
		AR coating	Ta_2O_5
		contacts	Ti:Pd:Ag
		busbars	silver (Ag) mesh
	• COVERSLIDE	material	fused silica (SiO_2)
		thk	152 μm (6 mil)
		AR coating	MgF_2
		UV filter	YES
	• ADHESIVES	coverslide-to-cell	Dow Corning 93-500
		cell-to-faceplate	Dow Corning 93-500
LD-11	• CELL	type	2 cm X 6 cm K-6.5 silicon
		thk	305 μm (12 mil)
		AR coating	Ta_2O_5
		contacts	Ti:Pd:Ag
		busbars	silver (Ag) mesh
	• COVERSLIDE	material	fused silica (SiO_2)
		thk	1.02 mm (40 mil)
		AR coating	MgF_2
		UV filter	NO
	• ADHESIVES	coverslide-to-cell	Dow Corning 93-500
		cell-to-faceplate	Dow Corning 93-500
LD-12	• CELL	type	2 cm X 6 cm K-6.5 silicon
		thk	305 μm (12 mil)
		AR coating	Ta_2O_5
		contacts	Ti:Pd:Ag
		busbars	silver (Ag) mesh
	• COVERSLIDE	material	fused silica (SiO_2)
		thk	1.02 mm (40 mil)
		AR coating	MgF_2
		UV filter	YES
	• ADHESIVES	coverslide-to-cell	Dow Corning 93-500
		cell-to-faceplate	Dow Corning 93-500

Cell ID	CONFIGURATION & MATERIALS		
LD-13	• CELL	type	2 cm X 6 cm K-6.5 silicon
		thk	305 µm (12 mil)
		AR coating	Ta_2O_5
		contacts	Ti:Pd:Ag
		busbars	silver (Ag) mesh
	• COVERSLIDE	material	fused silica (SiO_2)
		thk	305 µm (12 mil)
		AR coating	MgF_2
		UV filter	YES
	• ADHESIVES	coverslide-to-cell	Dow Corning 93-500
		cell-to-faceplate	Dow Corning 93-500
LD-14	• CELL	type	2 cm X 6 cm K-6.5 silicon
		thk	305 µm (12 mil)
		AR coating	Ta_2O_5
		contacts	Ti:Pd:Ag
		busbars	silver (Ag) mesh
	• COVERSLIDE	material	fused silica (SiO_2)
		thk	1.02 mm (40 mil)
		AR coating	MgF_2
		UV filter	NO
	• ADHESIVES	coverslide-to-cell	Dow Corning 93-500
		cell-to-faceplate	Dow Corning 93-500
LD-15	• CELL	type	2 cm X 6 cm K-6.5 silicon
		thk	305 µm (12 mil)
		AR coating	Ta_2O_5
		contacts	Ti:Pd:Ag
		busbars	silver (Ag) mesh
	• COVERSLIDE	material	fused silica (SiO_2)
		thk	1.02 mm (40 mil)
		AR coating	MgF_2
		UV filter	YES
	• ADHESIVES	coverslide-to-cell	Dow Corning 93-500
		cell-to-faceplate	Dow Corning 93-500

Space Power Institute

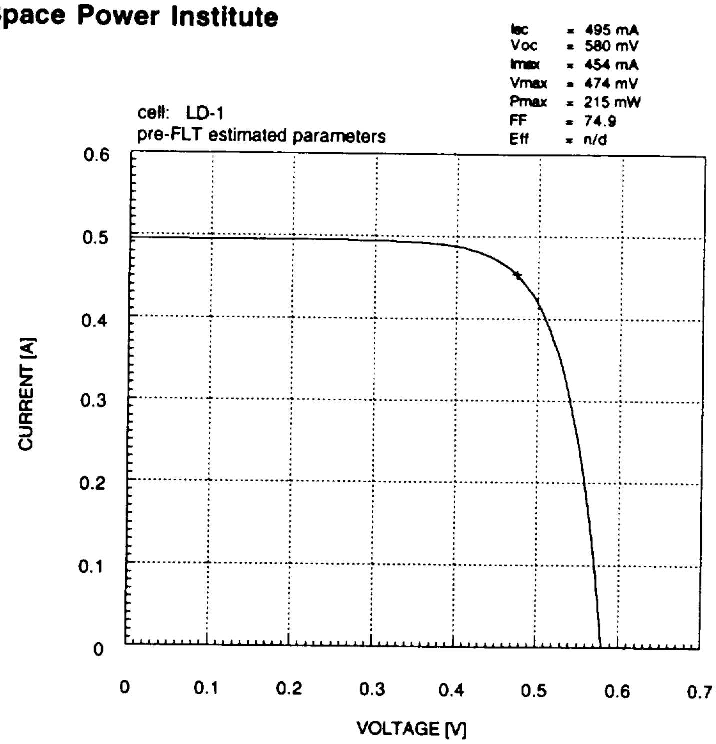

Space Power Institute

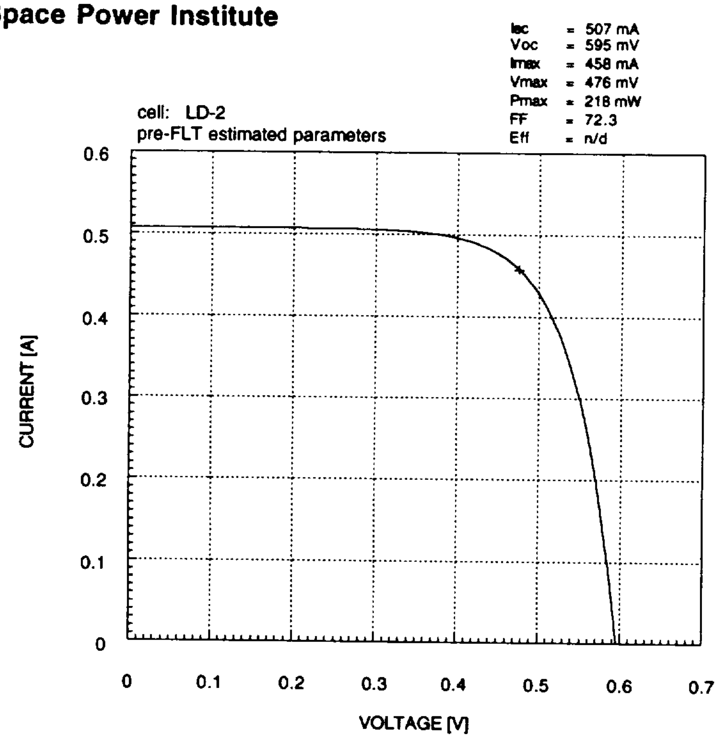

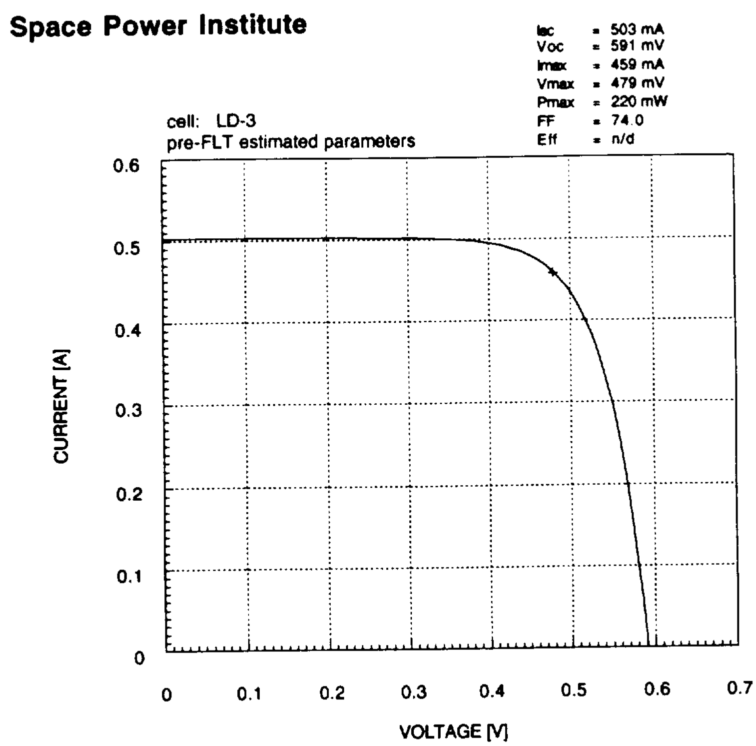
Space Power Institute
Isc = 503 mA
Voc = 591 mV
Imax = 459 mA
Vmax = 479 mV
Pmax = 220 mW
FF = 74.0
Eff = n/d
cell: LD-3
pre-FLT estimated parameters
CURRENT [A]
VOLTAGE [V]
0.6
0.5
0.4
0.3
0.2
0.1
0
0
0.1
0.2
0.3
0.4
0.5
0.6
0.7

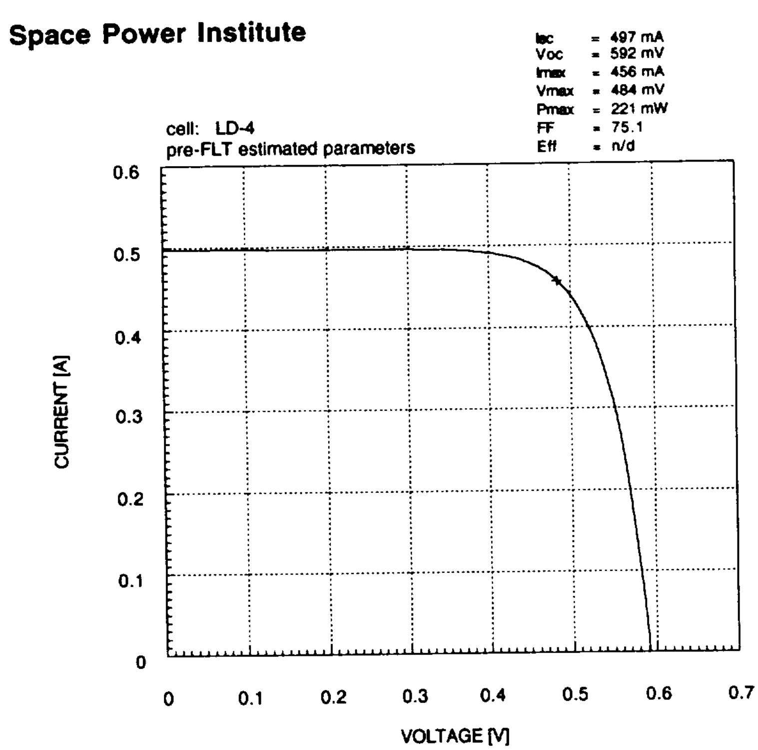
Space Power Institute
Isc = 497 mA
Voc = 592 mV
Imax = 456 mA
Vmax = 484 mV
Pmax = 221 mW
FF = 75.1
Eff = n/d
cell: LD-4
pre-FLT estimated parameters
CURRENT [A]
VOLTAGE [V]
0.6
0.5
0.4
0.3
0.2
0.1
0
0
0.1
0.2
0.3
0.4
0.5
0.6
0.7

Space Power Institute

Isc = 511 mA
Voc = 594 mV
Imax = 462 mA
Vmax = 476 mV
Pmax = 220 mW
FF = 72.5
Eff = n/d

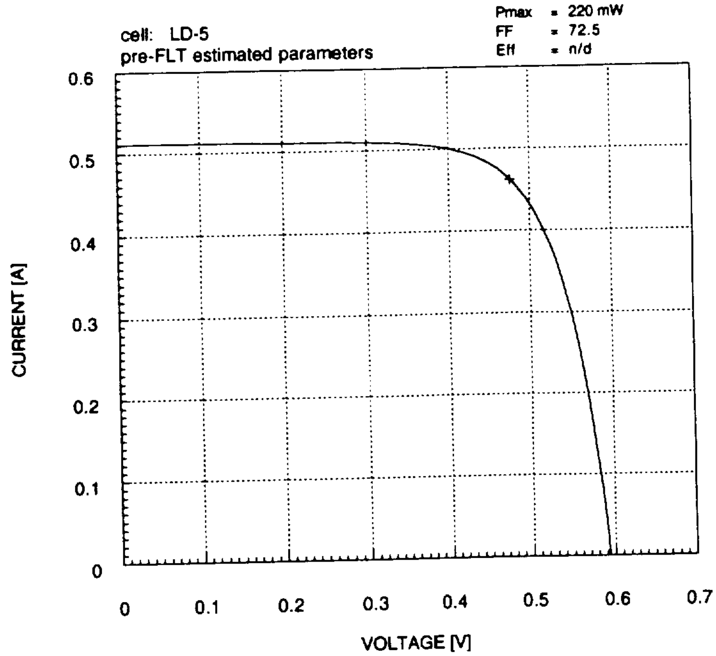

Space Power Institute

Isc = 507 mA
Voc = 587 mV
Imax = 467 mA
Vmax = 482 mV
Pmax = 225 mW
FF = 75.6
Eff = n/d

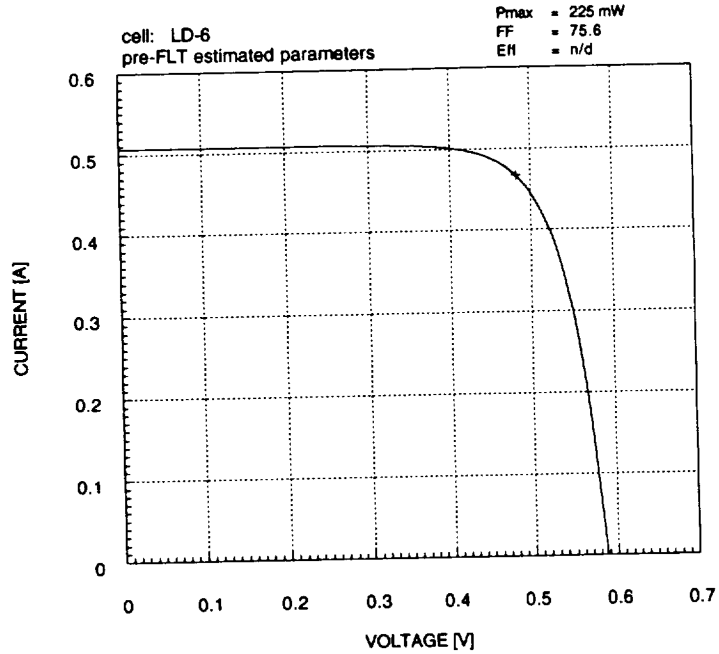

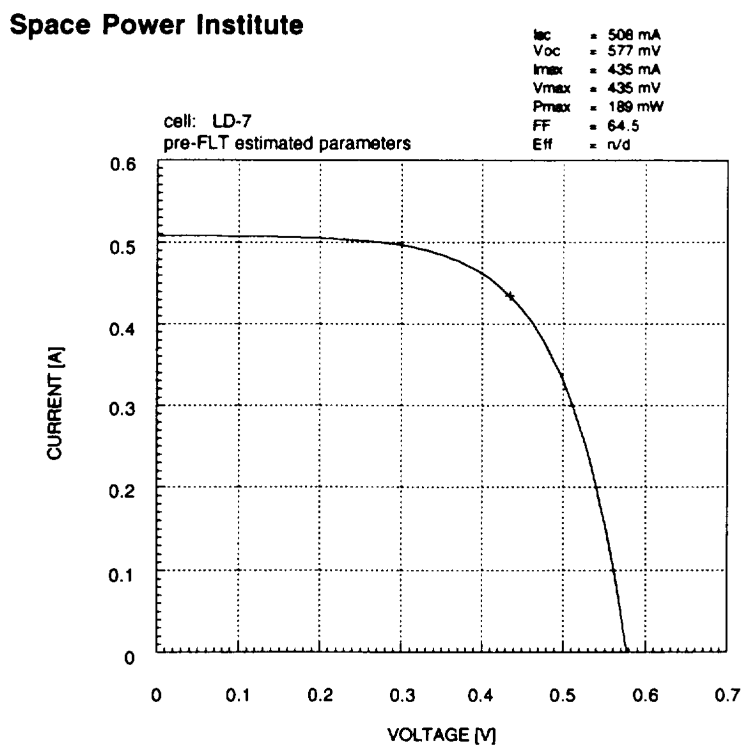
Space Power Institute
Isc = 508 mA
Voc = 577 mV
Imax = 435 mA
Vmax = 435 mV
Pmax = 189 mW
FF = 64.5
Eff = n/d
cell: LD-7
pre-FLT estimated parameters
CURRENT [A]
0.6
0.5
0.4
0.3
0.2
0.1
0
0
0.1
0.2
0.3
0.4
0.5
0.6
0.7
VOLTAGE [V]

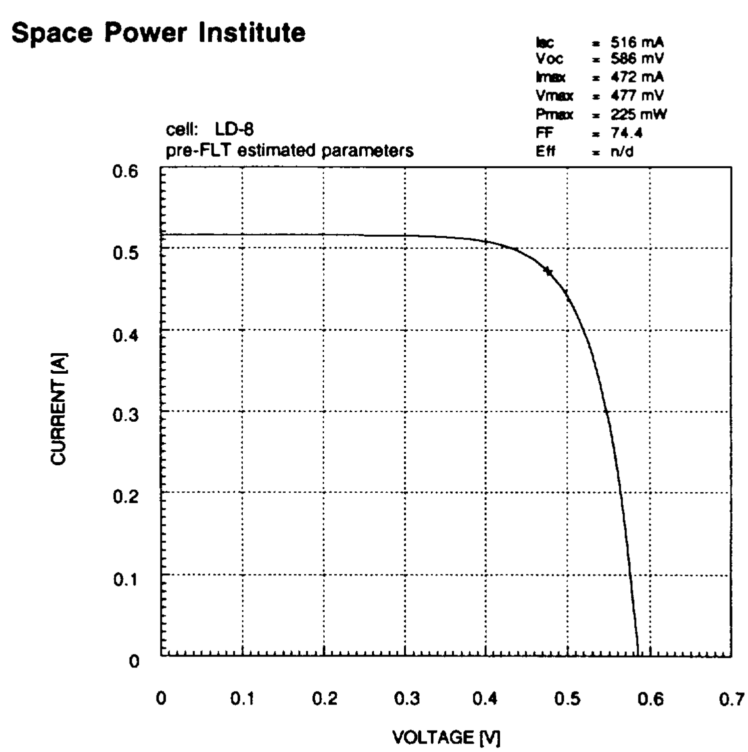
Space Power Institute
Isc = 516 mA
Voc = 586 mV
Imax = 472 mA
Vmax = 477 mV
Pmax = 225 mW
FF = 74.4
Eff = n/d
cell: LD-8
pre-FLT estimated parameters
CURRENT [A]
0.6
0.5
0.4
0.3
0.2
0.1
0
0
0.1
0.2
0.3
0.4
0.5
0.6
0.7
VOLTAGE [V]

Space Power Institute

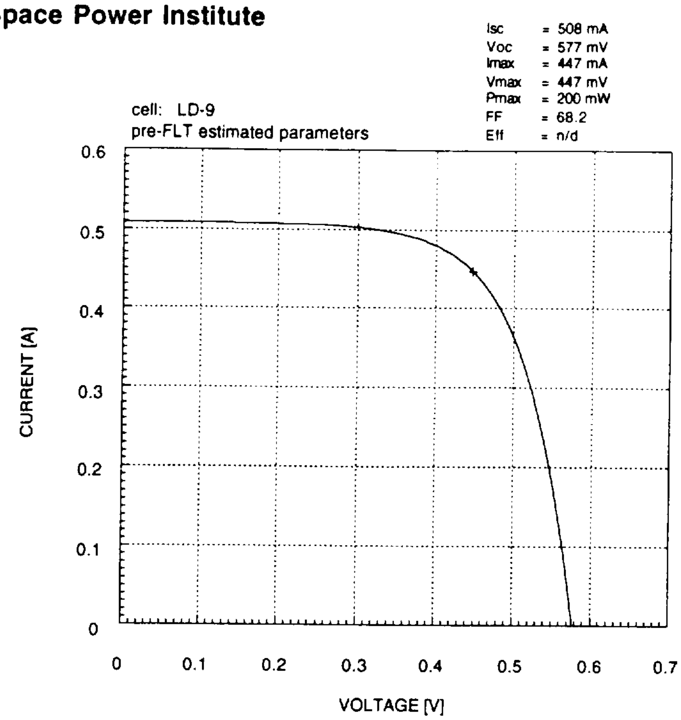

Space Power Institute

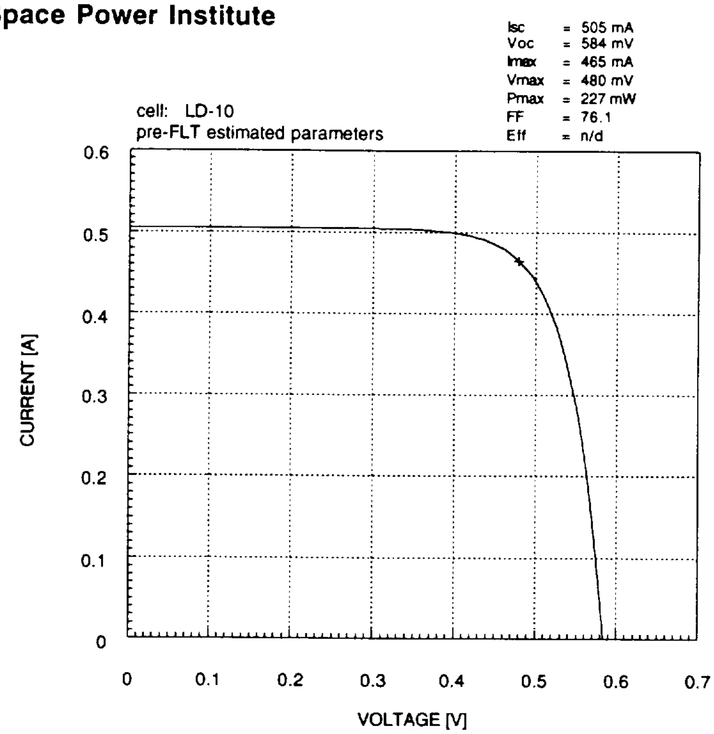

Space Power Institute

Isc = 519 mA
Voc = 593 mV
Imax = 478 mA
Vmax = 487 mV
Pmax = 233 mW
FF = 75.7
Eff = n/d

cell: LD-11
pre-FLT estimated parameters

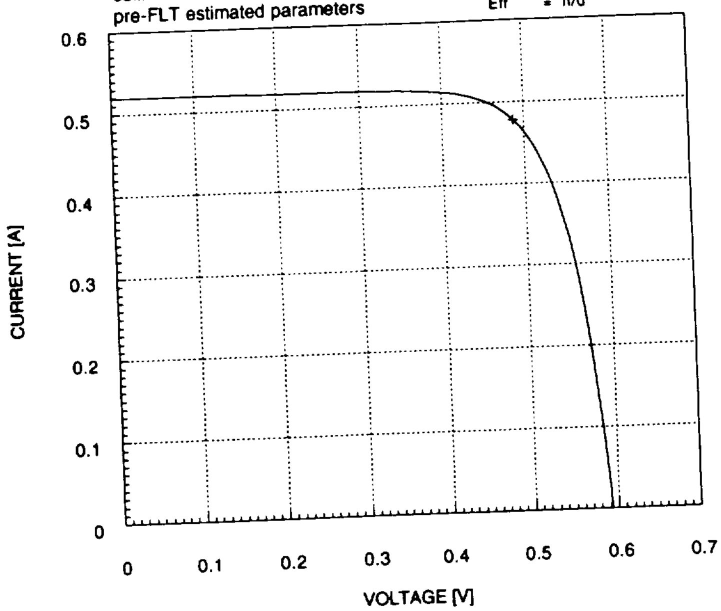

Space Power Institute

Isc = 521 mA
Voc = 591 mV
Imax = 478 mA
Vmax = 483 mV
Pmax = 231 mW
FF = 75.0
Eff = n/d

cell: LD-12
pre-FLT estimated parameters

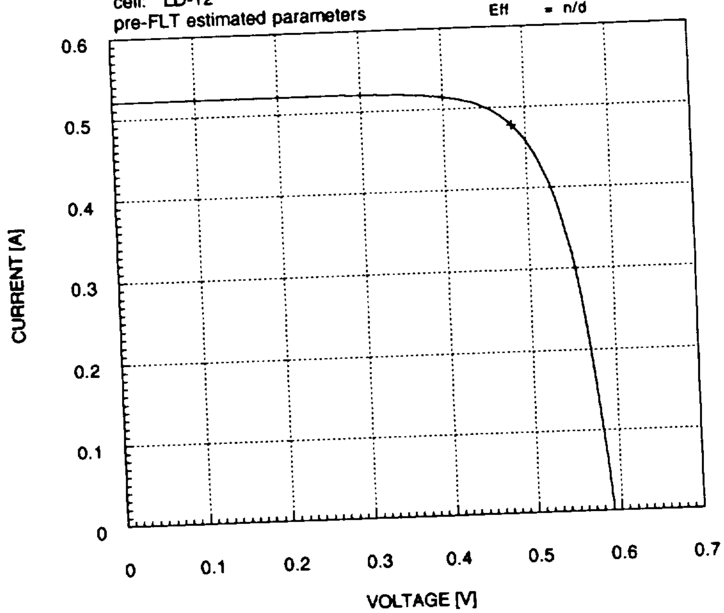

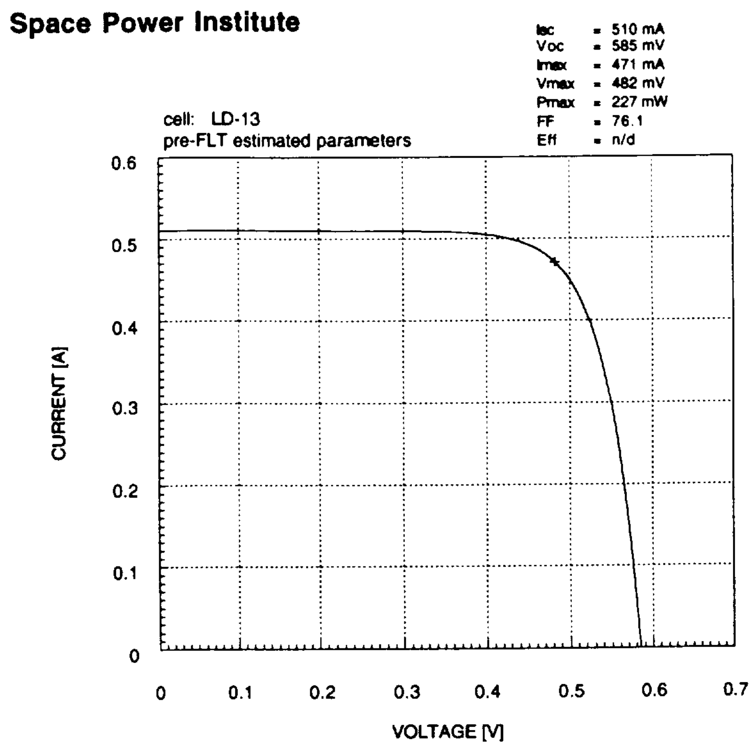

Space Power Institute
Isc = 510 mA
Voc = 585 mV
Imax = 471 mA
Vmax = 482 mV
Pmax = 227 mW
FF = 76.1
Eff = n/d
cell: LD-13
pre-FLT estimated parameters
0.6
0.5
0.4
0.3
0.2
0.1
0
CURRENT [A]
0
0.1
0.2
0.3
0.4
0.5
0.6
0.7
VOLTAGE [V]

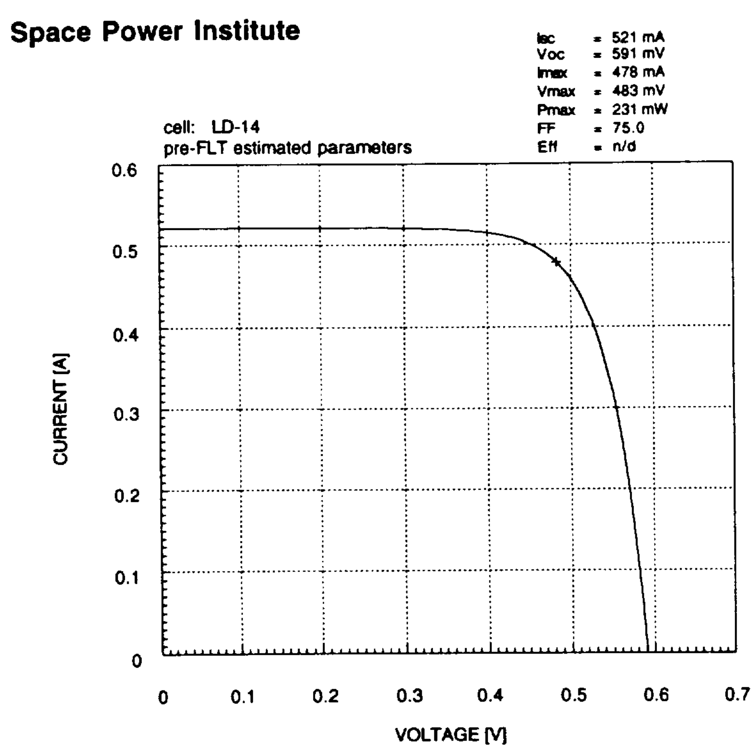

Space Power Institute
Isc = 521 mA
Voc = 591 mV
Imax = 478 mA
Vmax = 483 mV
Pmax = 231 mW
FF = 75.0
Eff = n/d
cell: LD-14
pre-FLT estimated parameters
0.6
0.5
0.4
0.3
0.2
0.1
0
CURRENT [A]
0
0.1
0.2
0.3
0.4
0.5
0.6
0.7
VOLTAGE [V]

Space Power Institute

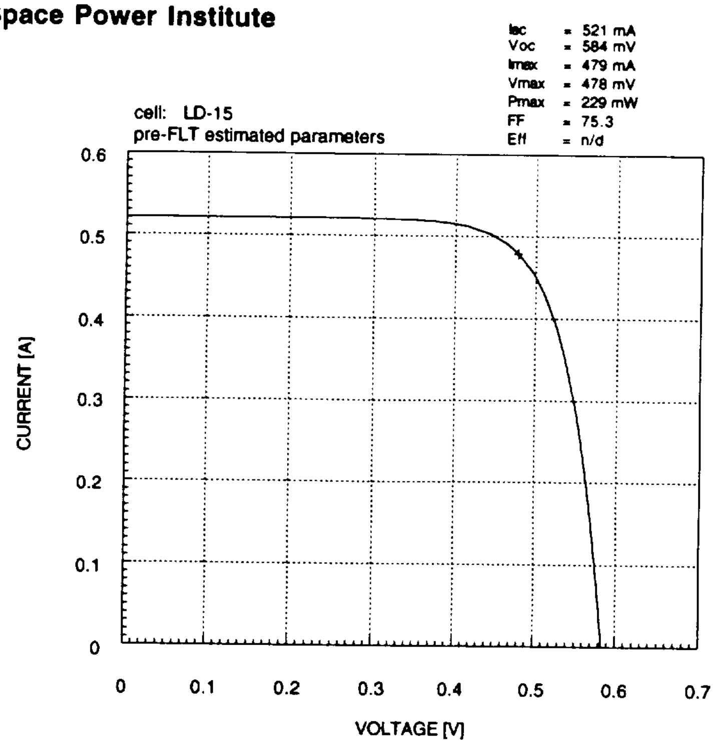

NASA

Lewis Research Center

Cell : LD-1
Date : 28 Jun 1994
Reference Cell : A-104
Area : 12 cm^2
Temperature : 25°C
Air Mass Zero
File Name : LD-1A.I_V

I_{sc} = -473.86 mA
V_{oc} = -450.9 mV
I_{max} = -356 mA
V_{max} = -309 mV
P_{max} = 110 mW
F.F. = 51.4
Eff. = 6.7 %

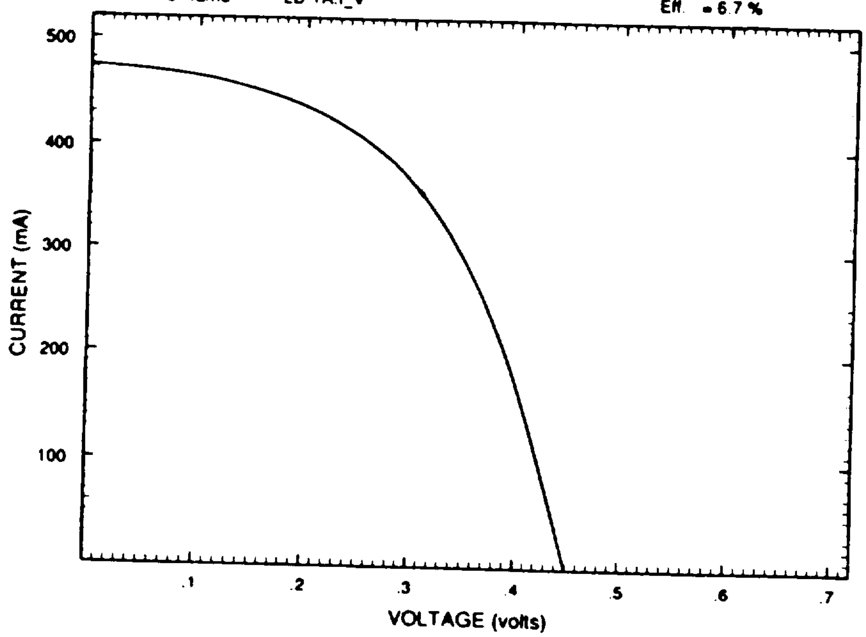

NASA

Lewis Research Center

Cell : LD-1
Date : 28 Jun 1994
Reference Cell : A-104
Area : 12 cm^2
Temperature : 25°C
Air Mass Zero
File Name : LD-1B.I_V

I_{sc} = -473.92 mA
V_{oc} = -447.5 mV
I_{max} = -357.2 mA
V_{max} = -304.6 mV
P_{max} = 108.8 mW
F.F. = 51.3
Eff. = 6.63 %

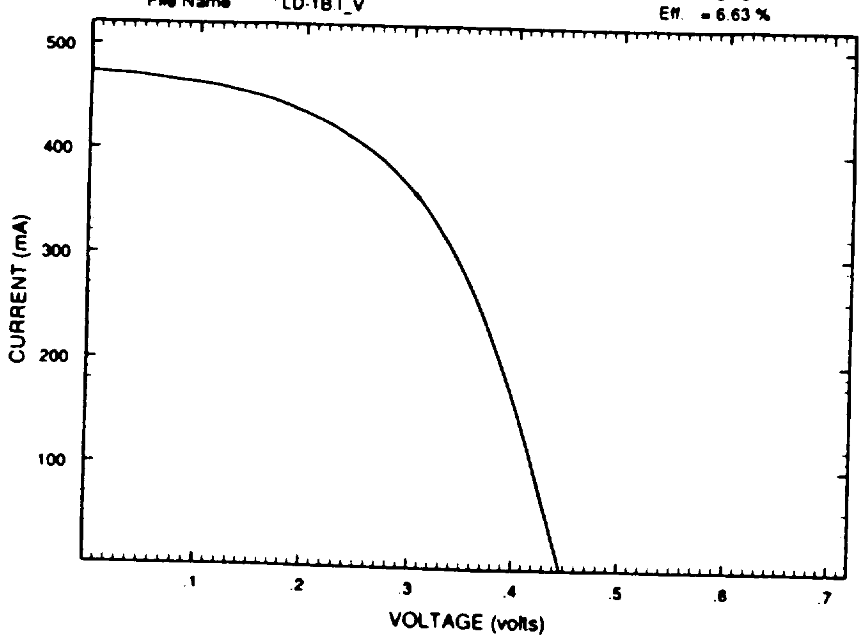

Lewis Research Center

Cell	LD-2
Date	28 Jun 1994
Reference Cell	A-104
Area	12 cm^2
Temperature	25°C
Air Mass Zero	
File Name	LD-2A.I_V

I_{sc} = -510 mA
V_{oc} = -580.6 mV
I_{max} = -465.3 mA
V_{max} = -461 mV
P_{max} = 214.5 mW
F.F. = 72.4
Eff. = 13.07 %

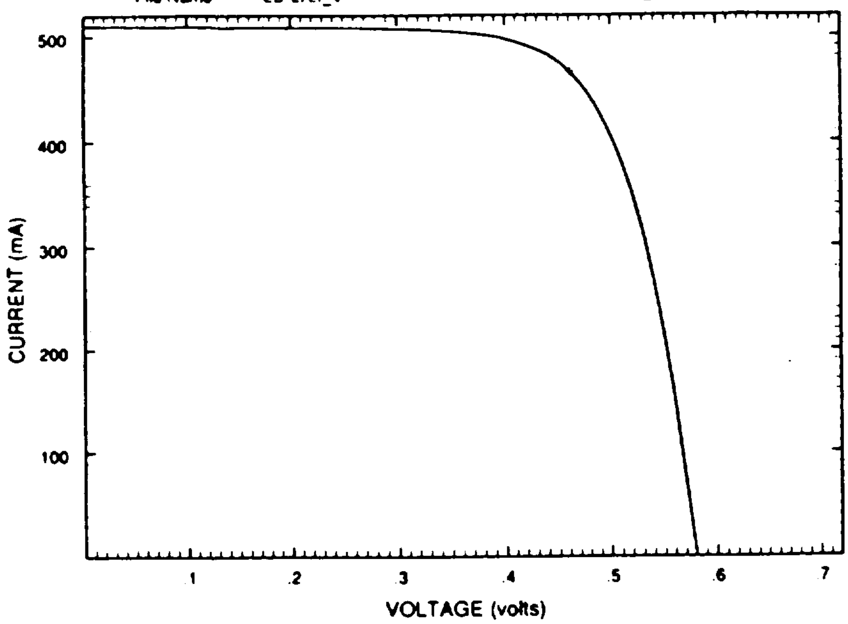

Lewis Research Center

Cell	LD-2
Date	28 Jun 1994
Reference Cell	A-104
Area	12 cm^2
Temperature	25°C
Air Mass Zero	
File Name	LD-2B.I_V

I_{sc} = -509.58 mA
V_{oc} = -579.7 mV
I_{max} = -462.6 mA
V_{max} = -462.9 mV
P_{max} = 214.1 mW
F.F. = 72.4
Eff. = 13.05 %

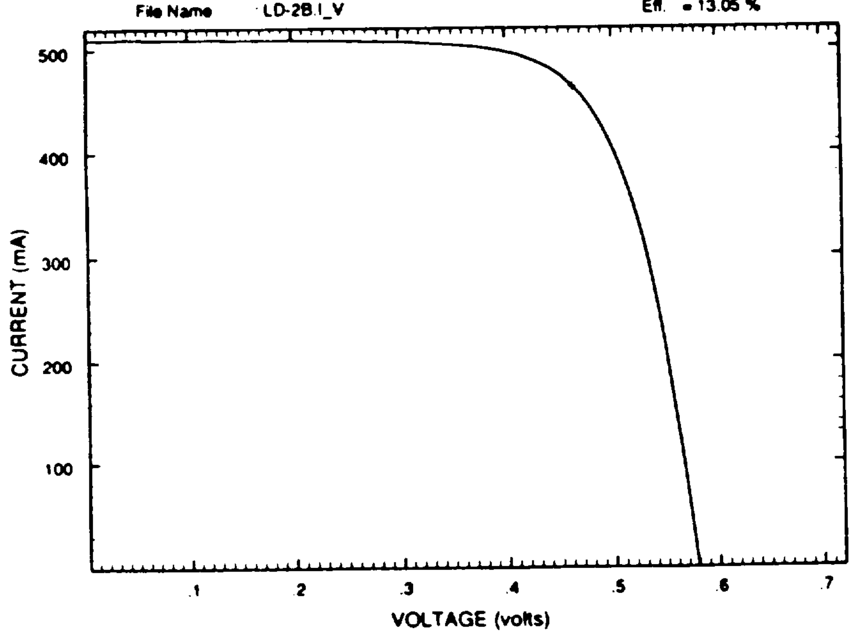

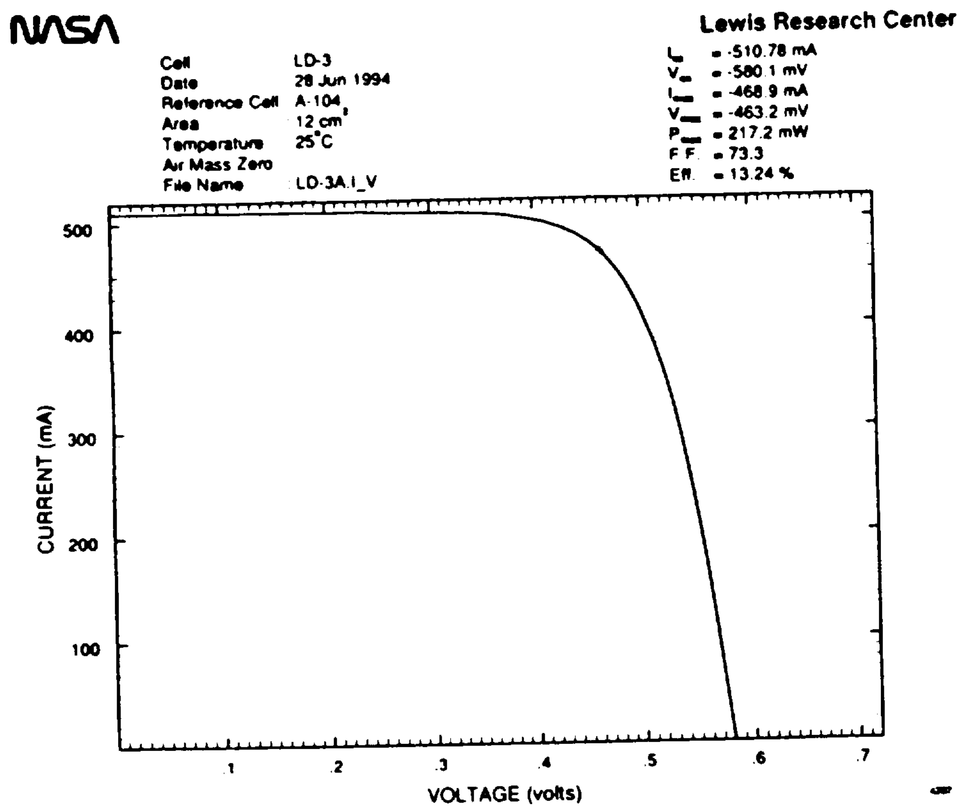
NASA
Lewis Research Center
Cell LD-3
Date 28 Jun 1994
Reference Cell A-104
Area 12 cm²
Temperature 25°C
Air Mass Zero
File Name LD-3A.I_V
Isc = -510.78 mA
Voc = -580.1 mV
Imax = -468.9 mA
Vmax = -463.2 mV
Pmax = 217.2 mW
F.F. = 73.3
Eff. = 13.24 %
CURRENT (mA)
500
400
300
200
100
.1
.2
.3
.4
.5
.6
.7
VOLTAGE (volts)

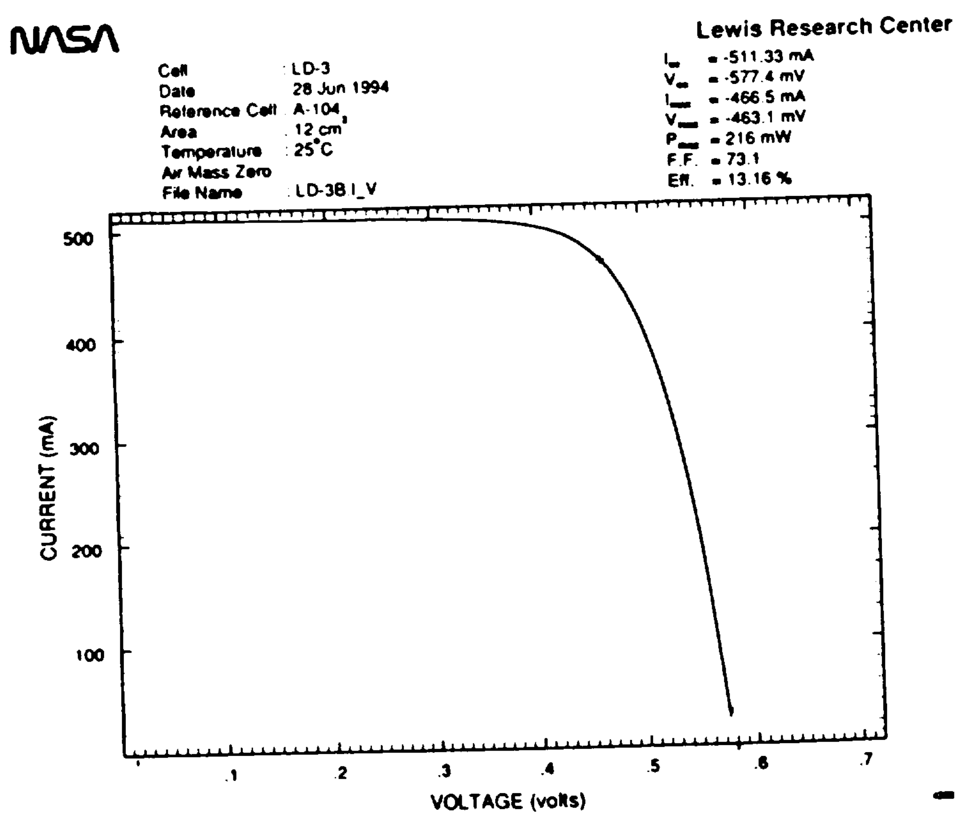
NASA
Lewis Research Center
Cell LD-3
Date 28 Jun 1994
Reference Cell A-104
Area 12 cm²
Temperature 25°C
Air Mass Zero
File Name LD-3B.I_V
Isc = -511.33 mA
Voc = -577.4 mV
Imax = -466.5 mA
Vmax = -463.1 mV
Pmax = 216 mW
F.F. = 73.1
Eff. = 13.16 %
CURRENT (mA)
500
400
300
200
100
.1
.2
.3
.4
.5
.6
.7
VOLTAGE (volts)

NASA

Lewis Research Center

Cell	LD-4	I_{sc}	= -469.76 mA
Date	28 Jun 1994	V_{oc}	= -445.2 mV
Reference Cell	A-104	I_{max}	= -407.4 mA
Area	12 cm^2	V_{max}	= -328.4 mV
Temperature	25°C	P_{max}	= 133.8 mW
Air Mass Zero		F.F.	= 63.9
File Name	LD-4B.I_V	Eff.	= 8.15 %

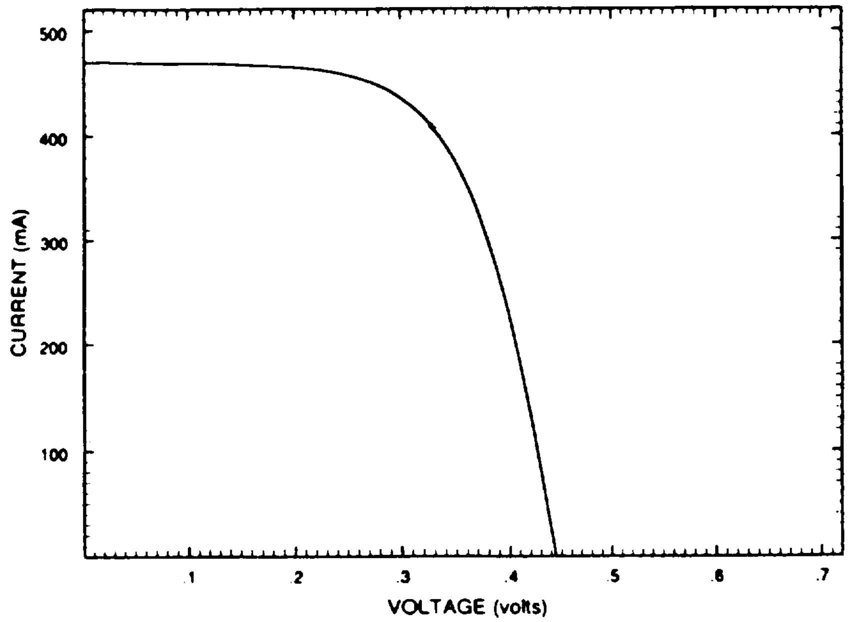

NASA

Lewis Research Center

Cell	LD-4	I_{sc}	= -469.74 mA
Date	28 Jun 1994	V_{oc}	= -449.9 mV
Reference Cell	A-104	I_{max}	= -411.4 mA
Area	12 cm^2	V_{max}	= -329.7 mV
Temperature	25°C	P_{max}	= 135.6 mW
Air Mass Zero		F.F.	= 64.1
File Name	LD-4A.I_V	Eff.	= 8.26 %

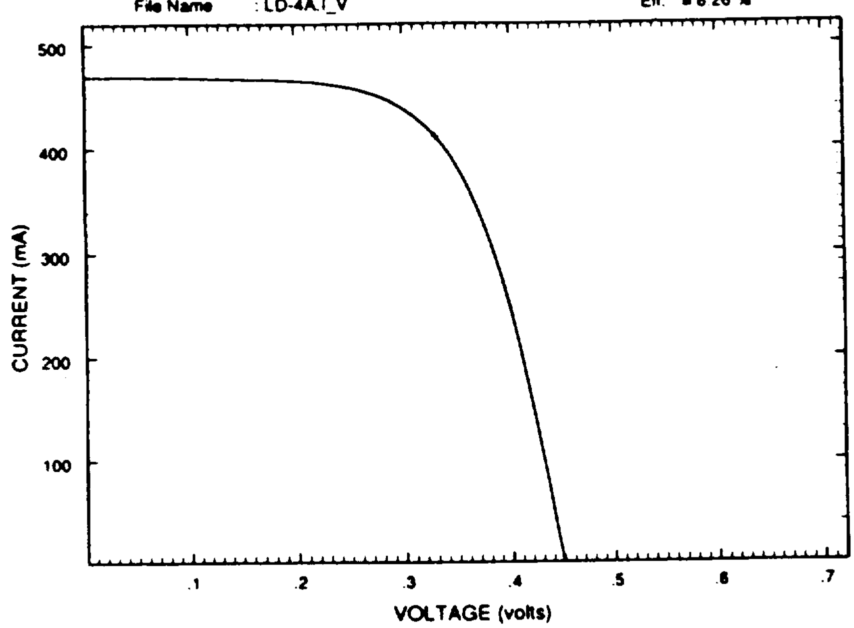

NASA

Lewis Research Center

Cell	LD-5
Date	28 Jun 1994
Reference Cell	A-104
Area	12 cm^2
Temperature	25°C
Air Mass Zero	
File Name	LD-5A.I_V

I_{sc}	= -512 68 mA
V_{oc}	= -581 9 mV
I_{max}	= -462 4 mA
V_{max}	= -466 1 mV
P_{max}	= 215 5 mW
F F	= 72 2
Eff	= 13.13 %

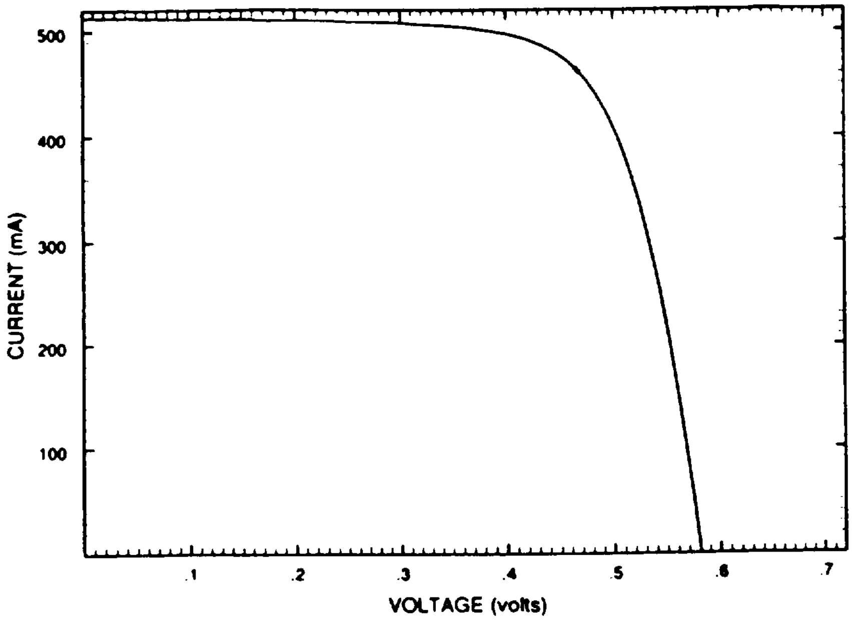

NASA

Lewis Research Center

Cell	LD-5
Date	28 Jun 1994
Reference Cell	A-104
Area	12 cm^2
Temperature	25°C
Air Mass Zero	
File Name	LD-5B.I_V

I_{sc}	= -513 5 mA
V_{oc}	= -579 mV
I_{max}	= -460.9 mA
V_{max}	= -465 3 mV
P_{max}	= 214 5 mW
F.F.	= 72.1
Eff.	= 13.07 %

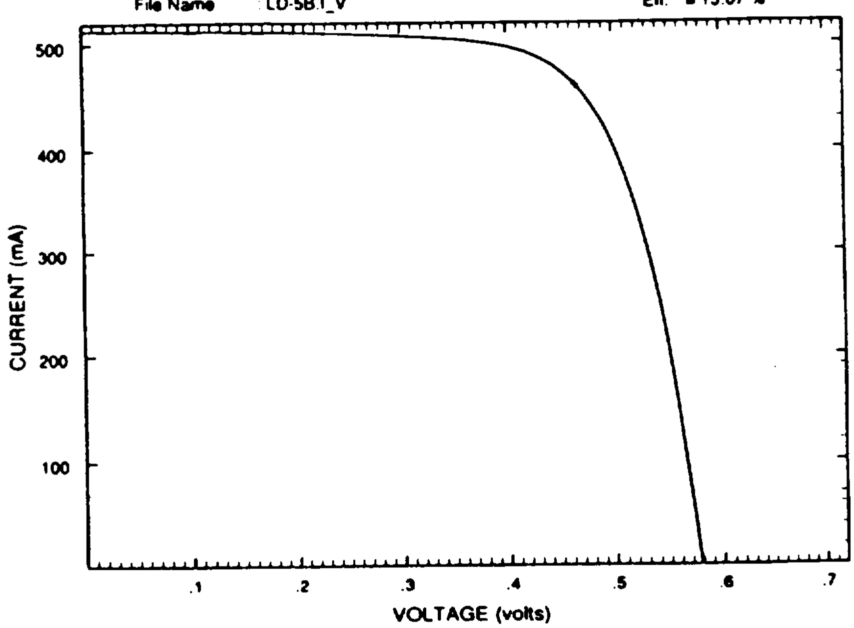

Lewis Research Center

Cell : LD-6
Date : 28 Jun 1994
Reference Cell : A-104
Area : 12 cm^2
Temperature : 25°C
Air Mass Zero
File Name : LD-6A.I_V

I_{sc} = -509.05 mA
V_{oc} = -579.8 mV
I_{max} = -474.3 mA
V_{max} = -469.3 mV
P_{max} = 222.6 mW
F.F. = 75.4
Eff. = 13.57 %

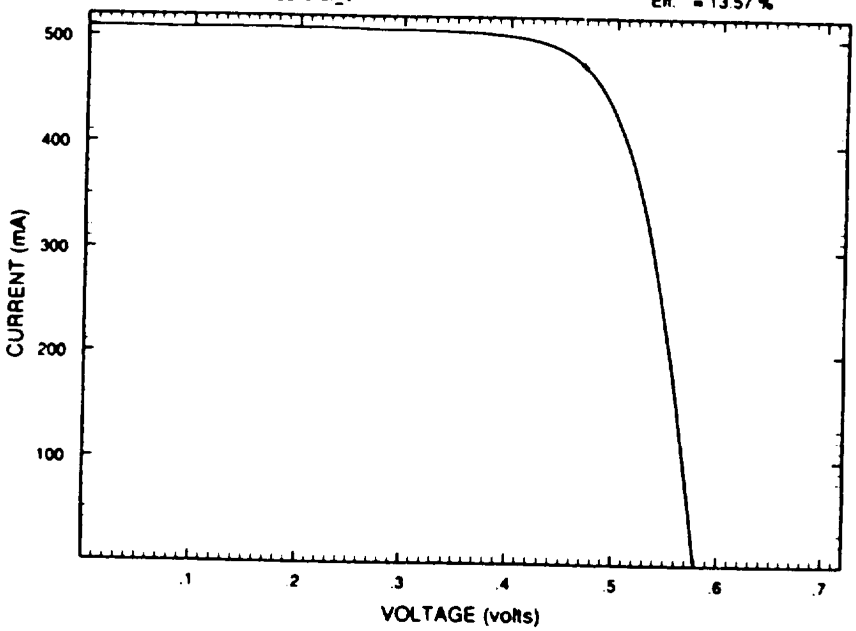

Lewis Research Center

Cell : LD-6
Date : 28 Jun 1994
Reference Cell : A-104
Area : 12 cm^2
Temperature : 25°C
Air Mass Zero
File Name : LD-6B.I_V

I_{sc} = -509 mA
V_{oc} = -577.5 mV
I_{max} = -473.4 mA
V_{max} = -468 mV
P_{max} = 221.5 mW
F.F. = 75.3
Eff. = 13.5 %

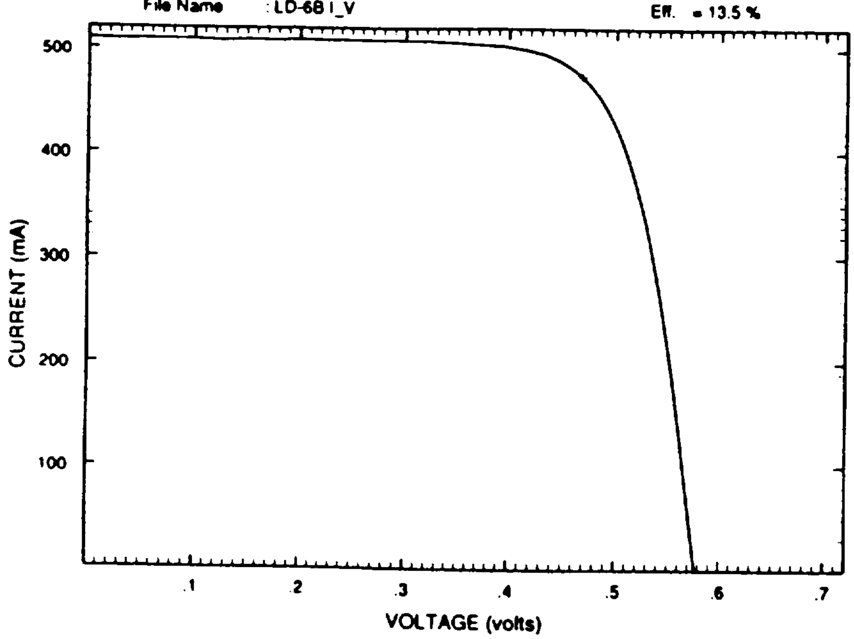

NASA

Lewis Research Center

Cell	LD-7	I_{sc}	= -508.28 mA
Date	28 Jun 1994	V_{oc}	= -569.3 mV
Reference Cell	A-104	I_{max}	= -426.2 mA
Area	12 cm^2	V_{max}	= -430.4 mV
Temperature	25°C	P_{max}	= 183.5 mW
Air Mass Zero		F.F.	= 63.4
File Name	LD-7A.I_V	Eff.	= 11.18 %

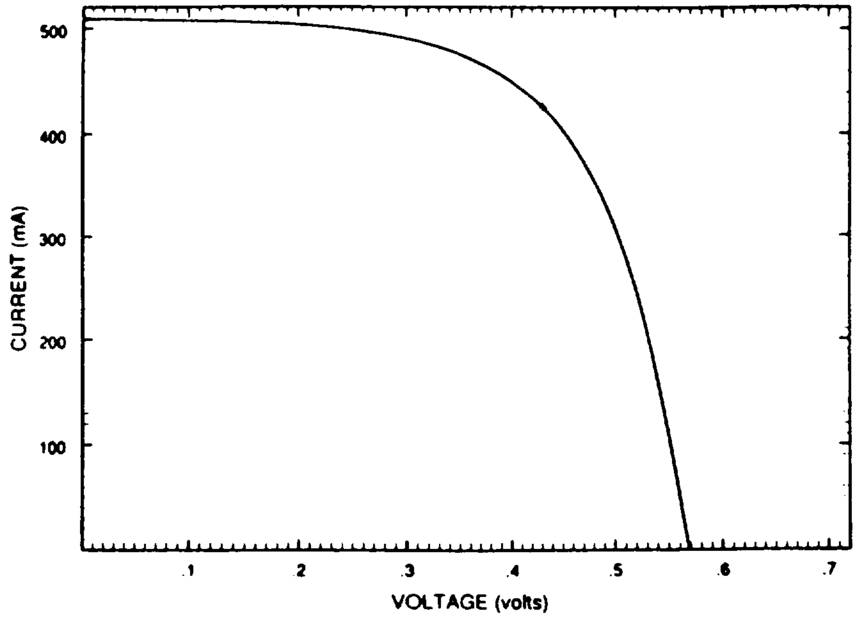

NASA

Lewis Research Center

Cell	: LD-7	I_{sc}	= -508.41 mA
Date	: 28 Jun 1994	V_{oc}	= -567.2 mV
Reference Cell	A-104	I_{max}	= -424.1 mA
Area	12 cm^2	V_{max}	= -430.5 mV
Temperature	25°C	P_{max}	= 182.6 mW
Air Mass Zero		F.F.	= 63.3
File Name	: LD-7B.I_V	Eff.	= 11.12 %

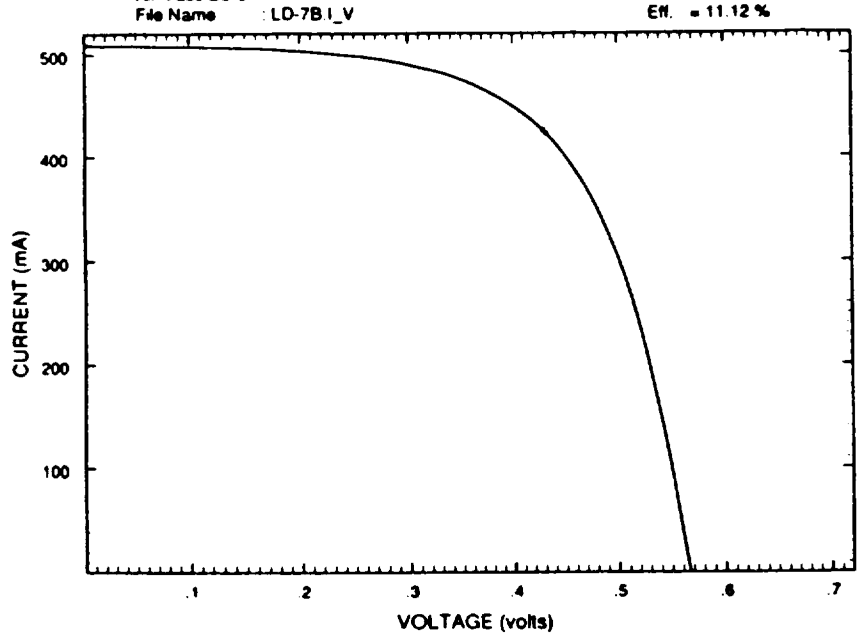

NASA

Lewis Research Center

Cell	LD-8
Date	28 Jun 1994
Reference Cell	A-104
Area	12 cm^2
Temperature	25°C
Air Mass Zero	
File Name	LD-8A.I_V

I_{sc} = -510.29 mA
V_{oc} = -572.9 mV
I_{max} = -464.2 mA
V_{max} = -466 mV
P_{max} = 216.3 mW
F.F. = 73.9
Eff = 13.18 %

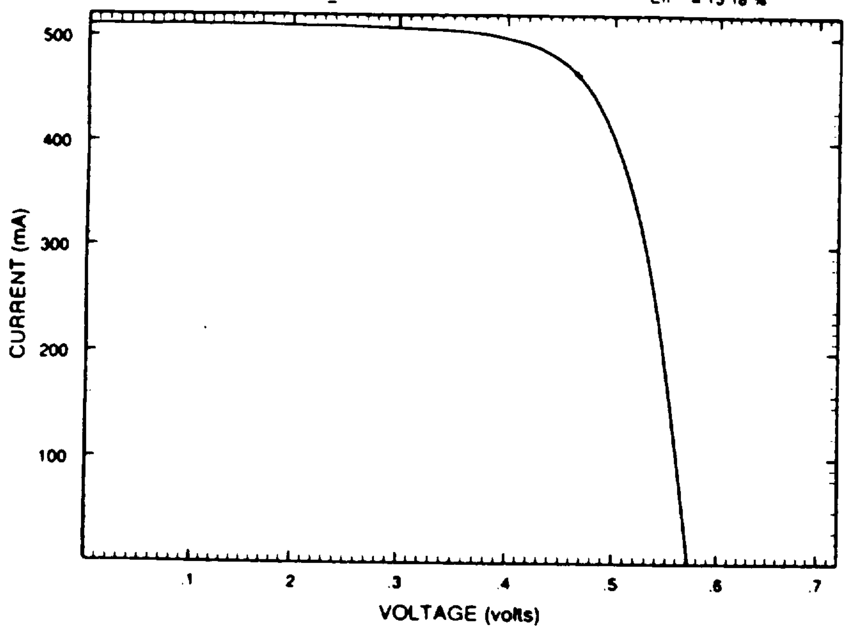

NASA

Lewis Research Center

Cell	LD-8
Date	28 Jun 1994
Reference Cell	A-104
Area	12 cm^2
Temperature	25°C
Air Mass Zero	
File Name	LD-8B.I_V

I_{sc} = -510.11 mA
V_{oc} = -570.6 mV
I_{max} = -468.8 mA
V_{max} = -459.2 mV
P_{max} = 215.3 mW
F.F. = 73.9
Eff. = 13.12 %

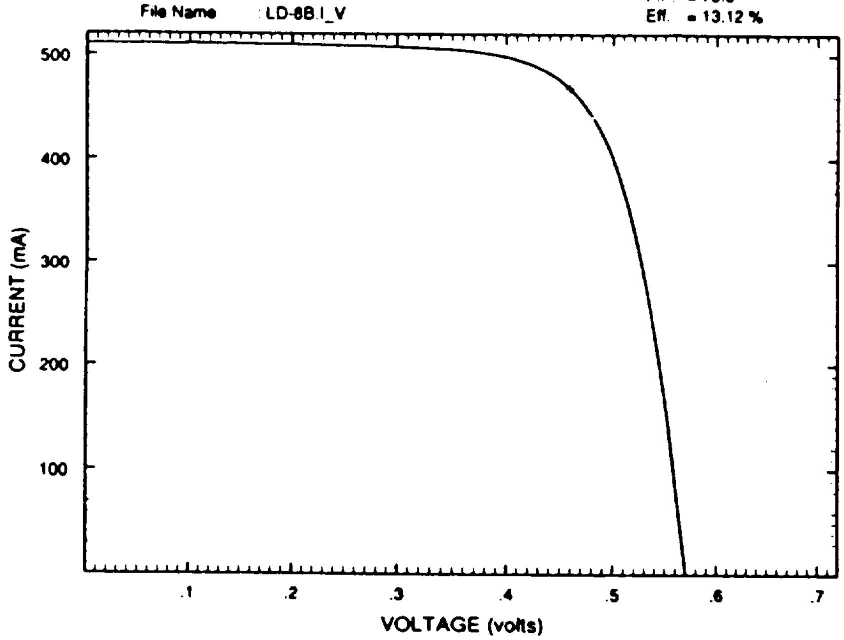

NASA

Lewis Research Center

Cell	LD-9
Date	28 Jun 1994
Reference Cell	A-104
Area	12 cm^2
Temperature	25°C
Air Mass Zero	
File Name	LD-9A I_V

I_{sc}	= -501.65 mA
V_{oc}	= -567.7 mV
I_{max}	= -437.2 mA
V_{max}	= -441 mV
P_{max}	= 192.8 mW
F.F.	= 67.6
Eff	= 11.75 %

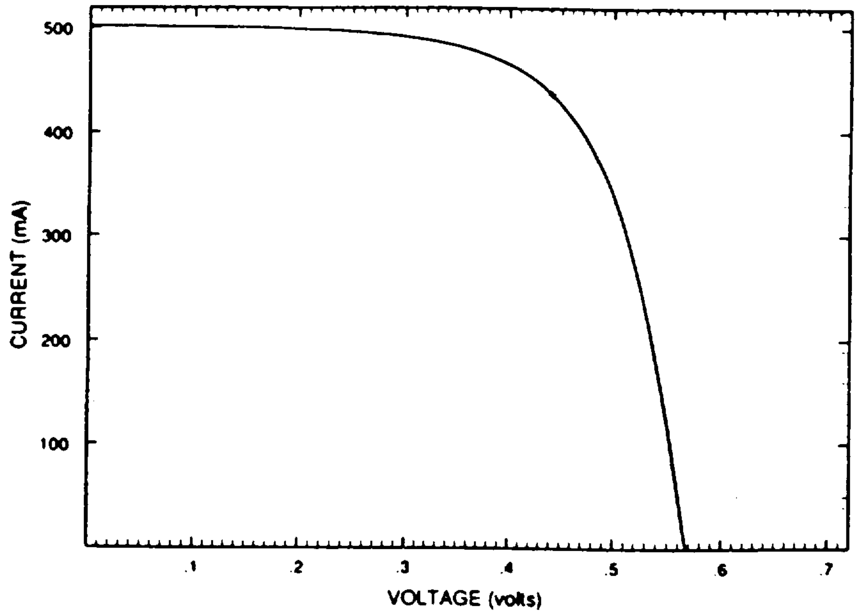

NASA

Lewis Research Center

Cell	LD-9
Date	28 Jun 1994
Reference Cell	A-104
Area	12 cm^2
Temperature	25°C
Air Mass Zero	
File Name	LD-9B I_V

I_{sc}	= -501.69 mA
V_{oc}	= -565.2 mV
I_{max}	= -433.4 mA
V_{max}	= -442.7 mV
P_{max}	= 191.9 mW
F.F.	= 67.6
Eff.	= 11.69 %

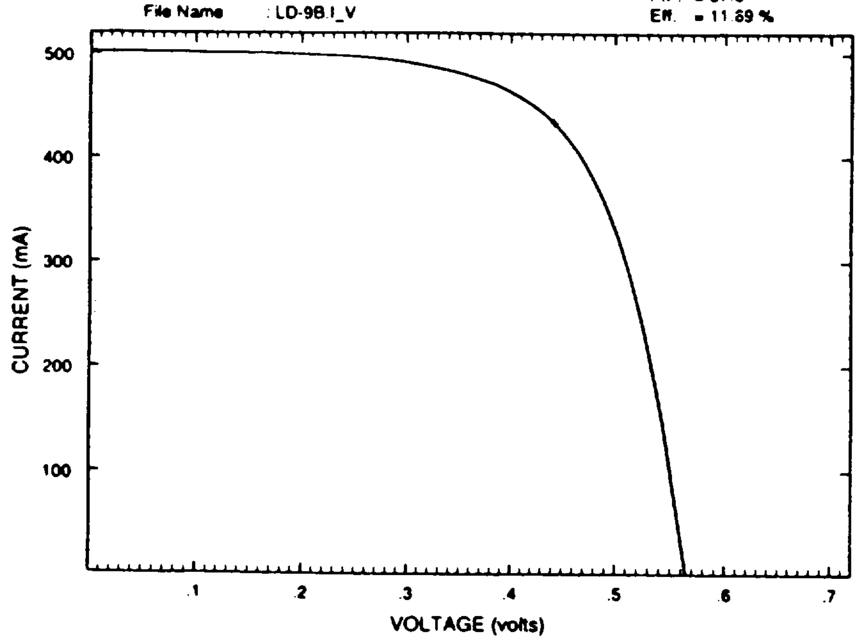

NASA

Cell	LD-10
Date	28 Jun 1994
Reference Cell	A-104
Area	12 cm^2
Temperature	25°C
Air Mass Zero	
File Name	LD-10A.I_V

Lewis Research Center

I_{sc} = -508.67 mA
V_{oc} = -570.4 mV
I_{max} = -475.6 mA
V_{max} = -458.7 mV
P_{max} = 218.2 mW
F.F. = 75.1
Eff. = 13.29 %

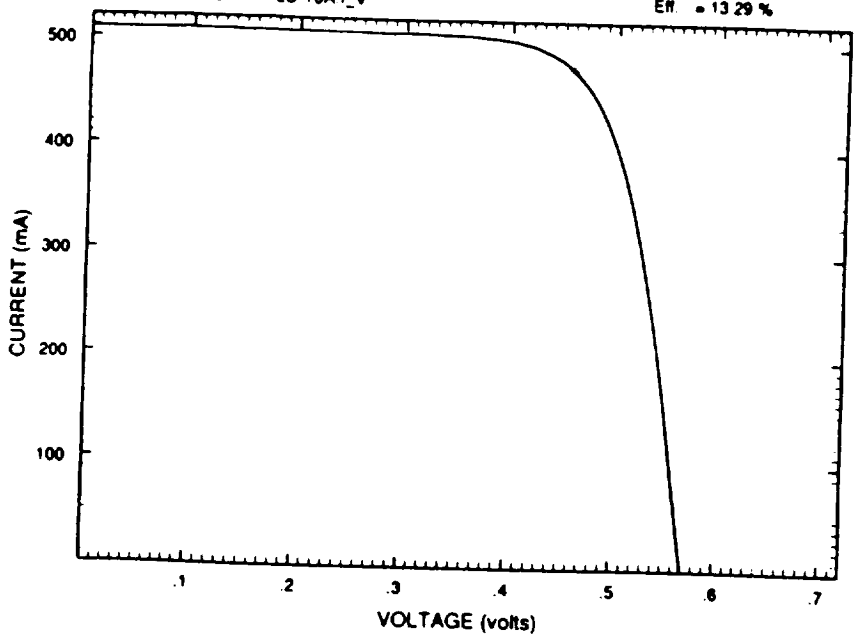

NASA

Cell	LD-10
Date	28 Jun 1994
Reference Cell	A-104
Area	12 cm^2
Temperature	25°C
Air Mass Zero	
File Name	LD-10B.I_V

Lewis Research Center

I_{sc} = -508.85 mA
V_{oc} = -569.4 mV
I_{max} = -474.7 mA
V_{max} = -459.1 mV
P_{max} = 217.9 mW
F.F. = 75.2
Eff. = 13.28 %

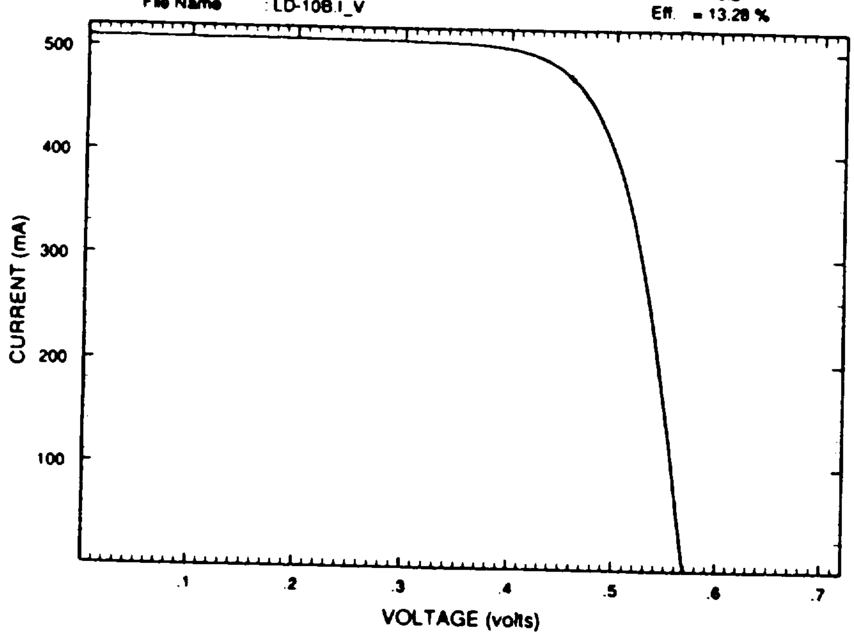

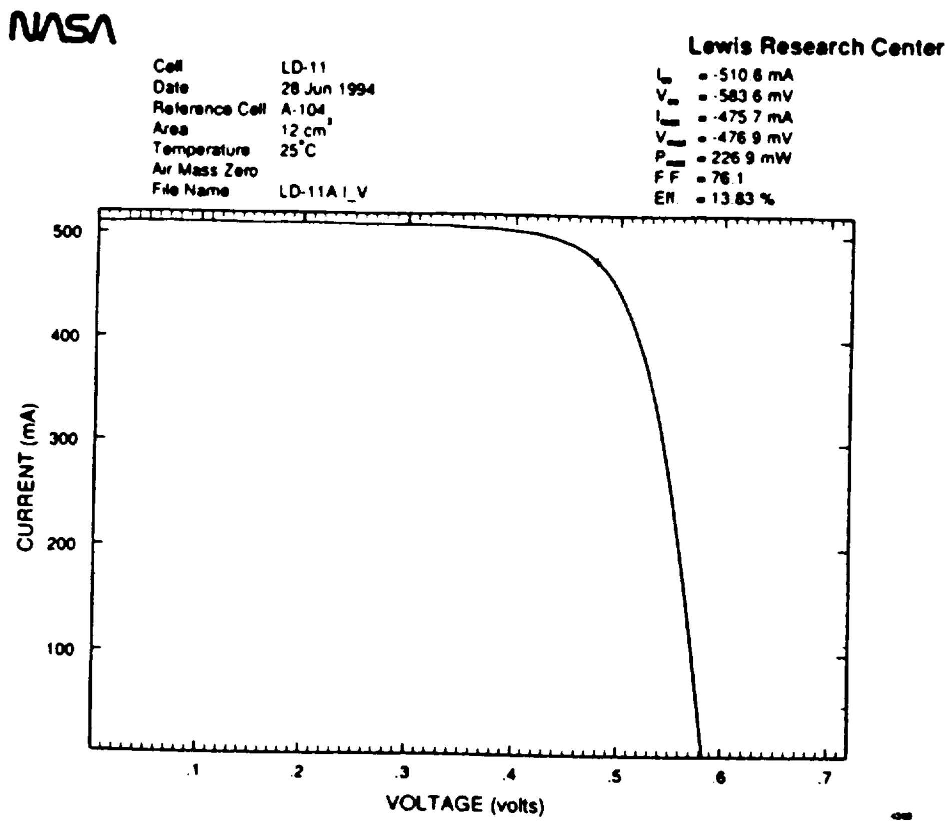

NASA
Lewis Research Center
Cell LD-11
Date 28 Jun 1994
Reference Cell A-104
Area 12 cm²
Temperature 25°C
Air Mass Zero
File Name LD-11A.I_V
= -510.6 mA
= -583.6 mV
= -475.7 mA
= -476.9 mV
= 226.9 mW
F.F. = 76.1
Eff. = 13.83 %
CURRENT (mA)
VOLTAGE (volts)

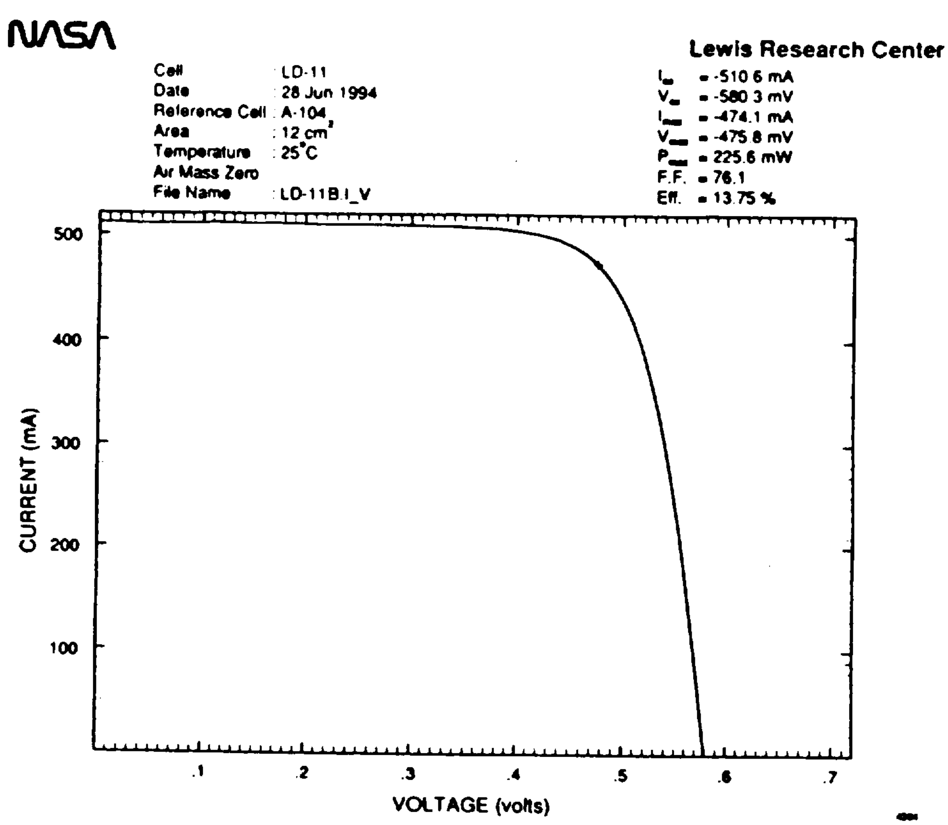

NASA
Lewis Research Center
Cell LD-11
Date 28 Jun 1994
Reference Cell A-104
Area 12 cm²
Temperature 25°C
Air Mass Zero
File Name LD-11B.I_V
= -510.6 mA
= -580.3 mV
= -474.1 mA
= -475.8 mV
= 225.6 mW
F.F. = 76.1
Eff. = 13.75 %
CURRENT (mA)
VOLTAGE (volts)

NASA

Lewis Research Center

Cell	LD-12
Date	28 Jun 1994
Reference Cell	A-104
Area	12 cm^2
Temperature	25°C
Air Mass Zero	
File Name	LD-12A.I_V

I_{sc} = -508.25 mA
V_{oc} = -576.1 mV
I_{max} = -467.3 mA
V_{max} = -470.1 mV
P_{max} = 219.6 mW
F.F. = 75
Eff = 13.38 %

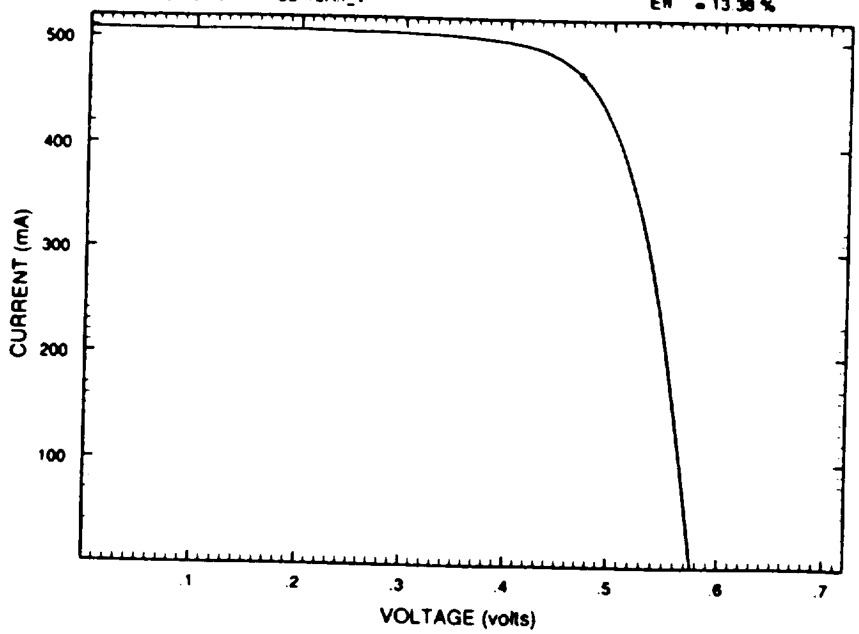

NASA

Lewis Research Center

Cell	LD-12
Date	28 Jun 1994
Reference Cell	A-104
Area	12 cm^2
Temperature	25°C
Air Mass Zero	
File Name	LD-12B.I_V

I_{sc} = -508.35 mA
V_{oc} = -572.7 mV
I_{max} = -466.7 mA
V_{max} = -468.4 mV
P_{max} = 218.6 mW
F.F. = 75
Eff. = 13.32 %

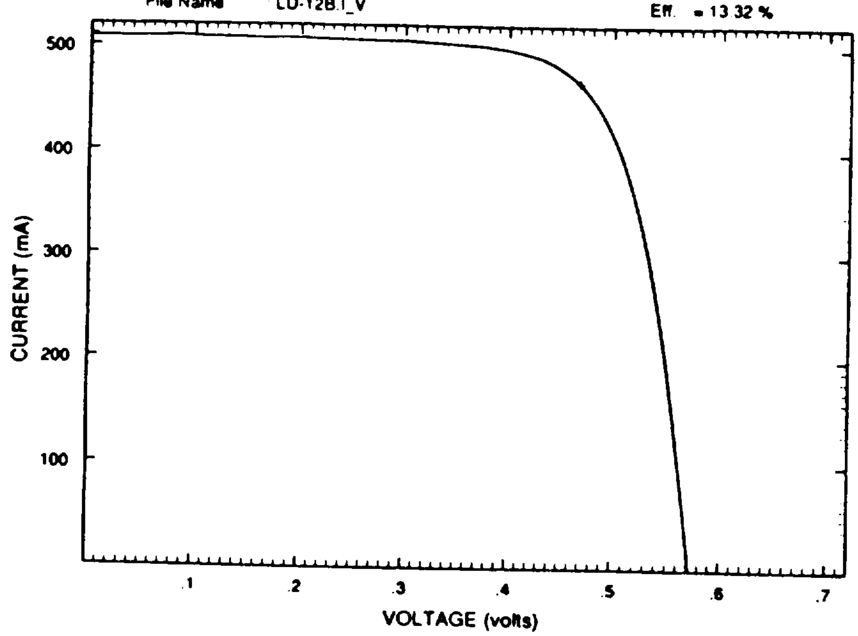

NASA

Lewis Research Center

Cell	LD-13	I_{sc}	= -498.1 mA
Date	28 Jun 1994	V_{oc}	= -576.6 mV
Reference Cell	A-104	I_{max}	= -463.9 mA
Area	12 cm^2	V_{max}	= -469.7 mV
Temperature	25°C	P_{max}	= 217.9 mW
Air Mass Zero		F.F.	= 75.8
File Name	LD-13A.I_V	Eff	= 13.28 %

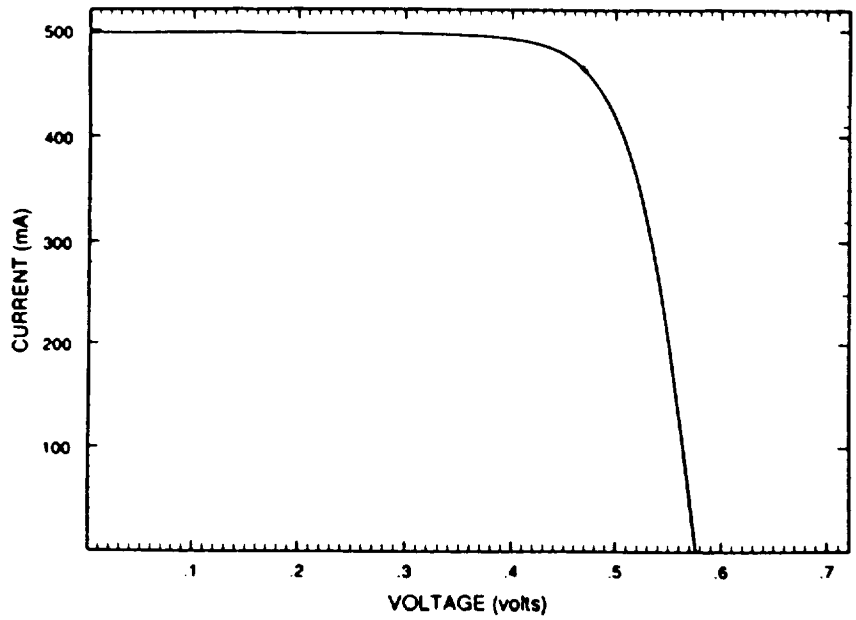

NASA

Lewis Research Center

Cell	: LD-13	I_{sc}	= -498.41 mA
Date	: 28 Jun 1994	V_{oc}	= -572.1 mV
Reference Cell	: A-104	I_{max}	= -460.9 mA
Area	: 12 cm^2	V_{max}	= -469 mV
Temperature	: 25°C	P_{max}	= 216.2 mW
Air Mass Zero		F.F.	= 75.8
File Name	: LD-13B.I_V	Eff.	= 13.17 %

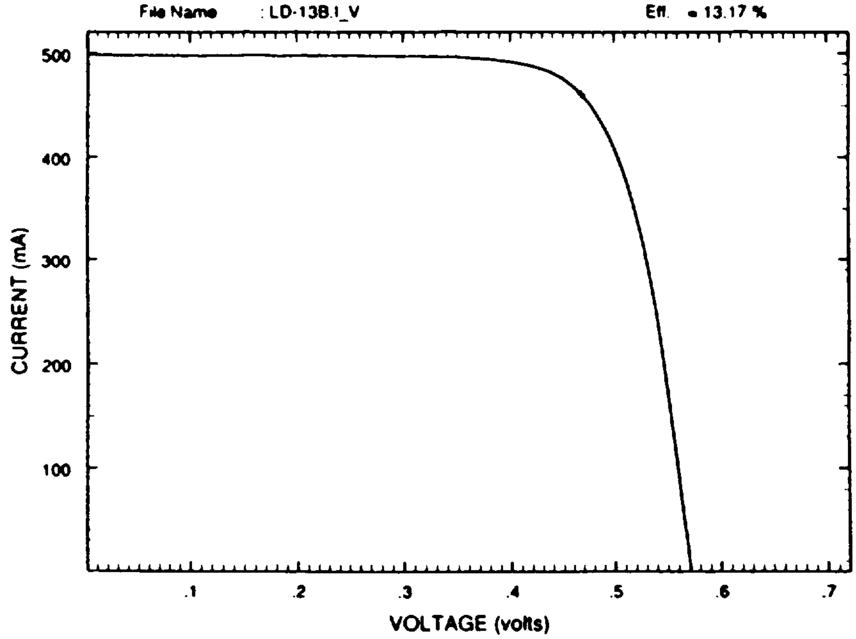

NASA

Cell : LD-14
Date : 28 Jun 1994
Reference Cell : A-104
Area : 12 cm^2
Temperature : 25°C
Air Mass Zero
File Name : LD-14A.I_V

Lewis Research Center

I_{sc} = -498.97 mA
V_{oc} = -582 mV
I_{max} = -461 mA
V_{max} = -472.3 mV
P_{max} = 217.7 mW
F.F. = 74.9
Eff. = 13.27 %

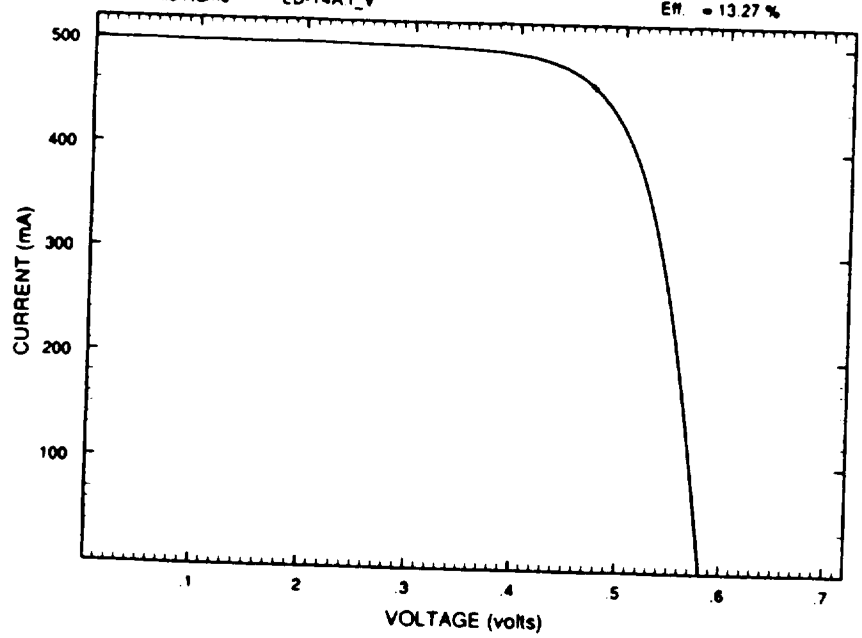

NASA

Cell : LD-14
Date : 28 Jun 1994
Reference Cell : A-104
Area : 12 cm^2
Temperature : 25°C
Air Mass Zero
File Name : LD-14B.I_V

Lewis Research Center

I_{sc} = -499.19 mA
V_{oc} = -578.4 mV
I_{max} = -459.3 mA
V_{max} = -471 mV
P_{max} = 216.4 mW
F.F. = 74.9
Eff. = 13.19 %

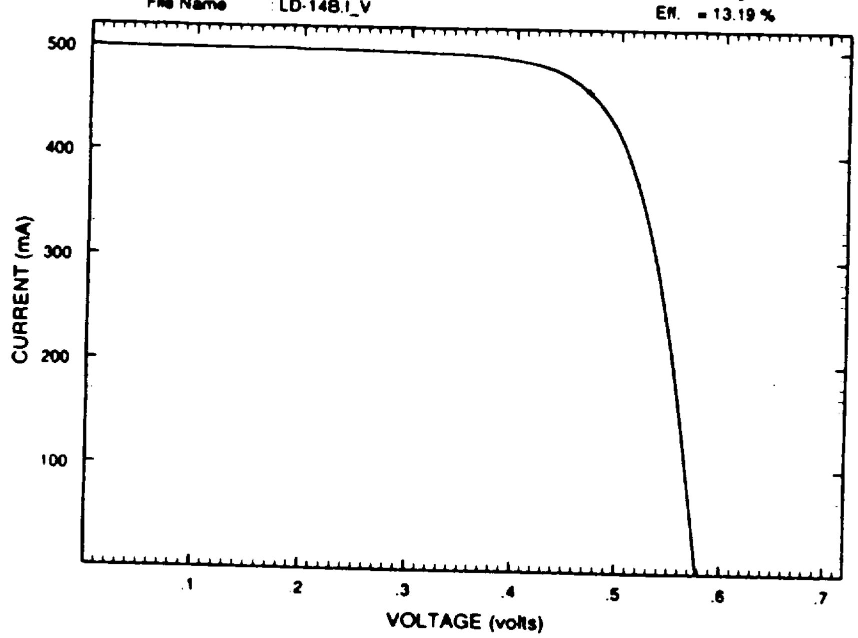

NASA

Cell	LD-15	
Date	28 Jun 1994	
Reference Cell	A-104	
Area	12 cm^2	
Temperature	25°C	
Air Mass Zero		
File Name	LD-15A I_V	

Lewis Research Center

I_{sc} = -511.99 mA
V_{oc} = -575.3 mV
I_{max} = -479.9 mA
V_{max} = -465.1 mV
P_{max} = 223.2 mW
F.F. = 75.7
Eff = 13.6 %

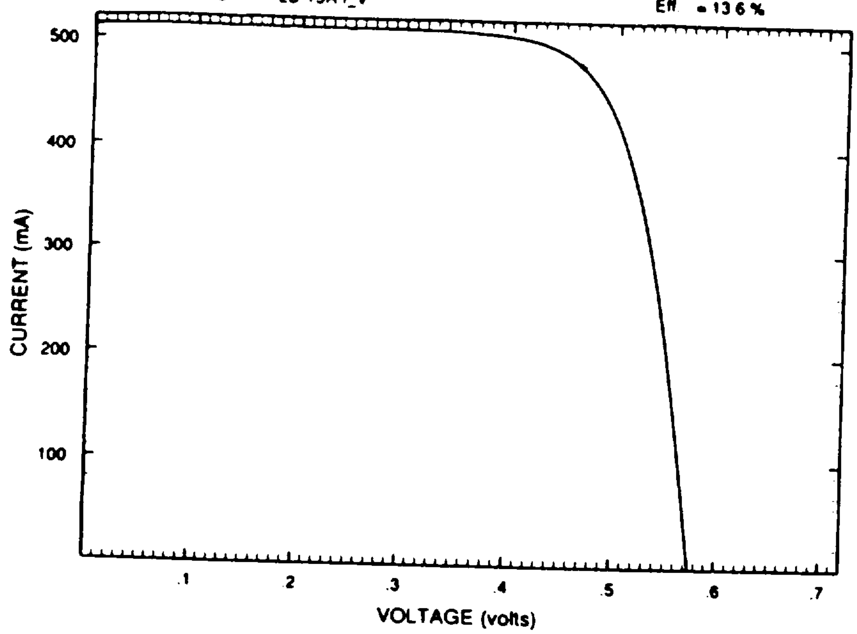

NASA

Cell	LD-15	
Date	28 Jun 1994	
Reference Cell	A-104	
Area	12 cm^2	
Temperature	25°C	
Air Mass Zero		
File Name	LD-15B I_V	

Lewis Research Center

I_{sc} = -511.76 mA
V_{oc} = -572.8 mV
I_{max} = -476 mA
V_{max} = -466.8 mV
P_{max} = 222.2 mW
F.F. = 75.8
Eff. = 13.54 %